Spring 1997

Adaptive space-time processing for digital mobile radio communication systems

Amit Shah
New Jersey Institute of Technology

Copyright Warning & Restrictions

The copyright law of the United States (Title 17, United States Code) governs the making of photocopies or other reproductions of copyrighted material.

Under certain conditions specified in the law, libraries and archives are authorized to furnish a photocopy or other reproduction. One of these specified conditions is that the photocopy or reproduction is not to be "used for any purpose other than private study, scholarship, or research." If a, user makes a request for, or later uses, a photocopy or reproduction for purposes in excess of "fair use" that user may be liable for copyright infringement,

This institution reserves the right to refuse to accept a copying order if, in its judgment, fulfillment of the order would involve violation of copyright law.

Please Note: The author retains the copyright while the New Jersey Institute of Technology reserves the right to distribute this thesis or dissertation

Printing note: If you do not wish to print this page, then select "Pages from: first page # to: last page #" on the print dialog screen

ABSTRACT

ADAPTIVE SPACE-TIME PROCESSING FOR DIGITAL MOBILE RADIO COMMUNICATION SYSTEMS

by
Amit Shah

The performance of digital mobile radio communication systems is primarily limited by cochannel interference and multipath fading. Antenna arrays, with *optimum combining* (OC), have been shown to combat multipath fading of the desired signal and are capable of reducing the power of interfering signals at the receiver through spatial filtering. With OC, the signals received by several antenna elements are weighted and combined to maximize the output signal-to-interference-plus-noise ratio (SINR). We derive new closed-form expressions for (1) the probability density function (PDF) of the SINR at the output of the optimum combiner, (2) the average probability of bit error rate (BER) and its upper bound, and (3) the outage probability in a Rayleigh fading environment with multiple cochannel interferers. The study covers both the case when the number of antenna elements exceeds the number of interferers and vice versa. We consider independent fading at each antenna element, as well as the effect of fading correlation. The analysis is also extended to processing using *maximal ratio combining* (MRC). The performance of the optimum combiner is compared to that of the maximal ratio combiner and results show that OC performs significantly better than MRC.

We investigate the performance of OC in a microcellular environment where the desired signal and the cochannel interference can have different statistical characteristics. The desired signal is assumed to have Rician statistics implying that a dominant multipath reflection or a line-of-sight (LOS) propagation exists within-cell transmission. Interfering signals from cochannel cells are assumed to be subject to Rayleigh fading due to the absence of LOS propagation. This is

the so called Rician/Rayleigh model. We also study OC for a special case of the Rician/Rayleigh model, the Nonfading/Rayleigh model. We derive expressions for the PDF of the SINR, the BER and the outage probability for both Rician/Rayleigh and Nonfading/Rayleigh models. Similar expressions are derived with MRC.

Another area in which space-time processing may provide significant benefits is when wideband signals (such as code division multiple access (CDMA) signals) are overlaid on existing narrowband user signals. The conventional approach of rejecting narrowband interference in direct-sequence (DS) CDMA systems has been to sample the received signal at the *chip interval*, and to exploit the high correlation between the interference samples prior to *spread spectrum* demodulation. A different approach is space-time processing. We study two space-time receiver architectures, referred to as cascade and joint, respectively, and evaluate the performance of a DS-CDMA signal overlaying a narrowband signal for personal communication systems (PCS). We define and evaluate the asymptotic efficiency of each configuration. We develop new closed-form expressions for the PDF of the SINR at the array output, the BER and its upper bound, for both cascade and joint configurations. We also analyze the performance of this system in the presence of multiple access interference (MAI).

ADAPTIVE SPACE-TIME PROCESSING FOR DIGITAL MOBILE RADIO COMMUNICATION SYSTEMS

by
Amit Shah

A Dissertation
Submitted to the Faculty of
New Jersey Institute of Technology
in Partial Fulfillment of the Requirements for the Degree of
Doctor of Philosophy

Department of Electrical and Computer Engineering

May 1997

APPROVAL PAGE

ADAPTIVE SPACE-TIME PROCESSING FOR DIGITAL MOBILE RADIO COMMUNICATION SYSTEMS

Amit Shah

Dr. Alexander Haimovich, Dissertation Advisor — Date
Associate Professor of Electrical and Computer Engineering, NJIT

Dr. Yeheskel Bar-Ness, Committee Member — Date
Distinguished Professor of Electrical and Computer Engineering, NJIT

Dr. Joseph Frank, Committee Member — Date
Associate Professor of Electrical and Computer Engineering, NJIT

Dr. Michael Porter, Committee Member — Date
Professor of Mathematics, NJIT

Dr. Jack Winters, Committee Member — Date
Member of Technical Staff, AT&T Labs-Research, Holmdel, NJ

BIOGRAPHICAL SKETCH

Author: Amit Shah

Degree: Doctor of Philosophy

Date: May, 1997

Undergraduate and Graduate Education:

- Doctor of Philosophy in Electrical Engineering,
  New Jersey Institute of Technology, Newark, NJ, 1997
- Bachelor of Science in Electrical Engineering,
  New Jersey Institute of Technology, Newark, NJ, 1992

Major: Electrical Engineering

Presentations and Publications:

A. Shah and A. M. Haimovich, "Space-Time Optimum Combining for CDMA Overlay for Personal Communication Systems," to appear in *Wireless Personal Communications*, 1997.

A. M. Haimovich and A. Shah, "The Performance of Space-Time Processing for Suppressing Narrowband Interference in CDMA Communications," *"The special Issue on CDMA for Universal Personal Communications Systems," Wireless Personal Communications*, 1997, accepted for publication.

A. Shah and A. M. Haimovich, "On the Probability of Bit Error of the Optimum Combiner in Space Diversity Reception with a Rayleigh Fading Cochannel Interferer," submitted to *IEEE Communications Letters*, August 1996.

A. Shah and A. M. Haimovich, "Performance Analysis of Optimum Combining in Wireless Communications with Rayleigh Fading and Cochannel Interference," submitted to *IEEE Transactions on Communications*, January 1997.

A. Shah and A. M. Haimovich, "A Performance Comparison of Optimum Combining and Maximal Ratio Combining for Digital Cellular Mobile Radio Communication Systems with Cochannel Interference," submitted to *IEEE Transactions on Vehicular Technology*, January 1997.

A. M. Haimovich, A. Shah and X. Bernstein, "Reduced-Rank Array Processing for Wireless Communications with Applications to IS-54/IS-136," submitted to *IEEE Transactions on Communications*, April 1997.

A. Shah and A. M. Haimovich, "On Optimum Combining in Digital Microcellular Mobile Radio Communication Systems with Cochannel Interference," to be submitted to *IEEE Transactions on Vehicular Technology*, April 1997.

A. Shah and A. M. Haimovich, "Bit Error Computations for Space-Time Narrowband Interference Suppression in CDMA Communications," *IEEE International Conference on Communications*, Montreal, Canada, June 1997, accepted for presentation.

A. Shah and A. M. Haimovich, "Performance Analysis of Space-Time Receiver Architectures for CDMA Overlay of Narrowband Waveforms for Personal Communication Systems," *IEEE International Conference on Communications*, Montreal, Canada, June 1997, accepted for presentation.

A. Shah and A. M. Haimovich, "On Spatial and Temporal Processing for CDMA Overlay Situations," *First IEEE Signal Processing Workshop on Signal Processing Advances in Wireless Communications*, Paris, France, 1997, accepted for presentation.

A. M. Haimovich and A. Shah, "STAP in Wireless Communications: Performance Analysis," *The Fifth Annual Workshop on Adaptive Sensor Array Processing*, MIT Lincoln Laboratory, Lexington, MA, March 1997.

D. J. Moelker, A. Shah and Y. Bar-Ness, "The Generalized Maximum SINR Array Processor for Personal Communication Systems in a Multipath Environment," *The Seventh IEEE International Symposium on Personal, Indoor and Mobile Radio Communications*, Taipei, Taiwan, ROC, October 1996.

A. M. Haimovich and A. Shah, "Space-Time Processing for Overlay Applications in PCS," *Proceedings of Interference Rejection and Signal Separation in Wireless Communications*, NJIT, Newark, USA, pp. 191-216, March 1996.

This dissertation is dedicated to
my uncle Kishor Shah and aunt Nayana Shah

ACKNOWLEDGMENT

I wish to express my sincere gratitude to my advisor, Dr. Alexander Haimovich, who has provided me with a lot of knowledge and encouragement throughout this research. I have been greatly influenced by his organized and disciplined style of research. It was my pleasure to do the research under his supervision.

I extend my gratitude to Drs. Jack Winters, Michael Porter, Yeheskel Bar-Ness and Joseph Frank for serving as members of the dissertation committee and for their comments.

A debt of gratitude is owed to Dr. Edith Frank for moral support, encouragement, and reassurance. This work would not have been possible otherwise.

Special thanks to Lisa Fitton for her suggestions during the editing of this dissertation.

I would like to express my deepest appreciation to my uncle Kishor Shah and aunt Nayana Shah, for their continuing support, encouragement, and love; without them, I would not be where I am today. They have contributed to this dissertation in more ways than they know, and for that and many other things, I thank them. I would also like to thank Mukesh Shah and Anjana Shah, for their help and support.

I would like to thank my parents and sister, for their invaluable support and help throughout my college career.

I would like to thank my present and former colleagues at the Center for Communications and Signal Processing Research at NJIT, for their help, encouragement, and friendship.

TABLE OF CONTENTS

Chapter Page

LIST OF TABLES

LIST OF FIGURES

CHAPTER 1

INTRODUCTION

Wireless communication is a field that is growing at a very fast rate. The goal of wireless communication is to allow the user access to the capabilities of the global network at any time without regard to location or mobility [1]. The principal resource underlying wireless communication is the radio frequency (RF) spectrum, which unfortunately is limited. The rapid increase in demand for wireless systems, without a corresponding increase in RF spectrum allocation, motivates the need for new techniques to improve spectrum utilization. System providers and equipment manufacturers are faced with the daunting task of catering to the needs of an ever-increasing subscriber community who demand better service and coverage area. The challenge is to increase system capacity, that is, the number of users that can access the system simultaneously while maintaining a specified quality of service [2].

The cellular concept was a major breakthrough in alleviating the problem of spectral congestion and system capacity. In cellular systems, a geographic area is partitioned into cells and each cell is allocated a set of frequencies. Interference between cells is minimized by assigning different frequency sets to neighboring cells. The cellular concept allows the reuse of the same spectrum at multiple locations. The frequency-reuse factor, however, determines the number of cells that can share an entirely allocated spectrum [3]. Reducing the frequency-reuse factor can increase system capacity, but inevitably increases the cochannel interference, which in turn degrades the system performance. The presence of cochannel interference because of frequency-reuse is a significant problem in cellular radio systems regardless of cell size and ultimately limits the system capacity. A further increase in the capacity is possible by reducing cell size (cell splitting). The degree of cell splitting, however, is

limited by the overhead of handoffs between cells and the number of base stations required.

Frequency division multiple access (FDMA), time division multiple access (TDMA), and code division multiple access (CDMA) are three schemes used to share the available bandwidth in a wireless communication system [4]. The "first-generation" cellular systems use the FDMA scheme for spectrum sharing, analog *frequency modulation* (FM) for speech transmission, and *frequency shift keying* (FSK) for signaling. The *Advanced Mobile Phone System* (AMPS), developed by AT&T for the USA, and the *Total Access Communication System* (TACS), used in the UK and a number of other countries, belong to the "first-generation."

The "second-generation" cellular systems are entirely digital. This allows TDMA and CDMA to be feasible. The TDMA system adds time slots on each radio channel, thus allowing more users to share the same spectrum. The *Global System for Mobile Communications* (GSM), specified by the European Telecommunications Standards Institute (ETSI), as well as IS-54, adopted by the Electronic Industries Association (EIA) and Telecommunications Industry Association (TIA) in North America, are TDMA cellular systems. CDMA, as a spread spectrum system, has distinct advantages over FDMA and TDMA systems. It has the potential to achieve a larger capacity than either FDMA or TDMA. The IS-95 CDMA standard is adopted by the EIA/TIA in North America. Multiple Access Interference (MAI), however, limits the CDMA system's capacity.

In a wireless system environment, the signal can reach the receiver after multiple reflections rather than a single direct path. The signal contributions may combine in a destructive manner, causing *multipath fading*. Fading may cause serious disruptions of the communication links and is one of the major factors to be considered in the system design. Diversity techniques, such as space, frequency, time, etc., are used to combat signal fading.

As mentioned above, the performance of cellular communication systems, is primarily limited by cochannel interference and multipath fading. Cochannel interference can be reduced by exploiting signal processing techniques. The rapid advance of VLSI technology and computers practically guarantees that signal processing will be a major component in the infrastructure of the next generation of wireless systems [5]. In particular, adaptive antenna arrays can be used to mitigate effects of fading and cochannel interference.

Antenna arrays can provide spatial diversity to combat multipath fading and are capable of reducing the power of the interferers through spatial filtering [6]. These improvements are measured quantitatively by the carrier-to-interference ratio (CIR). In classical beamforming, narrow beams are formed in specified directions. In a multipath environment, however, a generalized form of beamforming is required, in which beams are not associated with physical directions, but rather with a propagation vector representing the aggregate of all the propagation paths resulting from a specific source. In cellular mobile radio systems, there are several interfering signals whose power is close to that of the desired signal, and numerous interfering signals whose power is much less than that of the desired signal [7]. The cochannel cells in different tiers cause these successive power levels. Assuming more interferers than antenna elements, the array is unable to cancel every interfering signal. The adaptive array, however, does not have to greatly suppress interfering signals or vastly increase the output signal-to-interference-plus-noise ratio (SINR). A moderate increase in SINR at the output of the antenna array can result in significant increase in the capacity of the system. Consequently, spatial processing can provide a cost efficient means of increasing the capacity of cellular mobile radio communication systems.

Antenna arrays, with optimum combining (OC), combat both multipath fading of the desired signal and cochannel interference, subsequently increasing the performance and capacity of mobile radio systems [7, 8, 9, 10, 11, 12, 13]. With

OC, the signals received by several antenna elements are weighted and combined to maximize output SINR. Optimum combining has shown to reduce interference substantially both in systems with [7] and without [14] fading. A rich literature in the area of *Optimum Diversity Reception* can be found in translations of Russian authors from the sixties. These obscure publications are largely unknown to current authors, nevertheless they contain useful information [15, 16, 17, 18, 19]. The concept of OC is not new, and has been thoroughly investigated by the radar community, where it is usually referred to as adaptive array processing [14]. The use of adaptive arrays never managed to break out of niche applications, but the new application to wireless communication systems might finally make the use of adaptive arrays more widespread.

Winters studied the application of an adaptive antenna array at the base station to maximize SINR. He assumed a flat Rayleigh fading channel and independent fading between antennas. In [7], a closed-form expression is given for the average probability of bit error rate (BER) of the optimum combiner of BPSK signals with flat Rayleigh fading and a cochannel interferer. In [10], a closed-form expression for the upper bound on the BER with OC is given for N antenna elements and L ($L < N$) interferers. This is the *Zero-Forcing* solution, which is an upper bound for minimum-mean-square-error (MMSE) combining. Therein it is also shown that an antenna array may allocate available degrees of freedom (DOF) either to null interferences or for path diversity to combat fading. In [20], a closed-form expression for an upper bound on BER with OC is given for ($L < N$) as well as ($L \geq N$). Additional applications of adaptive arrays in mobile communications can be found in [21, 22].

Personal communication systems (PCS) strive to offer universal network access while freeing users of location, time and mobility restrictions. In October 1993, the U.S. Federal Communications Commission (FCC) released 140 MHz of spectrum in

the 1.85 to 1.99 GHz region for use in PCS applications [23]. The IS-95 direct-sequence (DS) CDMA has been proposed for use in the PCS frequency band [24]. This PCS spectrum, however, is currently occupied by point-to-point, fixed service, with relatively narrowband microwave radio links [25]. The coexistence of these two different systems within the same frequency spectrum will cause interference to both systems.

The concept of an overlay has been proposed for both the PCS band [26] and the cellular band [27]. In such a scenario, DS-CDMA signals are overlaid on top of existing narrowband user signals, thereby increasing overall spectrum efficiency, even more so than just through the use of the DS-CDMA network [28]. The inherent processing gain of DS spread spectrum techniques permits a DS-CDMA signal to operate in the presence of narrowband interference. Since a DS-CDMA signal spreads its power over a large bandwidth, the additional degradation it causes to a narrowband receiver is often just an imperceptible rise in its noise level. Measures must be taken so as not to cause intolerable interference to existing narrowband user signals. Signal processing techniques [29] can be employed to suppress these narrowband signals that occupy the spread spectrum bandwidth. Clearly, this will further lessen the interference level for CDMA users, more so than just that which is due to inherent processing gain. This, however, will also be beneficial to narrowband users, because now it is possible to operate a CDMA network at a reduced power level. It is important to note that the narrowband interference is not intentional, but rather an inevitable result of such a spectral sharing attempt. A number of authors have explored the performance of DS-CDMA overlay system [30, 31, 32, 33], with a narrowband BPSK signal as an interference.

Starting with the days when spread spectrum was contemplated mainly for military communications and through recent work concerned with commercial applications (e.g. overlay), a considerable body of knowledge exists on the topic of

narrowband interference rejection in DS-CDMA systems [34, 35, 36]. The conventional approach of rejecting narrowband interference has been to sample the received signal at the chip interval, and to exploit the high correlation between the interference samples prior to spread spectrum demodulation. The suppression filter used in this case is usually a two-sided transversal filter with weights being adapted according to the LMS algorithm. The filter attempts to remove the narrowband interference by using the great disparity in the bandwidth between a DS-CDMA waveform and a narrowband interference waveform. Since both DS-CDMA and thermal noise are wideband processes, their future values cannot be predicted from their past values. On the contrary, the interference, being a narrowband process, can indeed have its future values predicted from past values. The suppression filter predicts the narrowband interference component of the received signal and cancels it. A two-sided transversal filter uses both past and future values of the received signal to predict its current value. This method essentially places a notch at the narrowband interference frequency. The notch, however, also removes a portion of the DS-CDMA signal. As the bandwidth of the interference increases, the notch widens and the DS-CDMA signal loss becomes more significant.

A different approach is the use of antenna arrays. The main advantage of spatial over temporal (whitening filter) processing is in the bandwidth reference; in spatial processing the reference can be the carrier frequency, while in temporal processing the reference is the bandwidth of the spread spectrum signal. With respect to the carrier frequency, even the spread spectrum signal is essentially narrowband. Thus, unlike the performance of the whitening filter, the spatial processor is very robust with respect to the interference bandwidth. In [6], various space-time receiver architectures were considered for MAI cancellation in a CDMA based wireless communication system. Here, these architectures are evaluated for their performance in suppressing narrowband interference overlaid with a DS-CDMA signal for PCS.

The primary focus of this dissertation is to study application of adaptive space-time processing to digital cellular mobile radio communication systems. In this dissertation we make the following contributions.

1. We derive an expression for the BER, for the detection of BPSK signals, of the optimum combiner employing space diversity when both the desired signal and a cochannel interferer undergo flat Rayleigh fading. A computationally efficient closed-form expression for the upper bound on this BER is also derived.

2. We derive expressions for the BER and its upper bound with OC for N antenna elements and L ($L < N$) Rayleigh fading cochannel interferers.

3. We derive, with OC, the expression for the probability density function (PDF) of signal-to-interference ratio (SIR) at the antenna array output with N antenna elements and L ($L \geq N$) equal power Rayleigh fading cochannel interferers. We present closed-form expressions for both the BER and the outage probability. We consider independent fading at each antenna element, as well as the effect of fading correlation.

4. We derive, with maximal ratio combining (MRC), the expression for the PDF of SIR at the antenna array output with N antenna elements and L equal power Rayleigh fading cochannel interferers. We present closed-form expressions for both the BER and the outage probability. The performance of the optimum combiner is compared to that of the maximal ratio combiner.

5. We investigate the performance of OC for a microcellular system. In a microcellular environment, the desired and interfering signals can have different statistical characteristics. One such model is Rician/Rayleigh model. The desired signal is assumed to have Rician statistics implying that a dominant multipath reflection exists within-cell transmission. The interfering signals

from cochannel cells are assumed to be subject to Rayleigh fading because of the absence of line-of-sight (LOS) propagation. We also study OC for a special case of the Rician/Rayleigh model, the Nonfading/Rayleigh model. We derive expressions for the PDF of SIR, the BER and the outage probability for both Rician/Rayleigh and Nonfading/Rayleigh models. Similar expressions are derived with MRC.

6. We study the performance of space-time receiver architectures, cascade and joint, for suppressing a narrowband interference overlaid with a DS-CDMA signal for PCS. We develop expressions for the PDF of SINR at the array output, asymptotic efficiency, the BER and its upper bound, for both cascade and joint configurations. We also analyze the performance of these receiver architectures in the presence of MAI. The performance is evaluated in terms of BER, and how this performance is influenced by various parameters is also examined.

CHAPTER 2

OPTIMUM COMBINING FOR DIGITAL MACROCELLULAR MOBILE RADIO COMMUNICATION SYSTEMS

Adaptive array theory is well understood and documented [14]. Applications, however, were slow to exploit this body of knowledge, due to costs of building arrays and high demands on the required real-time computing power usually associated with array processing. Significant improvement in VLSI technology, computing power, and advances in adaptive signal processing, however, have made the use of antenna arrays a viable alternative to increase the capacity and performance of cellular radio systems. The additional cost of using antenna array may well be offset by increased revenues as the subscriber community continues to grow.

In this chapter we study the performance of optimum combining (OC) for digital mobile radio communication systems. We consider N antenna elements and L ($L < N$) Rayleigh fading cochannel interferers.

2.1 System Model

Consider the reverse link (mobile to base) of a digital cellular mobile radio communication system. The base station consists of an N element antenna array (micro-diversity). In contrast to traditional array processing (in a nonfading environment), in which antenna elements are placed at half-wavelength or at smaller intervals such that a high correlation exists between signals across the antenna array, spatial diversity is achieved by placing the antenna elements at larger intervals to provide for independent signal paths. If multipath reflections are uniformly distributed around the receive antenna elements, however, a spacing of atleast half-wavelength would suffice for the independence of signals at each antenna element [37]. The BPSK signals are assumed to be narrowband, hence they can be represented by

samples of their complex envelopes. The channel is characterized by flat (nondispersive) Rayleigh fading, independent between the antenna elements. The channel is assumed to be slowly fading, and therefore, the receiver has perfect knowledge of the instantaneous channel realization and a coherent receiver can be implemented. The multipath delay spread is assumed to be much smaller than the bit duration, hence we can neglect intersymbol interference.

After complex carrier demodulation, the received signal vector, at the outputs of the N separate antenna elements is given by

$$\mathbf{r}(t) = \sqrt{P}\mathbf{c}s(t) + \sum_{k=1}^{L} \sqrt{P_k}\mathbf{c}_k s_k(t) + \mathbf{v}(t), \tag{2.1}$$

where $s(t) \in \{-1, 1\}$ and $s_k(t) \in \{-1, 1\}$ are the desired and the k-th interfering signals, respectively, $\mathbf{c}$ and $\mathbf{c}_k$ are their respective channel propagation vectors. The binary symbols of the desired user and cochannel interferers are assumed time synchronized, equally probable and mutually independent. The number of interferers $L < N$, the order of diversity. P and P_k are the powers of the desired signal and the k-th interfering signal, respectively. We have

$$\mathrm{E}\left[s(t)\right] = \mathrm{E}\left[s_k(t)\right] = 0, \quad \mathrm{E}\left[s^2(t)\right] = \mathrm{E}\left[s_k^2(t)\right] = 1 \qquad k = 1, \ldots, L, \tag{2.2}$$

where E denotes expectation. With independent Rayleigh fading at each antenna element, the elements of $\mathbf{c}$ and $\mathbf{c}_k$ are independent, identically distributed (iid) complex Gaussian random variables with zero means and σ^2 variances. The magnitudes of the elements of $\mathbf{c}$ and $\mathbf{c}_k$ are Rayleigh distributed, and their phases are uniformly distributed between $[0, 2\pi]$. With Rayleigh fading, the inphase and quadrature components of each of the received signals have a Gaussian distribution (see Appendix D). The thermal noise $\mathbf{v}(t)$ is additive white complex Gaussian with a zero mean and a variance σ_n^2. The desired signal, interferers and thermal noise are assumed mutually independent.

2.2 Optimum Combining

The weight vector that maximizes signal-to-interference-plus-noise ratio (SINR) at the output of the array is [38]

$$\mathbf{w} = \alpha \mathbf{R}^{-1}\mathbf{c}, \tag{2.3}$$

where α is an arbitrary constant and the superscript $\{-1\}$ denotes the matrix inverse. The interference-plus-noise covariance matrix

$$\begin{aligned} \mathbf{R} &= \mathrm{E}\left[\left(\sum_{k=1}^{L}\sqrt{P_k}\mathbf{c}_k s_k(t) + \mathbf{v}(t)\right)\left(\sum_{k=1}^{L}\sqrt{P_k}\mathbf{c}_k s_k(t) + \mathbf{v}(t)\right)^{H}\right] \\ &= \sum_{k=1}^{L} P_k \mathbf{c}_k \mathbf{c}_k^{H} + \sigma_n^2 \mathbf{I}_N, \end{aligned} \tag{2.4}$$

where the superscript $\{H\}$ stands for transpose complex conjugate and $\mathbf{I}_N$ is an identity matrix of dimension N. The expected value operation in eq. (2.4) is taken with respect to noise and over the time interval during which $\mathbf{c}$ and $\mathbf{c}_k$ are considered constant (at least one signaling interval). The constant α does not affect the performance of the optimum combiner, i.e., the SINR at the array output. The output of the optimum combiner is given by

$$y = \mathbf{w}^{H}\mathbf{r} \tag{2.5}$$

The maximum SINR at the array output is given by [39]

$$\mu = P\mathbf{c}^{H}\mathbf{R}^{-1}\mathbf{c}. \tag{2.6}$$

Using unitary transformation Q in eq. (2.6), we get

$$\mu = P\mathbf{c}^{H}Q\Lambda^{-1}Q^{H}\mathbf{c}, \tag{2.7}$$

where Λ is a diagonal matrix with eigenvalues $\{\lambda_1, \ldots, \lambda_N\}$ of the matrix $\mathbf{R}$. Let $\mathbf{s} = Q^{H}\mathbf{c}$. Since Q is a unitary matrix, the elements of $\mathbf{s}$ have the same statistics as that of the elements of $\mathbf{c}$. Equation (2.7) can be rewritten as

$$\mu = P\sum_{l=1}^{N}\frac{|s_l|^2}{\lambda_l}, \tag{2.8}$$

where $\mathbf{s}^T = [s_1, \ldots, s_N]$. Since the elements of $\mathbf{c}$ have Rayleigh distributed amplitudes, each of $\{|s_l|^2\}$ is a chi-square random variable with two degrees of freedom (DOF).

2.3 BER of the Optimum Combiner

First, we will evaluate the performance, i.e., the average probability of bit error rate (BER), of the optimum combiner for $L = 1$ interferer and in the later section for any $L < N$.

2.3.1 BER for One Rayleigh Fading Interferer

In the case of one interferer, the eigenvalues $\{\lambda_l\}$ of $\mathbf{R}$ are

$$\lambda_l = \begin{cases} P_1 \sum_{n=1}^{N} \mid c_{1n} \mid^2 + \sigma_n^2 & l = 1 \\ \sigma_n^2 & l = 2, \ldots, N, \end{cases}$$

where $\mathbf{c}_1^T = [c_{11}, \ldots, c_{1N}]$. Each of $\{\mid c_{1l} \mid^2\}$ is a chi-square random variable with two DOF.

Due to the mutual independence of the terms in eq. (2.8), the characteristic function of μ conditioned on λ_1 is given by [40]

$$\phi_{\mu/\lambda_1}(jw) = \frac{1}{\left(1 - jw\frac{P_s}{\lambda_1}\right)\left(1 - jw\frac{P_s}{\sigma_n^2}\right)^{N-1}}, \tag{2.9}$$

where $P_s = P\mathrm{E}[|c_l|^2], l = 1, \ldots, N$, is the mean desired signal power per antenna and $\mathbf{c}^T = [c_1, \ldots, c_N]$. Define $h = \frac{P_s}{\sigma_n^2}$ as the mean signal-to-noise ratio (SNR) per antenna (channel). Therefore, the conditional probability density function (PDF) of μ can now be obtained by applying the inverse Fourier transformation to eq. (2.9) and is given by [41]

$$f_{\mu/\lambda_1}(\mu) = \frac{\lambda_1 \mu^{N-1} e^{\frac{-\lambda_1 \mu}{P_s}} {}_1F_1\left(N-1; N; \frac{(\lambda_1 - \sigma_n^2)\mu}{P_s}\right)}{\sigma_n^2 \Gamma(N) h^N}, \ \mu \geq 0, \ \lambda_1 \geq \sigma_n^2, \ N \geq 1, \tag{2.10}$$

where ${}_1F_1(\cdot)$ is the Kummer's confluent hypergeometric function and $\Gamma(\cdot)$ is th standard gamma function. The function ${}_1F_1(\cdot)$ is defined as [42]

$$ {}_1F_1(a,b,x) = \sum_{n=0}^{\infty} \frac{\Gamma(a+n)\Gamma(b)}{\Gamma(a)\Gamma(b+n)} \frac{x^n}{n!}. \tag{2.11} $$

The series converges for all finite x, i.e., $-\infty < x < \infty$.

In [7], λ_1 in eq. (2.10) was assumed constant. That is, the PDF in eq. (2.10) was considered unconditional with λ_1 replaced by $NP_I + \sigma_n^2$, where $P_I = P_1 \mathrm{E}[|c_{1l}|^2]$ is the mean interference power per antenna. If the interference is assumed fading, clearly, λ_1 is a random variable.

As mentioned earlier, subsequent to Rayleigh fading, the inphase and quadratur components of each of the received signals have a Gaussian distribution. That is, $\sqrt{P_1}\mathbf{c}_1 s_1(t)$, has a complex Gaussian distribution. The sum of the interference and noise is also complex Gaussian. Since the optimum combiner is a linear filter, the sum of the interference and noise at the output of the optimum combiner (antenna array) is also complex Gaussian. Therefore, the conditional BER can now be evaluated as

$$ \begin{aligned} P_{e/\lambda_1} &= \int_0^{\infty} \frac{1}{2}\mathrm{erfc}(\sqrt{\mu}) f_{\mu/\lambda_1}(\mu) d\mu \\ &= \frac{1}{2} - \frac{1}{2}\int_0^{\infty} \mathrm{erf}(\sqrt{\mu}) f_{\mu/\lambda_1}(\mu) d\mu, \end{aligned} \tag{2.12} $$

where $\mathrm{erf}(\cdot)$ and $\mathrm{erfc}(\cdot)$ are the error function and the complementary error functions, respectively. Using the identity [42]

$$ \mathrm{erf}(\sqrt{\mu}) = \frac{2}{\sqrt{\pi}}\sqrt{\mu}\, e^{-\mu}\, {}_1F_1\left(1; \frac{3}{2}; \mu\right) $$

in eq. (2.12) we get

$$ \begin{aligned} P_{e/\lambda_1} &= \frac{1}{2} - \frac{\lambda_1}{\sqrt{\pi}\sigma_n^2\Gamma(N)h^N} \int_0^{\infty} \mu^{(N-\frac{1}{2})} e^{-(\frac{\lambda_1}{P_s}+1)\mu} \\ &\quad {}_1F_1\left(1; \frac{3}{2}; \mu\right) {}_1F_1\left(N-1; N; \frac{(\lambda_1 - \sigma_n^2)\mu}{P_s}\right) d\mu. \end{aligned} \tag{2.13} $$

The integral in eq. (2.13) can be evaluated in closed-form [43] and is

$$ P_{e/\lambda_1} = \frac{1}{2} - \frac{\lambda_1\Gamma(N+\frac{1}{2})P_s^{N+\frac{1}{2}} F_2\left(N+\frac{1}{2}, 1, N-1; \frac{3}{2}, N; \frac{P_s}{\lambda_1+P_s}, \frac{\lambda_1-\sigma_n^2}{\lambda_1+P_s}\right)}{\sqrt{\pi}\sigma_n^2\Gamma(N)h^N(\lambda_1+P_s)^{N+\frac{1}{2}}}, \tag{2.14} $$

where $F_2(\cdot)$ is Appell's hypergeometric function of two variables. The function $F_2(\cdot)$ is defined as [44]

$$F_2(\alpha,\beta,\beta';\gamma,\gamma';x,y) = \sum_{m=0}^{\infty}\sum_{n=0}^{\infty}\frac{(\alpha)_{m+n}(\beta)_m(\beta')_n}{m!n!(\gamma)_m(\gamma')_n}x^m y^n. \tag{2.15}$$

The notation $(\alpha)_{m+n}$ is called the Pochhammer symbol [42] and is defined as $(\alpha)_{m+n} = \frac{\Gamma(\alpha+m+n)}{\Gamma(\alpha)}, m,n = 0,1,2,\ldots$. The double infinite series in eq. (2.15) is absolutely convergent for $|x| + |y| < 1$ as shown in [44]. Hence, the series in eq. (2.14) converges.

Since each of $\{| c_{1l} |^2\}$ has a chi-square distribution, $\lambda_1 = P_1 \sum_{l=1}^{N} | c_{1l} |^2 + \sigma_n^2$, has the PDF [40]

$$f_{\lambda_1}(\lambda_1) = \frac{1}{\Gamma(N)P_I^N}(\lambda_1 - \sigma_n^2)^{N-1}e^{-\frac{(\lambda_1-\sigma_n^2)}{P_I}}, \qquad \lambda_1 \geq \sigma_n^2. \tag{2.16}$$

Therefore the BER averaged over all values of λ_1 is

$$\begin{aligned} P_e &= \frac{1}{2} - \frac{\Gamma(N+\frac{1}{2})P_s^{N+\frac{1}{2}}}{\sqrt{\pi}\sigma_n^2\Gamma(N)h^N}\frac{1}{\Gamma(N)P_I^N}\int_{\sigma_n^2}^{\infty}\frac{\lambda_1}{(\lambda_1+P_s)^{N+\frac{1}{2}}}(\lambda_1-\sigma_n^2)^{N-1}e^{-\frac{(\lambda_1-\sigma_n^2)}{P_I}} \\ &\quad F_2\left(N+\frac{1}{2},1,N-1;\frac{3}{2},N;\frac{P_s}{\lambda_1+P_s},\frac{\lambda_1-\sigma_n^2}{\lambda_1+P_s}\right)d\lambda_1. \end{aligned} \tag{2.17}$$

A closed-form expression for the integral in eq. (2.17) is not known, however, it can be evaluated numerically. For the special case of $N = 1$, i.e., one antenna element, there is a closed-form expression for the BER in eq. (2.17):

$$P_e = \frac{1}{2} - \frac{\sqrt{\pi}}{2}\sqrt{\frac{P_s}{P_I}}e^{\frac{P_s+\sigma_n^2}{P_I}}\operatorname{erfc}\left(\sqrt{\frac{P_s+\sigma_n^2}{P_I}}\right). \tag{2.18}$$

As $\sigma_n^2 \to 0$, the evaluation of the BER in eq. (2.17) becomes computationally involved.

2.3.2 BER for One Rayleigh Fading Interferer: An Alternate Approach

Using eqs. (2.10), (2.16), we can obtain [45] the unconditional distribution of μ:

$$\begin{aligned} f_\mu(\mu) &= \int_{\sigma_n^2}^{\infty} f_{\mu/\lambda_1}(\mu)f_{\lambda_1}(\lambda_1)d\lambda_1 \\ &= \frac{\mu^{N-1}e^{-\frac{\mu}{h}}\left[NP_sP_I + P_s\sigma_n^2 + \mu P_I^2(N-1) + \mu P_I\sigma_n^2\right]}{\Gamma(N)h^{N-1}(P_s+P_I\mu)^2}. \end{aligned} \tag{2.19}$$

The BER can now be evaluated:

$$\begin{aligned} P_e &= \int_0^\infty \frac{1}{2}\text{erfc}(\sqrt{\mu}) f_\mu(\mu) d\mu \\ &= \int_0^\infty \frac{\mu^{N-1} e^{-\frac{\mu}{h}} \text{erfc}(\sqrt{\mu}) \left[N P_s P_I + P_s \sigma_n^2 + \mu P_I^2 (N-1) + \mu P_I \sigma_n^2\right]}{2h^{N-1}\Gamma(N)(P_s + P_I\mu)^2} d\mu \end{aligned} \tag{2.20}$$

A closed-form expression for the integral in eq. (2.20) is not known, however, it is simpler to numerically evaluate than eq. (2.17). Both, eq. (2.20) and eq. (2.17), do not provide any meaningful insight into the performance of the optimum combiner. Thus, a meaningful and computationally efficient upper bound on this BER is derived.

2.3.3 Upper Bound on the BER for One Rayleigh Fading Interferer

Using the bound [46]

$$\text{erfc}(\sqrt{\mu}) < e^{-\mu} \tag{2.21}$$

in eq. (2.12) we get

$$\begin{aligned} P_{e/\lambda_1} &< \frac{1}{2}\int_0^\infty e^{-\mu} f_{\mu/\lambda_1}(\mu) d\mu \\ &= \frac{\lambda_1}{2\sigma_n^2 \Gamma(N) h^N} \int_0^\infty e^{-(\frac{\lambda_1}{P_s}+1)\mu} \mu^{N-1} {}_1F_1\left(N-1; N; \frac{(\lambda_1 - \sigma_n^2)\mu}{P_s}\right) d\mu. \end{aligned} \tag{2.22}$$

The integral in eq. (2.22 can be evaluated in closed-form [43]:

$$P_{e/\lambda_1} < \frac{\lambda_1}{2(\lambda_1 + P_s)(1+h)^{N-1}}. \tag{2.23}$$

The BER expression in eq. (2.23) provides meaningful insight into a few special cases. When there is no interference, i.e., $P_1 = 0, \lambda_1 = \sigma_n^2$, the conditional BER of eq. (2.23) reduces to $P_e < \frac{1}{2(1+h)^N}$. This is the upper bound for the BER of an N-th order space diversity receiver employing maximal ratio combining (MRC) without interference, as expected. When the interference power is infinite, i.e., $P_1 \to \infty, \lambda_1 \to \infty$, eq. (2.23) reduces to $P_e < \frac{1}{2(1+h)^{N-1}}$. This is the upper bound for the BER of an $(N-1)$-th

order space diversity MRC receiver and no interference. This implies that presence of interference with infinite power in the channel, results in the loss of one diversity path, a result also mentioned in [7, 47].

The upper bound on the BER averaged over all the values of λ_1 is

$$P_e < \frac{1}{2\Gamma(N)P_I^N(1+h)^{N-1}} \int_{\sigma_n^2}^{\infty} \frac{\lambda_1(\lambda_1-\sigma_n^2)^{N-1}}{(\lambda_1+P_s)} e^{-\frac{(\lambda_1-\sigma_n^2)}{\bar{\gamma}}} d\lambda_1. \tag{2.24}$$

Using a change of variable and the identity [45]

$$\int_0^{\infty} \frac{x^n}{(x+y)} e^{-ax}\, dx = (-1)^{n+1} y^n e^{ay} \mathrm{Ei}(-ay) + \sum_{r=1}^{n} (-1)^{n-r} (r-1)!\, a^{-r} y^{n-r}, \tag{2.25}$$

in eq. (2.24), we get

$$\begin{aligned} P_e &< A\left[(-1)^{N+1}\left(P_s+\sigma_n^2\right)^N e^{\frac{P_s+\sigma_n^2}{P_I}} \mathrm{Ei}\left(-\frac{P_s+\sigma_n^2}{P_I}\right)\right. \\ &+ \left.\sum_{r=1}^{N}(-1)^{N-r}(r-1)!P_I^r\left(P_s+\sigma_n^2\right)^{N-r}\right] \\ &+ A\sigma_n^2\left[(-1)^N\left(P_s+\sigma_n^2\right)^{N-1} e^{\frac{P_s+\sigma_n^2}{P_I}} \mathrm{Ei}\left(-\frac{P_s+\sigma_n^2}{P_I}\right)\right. \\ &+ \left.\sum_{r=1}^{N-1}(-1)^{N-1-r}(r-1)!P_I^r\left(P_s+\sigma_n^2\right)^{N-1-r}\right], \end{aligned} \tag{2.26}$$

where $\mathrm{Ei}(\cdot)$ is the exponential integral and $A = \frac{1}{2\Gamma(N)P_I^N(1+h)^{N-1}}$.

In Figure 2.1, eqs. (2.17), (2.18), (2.26) and simulation results are plotted as a function of average total SNR defined as $N\frac{P_s}{\sigma_n^2}$, where N is the order of diversity. The mean power of the desired signal and interference are assumed equal, i.e., $P_s = P_I$. Note the good agreement between theory and simulation results. For $N = 1$, the performance of the optimum combiner becomes interference limited.

In the next section, we study the performance of the optimum combiner for $1 < L < N$ cochannel interferers.

2.3.4 BER for Multiple Rayleigh Fading Interferers

For $L < N$ interferers, the eigenvalues $\{\lambda_l\}$ of $\mathbf{R}$ are

$$\lambda_l = \begin{cases} \lambda_l & l = 1, \ldots, L \\ \sigma_n^2 & l = L+1, \ldots, N. \end{cases}$$

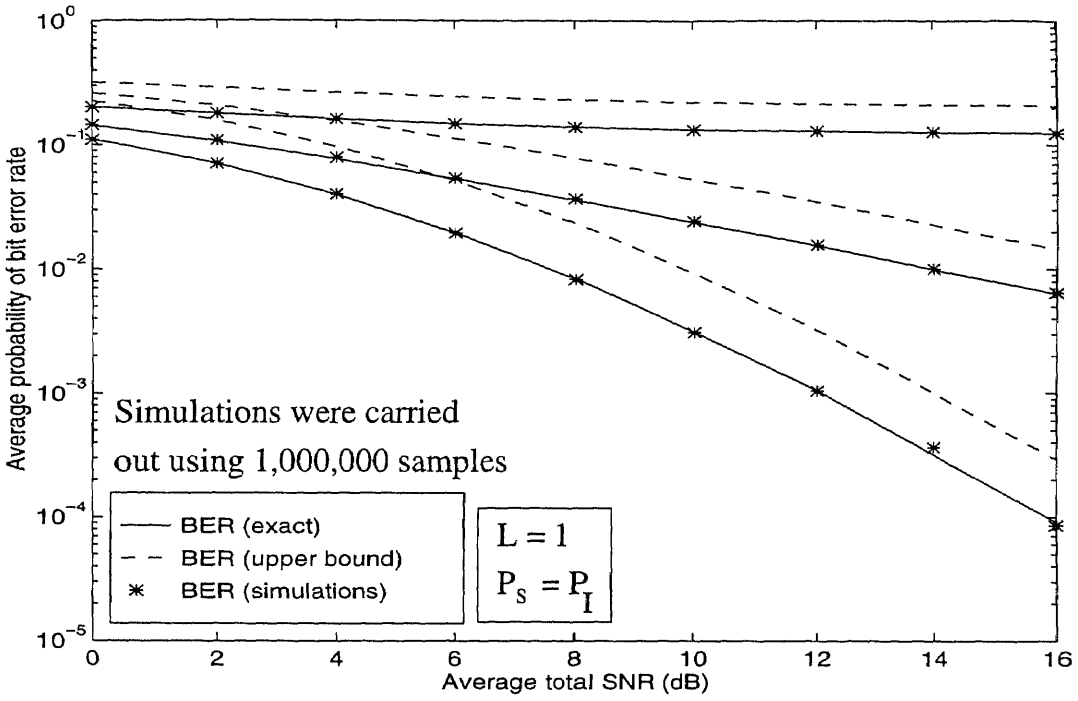

Figure 2.1 BER of the optimum combiner with a Rayleigh fading cochannel interference.

The characteristic function of μ conditioned on the eigenvalues λ_l, $l = 1, \ldots, L$, is given by

$$\phi_{\mu/\lambda_1,\ldots,\lambda_L}(jw) = \left(\prod_{l=1}^{L} \frac{1}{(1-jw\gamma_l)}\right) \frac{1}{(1-jwh)^{N-L}}, \tag{2.27}$$

where $\gamma_l = \frac{P_s}{\lambda_l}$ and $h = \frac{P_s}{\sigma_n^2}$. Therefore the conditional PDF of μ can now be obtained and is

$$f_{\mu/\lambda_1,\ldots,\lambda_L}(\mu) = \frac{h^{-(N-L)}\mu^{(N-L)}}{\Gamma(N-L+1)} \sum_{l=1}^{L} \frac{\pi_l e^{\frac{-\mu}{\gamma_l}} {}_1F_1\left(N-L; N-L+1; \left(\frac{1}{\gamma_l} - \frac{1}{h}\right)\mu\right)}{\gamma_l}, \tag{2.28}$$

where $\pi_l = \prod_{k=1,k\neq l}^{L} \frac{\gamma_l}{\gamma_l - \gamma_k}$. Here, it is assumed that $\{\lambda_l, l = 1, \ldots, L\}$ are distinct and $\lambda_1 > \lambda_2 > \ldots > \lambda_L$. Therefore, the conditional BER is

$$\begin{aligned} P_{e/\lambda_1,\ldots,\lambda_L} &= \int_0^\infty \frac{1}{2}\mathrm{erfc}(\sqrt{\mu}) f_{\mu/\lambda_1,\ldots,\lambda_L}(\mu) d\mu \\ &= \frac{1}{2} - \frac{1}{2}\int_0^\infty \mathrm{erf}(\sqrt{\mu}) f_{\mu/\lambda_1,\ldots,\lambda_L}(\mu) d\mu. \end{aligned} \tag{2.29}$$

Using the procedure shown in the previous section, the integral in eq. (2.29) can be evaluated yielding

$$P_{e/\lambda_1,\ldots,\lambda_L} = \frac{1}{2} - \sum_{l=1}^{L} \frac{\Gamma(N-L+\frac{3}{2})\pi_l F_2\left(N-L+\frac{3}{2}, 1, N-L; \frac{3}{2}, N-L+1; \frac{\gamma_l}{\gamma_l+1}, \frac{1-\frac{\gamma_l}{h}}{\gamma_l+1}\right)}{\sqrt{\pi}\Gamma(N-L+1)h^{(N-L)}\gamma_l(1+\frac{1}{\gamma_l})^{N-L+\frac{3}{2}}}. \tag{2.30}$$

Therefore the unconditional BER, i.e., the one averaged over all the values of $\lambda_1, \ldots, \lambda_L$, is given by

$$P_e = \int_{\sigma_n^2}^{\infty} \int_{\sigma_n^2}^{\lambda_1} \cdots \int_{\sigma_n^2}^{\lambda_{L-1}} P_{e/\lambda_1,\ldots,\lambda_L} f_{\lambda_1,\ldots,\lambda_L}(\lambda_1, \ldots, \lambda_L) d\lambda_L \ldots d\lambda_2 d\lambda_1, \tag{2.31}$$

where $f_{\lambda_1,\ldots,\lambda_L}(\lambda_1, \ldots, \lambda_L)$ is the joint PDF of the eigenvalues $\lambda_1, \ldots, \lambda_L$. It is extremely difficult to obtain the joint PDF of the eigenvalues.

2.3.5 Upper Bound on the BER for Multiple Rayleigh Fading Interferers

Since eq. (2.31) is very difficult to evaluate, in this section we derive an upper bound on the BER for $L < N$ interferers. Using the bound in eq. (2.21) in eq. (2.29) we get

$$\begin{aligned} P_{e/\lambda_1,\ldots,\lambda_L} &< \frac{1}{2}\int_0^\infty e^{-\mu} f_{\mu/\lambda_1,\ldots,\lambda_L}(\mu)d\mu \\ &= \frac{h^{-(N-L)}}{2\Gamma(N-L+1)}\int_0^\infty \sum_{l=1}^{L} \frac{\pi_l \mu^{N-L}\, {}_1F_1\left(N-L; N-L+1; \left(\frac{1}{\gamma_l}-\frac{1}{h}\right)\mu\right)}{e^{\left(\frac{1}{\gamma_l}+1\right)\mu}\gamma_l} d\mu. \end{aligned} \tag{2.32}$$

The integral in eq. (2.32) can be evaluated in closed-form [43] and is

$$\begin{aligned} P_{e/\lambda_1,\ldots,\lambda_L} &< \frac{1}{2}\sum_{l=1}^{L}\frac{\pi_l}{(1+\gamma_l)(1+h)^{N-L}} \\ &= \frac{1}{2}\frac{1}{(1+\gamma_1)(1+\gamma_2)\ldots(1+\gamma_L)(1+h)^{N-L}}. \end{aligned} \tag{2.33}$$

The BER expression in eq. (2.33) provides useful insight into the performance of the optimum combiner. When there is no interference, the conditional BER of eq. (2.33) reduces to $P_e < \frac{1}{2(1+h)^N}$, which is the upper bound on the BER for N-th order diversity MRC receiver without interference. When all interferers have infinite power, the conditional BER of eq. (2.33) reduces to $P_e < \frac{1}{2(1+h)^{(N-L)}}$, which is the upper bound on the BER for $(N-L)$-th order diversity MRC receiver and no interference. This indicates a loss of L diversity paths, a result first mentioned in [47]. Therefore, the optimum combiner with N antenna elements and L $(L < N)$ interferers will always do better than the maximal ratio combiner with $(N-L)$ antenna elements without interference. The interference cancellation entails a loss of DOF, with a corresponding loss in the diversity performance.

In the above derivations it was assumed that the eigenvalues $\{\lambda_l\}$ $l = 1,\ldots,L$ are distinct. If $\lambda_1 = \lambda_2 = \ldots = \lambda_L$, the conditional PDF of μ is given by

$$f_{\mu/\lambda_l}(\mu) = \frac{\mu^{N-1}e^{-\frac{\mu}{\gamma}}\, {}_1F_1\left(N-L; N; \left(\frac{1}{\gamma}-\frac{1}{h}\right)\mu\right)}{h^{(N-L)}\gamma^L\Gamma(N)}, \qquad \lambda_l \geq \sigma_n^2, \tag{2.34}$$

where $\gamma = \frac{P_s}{\lambda_l}$, $l = 1,\ldots,L$.

The upper bound on the BER in the case of equal eigenvalues is

$$P_{e/\lambda_l} < \frac{1}{2(1+\gamma)^L(1+h)^{N-L}}. \tag{2.35}$$

Clearly, the BER in expression eq. (2.35) adheres to the results mentioned above.

In the next chapter, we evaluate the performance of the optimum combiner for $L \geq N$ cochannel interferers.

CHAPTER 3

A PERFORMANCE COMPARISON OF OPTIMUM COMBINING AND MAXIMAL RATIO COMBINING

In the previous chapter, the performance of the optimum combiner was evaluated for N antenna elements and L ($L < N$) Rayleigh fading cochannel interferers. In this chapter, we consider the case of L ($L \geq N$) equal power cochannel interferers. This case is of practical interest. As mentioned in the introduction, in the case of $L \geq N$, the optimum combiner is unable to cancel every interfering signal. The optimum combiner, however, does not have to cancel every interfering signal or vastly increase the output signal-to-interference ratio (SIR). A few decibel increase in SIR at the output of the optimum combiner can result in a significant increase in the capacity of the system.

In this chapter, we derive expressions for the probability density function (PDF) of the maximum SIR at the output of the optimum combiner, the outage probability and the average probability of bit error rate (BER). We consider independent fading at each antenna element, as well as the effect of fading correlation. We also study maximal ratio combining (MRC) and derive similar expressions. The performance of the optimum combiner is then compared to that of the maximal ratio combiner.

The system model is similar to the one assumed in section 2.1. The communication system is assumed interference limited, hence, thermal noise is neglected. The received signal vector, at the outputs of the separate antenna elements is given by

$$\mathbf{r}(t) = \sqrt{P_s}\mathbf{c}s(t) + \sqrt{P}\sum_{k=1}^{L}\mathbf{c}_k s_k(t), \tag{3.1}$$

where $s(t) \in \{-1, 1\}$ and $s_k(t) \in \{-1, 1\}$ are the desired and the k-th interfering signals, respectively, $\mathbf{c}$ and $\mathbf{c}_k$ are their respective channel propagation vectors. The number of interferers $L \geq N$, the order of diversity. Results are for the case where

all interferers have equal power P, e.g., when they are equidistant from the desired mobile's base station. P_s is the desired signal power.

3.1 Maximal Ratio Combining

Without cochannel interference, for coherent reception with independent fading at each antenna element, MRC is the optimum linear combining technique [48]. With MRC, the signal received at each antenna element is weighted by the corresponding complex conjugate of the channel coefficient. The effect of this multiplication is to compensate for the phase shift in the channel and to weight the signal by a factor that is proportional to the signal strength. With cochannel interference, MRC helps combat the desired signal fading, however, it ignores the cochannel interference.

The MRC weight vector is [40]

$$\mathbf{w} = \sqrt{P_s}\mathbf{c}. \tag{3.2}$$

The signal-to-interference ratio at the output of the maximal ratio combiner is

$$\begin{aligned} \rho &= \frac{\mathbf{w}^H \mathbf{R}_s \mathbf{w}}{\mathbf{w}^H \mathbf{R} \mathbf{w}} \\ &= \frac{\mathbf{c}^H \mathbf{R}_s \mathbf{c}}{\mathbf{c}^H \mathbf{R} \mathbf{c}}, \end{aligned} \tag{3.3}$$

where $\mathbf{R}_s$ and $\mathbf{R}$ are the covariance matrices of the desired signal and interferences, respectively. The superscript $\{H\}$ stands for transpose complex conjugate. The covariance matrices are defined as

$$\mathbf{R}_s = P_s \mathrm{E}\left[\mathbf{c}\mathbf{c}^H\right] = P_s \mathbf{c}\mathbf{c}^H, \ \mathbf{R} = P \sum_{k=1}^{L} \mathrm{E}\left[\mathbf{c}_k \mathbf{c}_k^H\right] = P \sum_{k=1}^{L} \mathbf{c}_k \mathbf{c}_k^H, \tag{3.4}$$

where E denotes expectation. The expected value operation in eq. (3.4) is taken over the time interval during which $\mathbf{c}$ and $\mathbf{c}_k$ are considered constant (at least one signaling interval).

3.1.1 Distribution of SIR ρ

Equation (3.3) can be rewritten as

$$\begin{aligned}
\rho &= \frac{P_s}{P}\frac{\mathbf{c}^H\mathbf{c}\mathbf{c}^H\mathbf{c}}{\sum_{k=1}^{L}\mathbf{c}^H\mathbf{c}_k\mathbf{c}_k^H\mathbf{c}} \\
&= \frac{P_s}{P}\frac{\| \mathbf{c} \|^2}{\sum_{k=1}^{L}\frac{\mathbf{c}^H\mathbf{c}_k\mathbf{c}_k^H\mathbf{c}}{\|\mathbf{c}\|^2}} \\
&= \frac{P_s}{P}\frac{\| \mathbf{c} \|^2}{\sum_{k=1}^{L}\frac{\mathbf{c}^H\mathbf{c}_k}{\|\mathbf{c}\|}\frac{\mathbf{c}_k^H\mathbf{c}}{\|\mathbf{c}\|}} \\
&= \frac{P_s}{P}\frac{\| \mathbf{c} \|^2}{\sum_{k=1}^{L} b_k b_k^*},
\end{aligned} \tag{3.5}$$

where $\| \cdot \|$ and $*$ denote the Euclidean norm (length) of a vector and complex conjugate, respectively. The quantity $b_k = \frac{\mathbf{c}^H\mathbf{c}_k}{\|\mathbf{c}\|}$. Since the elements of $\mathbf{c}_k$ are iid complex Gaussian with zero mean and σ^2 variance, the distribution of b_k for a given $\mathbf{c}$, is also complex Gaussian. The mean and the variance of the random variable b_k conditioned on $\mathbf{c}$ are

$$\mathrm{E}\left[b_k\right] = \frac{\mathbf{c}^H}{\| \mathbf{c} \|}\mathrm{E}\left[\mathbf{c}_k\right] = 0, \tag{3.6}$$

and

$$\begin{aligned}
\mathrm{E}\left[\mid b_k \mid^2\right] &= \frac{\mathbf{c}^H\mathrm{E}\left[\mathbf{c}_k\mathbf{c}_k^H\right]\mathbf{c}}{\| \mathbf{c} \|^2} \\
&= \sigma^2\frac{\mathbf{c}^H\mathbf{I}_N\mathbf{c}}{\| \mathbf{c} \|^2} \\
&= \sigma^2,
\end{aligned} \tag{3.7}$$

respectively, where $\mathbf{I}_N$ is the identity matrix of dimension N. Hence, each of b_k is complex Gaussian with zero mean and variance σ^2, and is distributed independently of $\mathbf{c}$.

Equation (3.5) can be written as

$$\begin{aligned}\rho &= \frac{P_s}{P}\frac{\| \mathbf{c} \|^2}{\sum_{k=1}^{L} | b_k |^2} \\ &= \frac{P_s}{P}\frac{\sum_{j=1}^{N} | f_j |^2}{\sum_{k=1}^{L} | b_k |^2} \\ &= \frac{P_s}{P}\zeta, \end{aligned} \tag{3.8}$$

where $\mathbf{c}^T = [f_1, \ldots, f_N]$ is the desired user's channel propagation vector and the superscript $\{T\}$ denotes transpose. Since each of f_j and b_k are complex Gaussian random variables, each of $| f_j |^2$ and $| b_k |^2$ are chi-square random variables with two degrees of freedom (DOF). The quantity

$$\zeta = \frac{\sum_{j=1}^{N} | f_j |^2}{\sum_{k=1}^{L} | b_k |^2}, \tag{3.9}$$

can be recognized as the ratio of two independent chi-squared random variables, the numerator with $2N$ DOF and the denominator with $2L$ DOF. The distribution of ζ is therefore given by [49]

$$f_\zeta(\zeta) = \frac{\Gamma(L+N)}{\Gamma(L)\Gamma(N)}\frac{\zeta^{N-1}}{(1+\zeta)^{L+N}}, \qquad \zeta \geq 0,\ N \geq 1,\ L \geq 1, \tag{3.10}$$

where $\Gamma(\cdot)$ is the standard gamma function. The PDF in eq. (3.10) is a modified form of the central F distribution. The word 'modified' refers to the fact that the ratio of two independent chi-squared random variables divided by their respective DOF has a central F distribution. By using the transformation $\rho = \frac{P_s}{P}\zeta$, the PDF of the SIR ρ can easily be obtained and is

$$f_\rho(\rho) = \frac{\Gamma(L+N)}{\Gamma(L)\Gamma(N)}\left(\frac{P_s}{P}\right)^L \frac{\rho^{N-1}}{\left(\frac{P_s}{P}+\rho\right)^{L+N}}, \qquad \rho \geq 0,\ N \geq 1,\ L \geq 1. \tag{3.11}$$

The mean value of ρ can now be calculated [45]:

$$\begin{aligned}\bar{\rho} &= \mathrm{E}[\rho] \\ &= \frac{\Gamma(L+N)}{\Gamma(L)\Gamma(N)}\left(\frac{P_s}{P}\right)^L \int_0^\infty \frac{\rho^N}{\left(\frac{P_s}{P}+\rho\right)^{L+N}} \\ &= \frac{N}{L-1}\frac{P_s}{P}. \end{aligned} \tag{3.12}$$

3.1.2 Outage Probability of the Maximal Ratio Combiner

Probability of outage is an important statistical measure in the design of cellular mobile radio systems which operate in a fading environment with multiple interferers [50]. It represents the probability of unsatisfactory reception over the intended coverage area. A system planner can use outage probability calculations to assess the effects of various system configurations on the quality of service provided by the system. The outage probability is defined as the probability of failing to achieve a SIR sufficient to give satisfactory radio reception [51] and is expressed as

$$\begin{aligned} P_o &= \text{Probability}\left[\rho < \rho_p\right] \\ &= \int_0^{\rho_p} f_\rho(\rho) d\rho \\ &= \frac{\Gamma(L+N)}{\Gamma(L)\Gamma(N)} \left(\frac{P_s}{P}\right)^L \int_0^{\rho_p} \frac{\rho^{N-1}}{(\frac{P_s}{P}+\rho)^{L+N}} d\rho, \end{aligned} \tag{3.13}$$

where ρ_p is the SIR protection ratio which depends on the modulation technique used and performance desired [52]. Equation (3.13) can be evaluated in closed-form [53] and is

$$P_o = \frac{\Gamma(L+N)}{\Gamma(L)\Gamma(N+1)} \left(\frac{\rho_p P}{P_s}\right)^N {}_2F_1\left(L+N, N; N+1; -\frac{\rho_p P}{P_s}\right), \tag{3.14}$$

where ${}_2F_1\left(a, b; c; x\right)$ is the hypergeometric function defined as [42]

$${}_2F_1\left(a, b; c; x\right) = \sum_{n=0}^{\infty} \frac{(a)_n (b)_n}{(c)_n} \frac{x^n}{n!}. \tag{3.15}$$

The notation $(\cdot)_n$ is called the Pochhammer symbol and is defined as $(a)_n = \frac{\Gamma(a+n)}{\Gamma(a)}$.

3.1.3 BER of the Maximal Ratio Combiner

As mentioned earlier, subsequent to Rayleigh fading, the in-phase and quadrature components of each of the received signals have a Gaussian distribution. That is, $\sqrt{P}\mathbf{c}_k s_k(t)$, $k = 1, \ldots, L$, has a complex Gaussian distribution. The sum of the interference is also complex Gaussian. Since the maximal ratio combiner is a linear filter, the sum of the interference at the output of the maximal ratio combiner (antenna

array) is also complex Gaussian. Thus, the conditional probability of bit error (BER), i.e., the BER computed for a given value of ρ, is simply

$$P_{e|\rho} = \mathrm{Q}(\sqrt{2\rho}) = \frac{1}{2}\mathrm{erfc}(\sqrt{\rho}), \tag{3.16}$$

where $\mathrm{Q}(\cdot)$ is the area under the tail of the Gaussian probability density function and is defined as

$$\mathrm{Q}(x) = \frac{1}{\sqrt{2\pi}} \int_x^\infty e^{-t^2/2}\, dt, \tag{3.17}$$

$\mathrm{erfc}(\cdot)$ is the complementary error function and is defined as

$$\mathrm{erfc}(x) = \frac{2}{\sqrt{\pi}} \int_x^\infty e^{-t^2}\, dt. \tag{3.18}$$

The unconditional BER, i.e., the one averaged over all the values of ρ is

$$\begin{aligned} P_e &= \frac{1}{2}\int_0^\infty \mathrm{erfc}(\sqrt{\rho}) f_\rho(\rho) d\rho \\ &= \frac{1}{2}\frac{\Gamma(L+N)}{\Gamma(L)\Gamma(N)}\left(\frac{P_s}{P}\right)^L \int_0^\infty \mathrm{erfc}(\sqrt{\rho}) \frac{\rho^{N-1}}{(\frac{P_s}{P}+\rho)^{L+N}} d\rho. \end{aligned} \tag{3.19}$$

As shown in the Appendix A, eq. (3.19) can be evaluated as

$$\begin{aligned} P_e \;=\; & \frac{1}{2\sqrt{\pi}\Gamma(L)\Gamma(N)} \left[\left(\frac{P_s}{P}\right)^L \frac{\Gamma(\frac{1}{2}-L)\Gamma(L+N)}{(-L)} \right. \\ & {}_2F_2\left(L+N, L; L+\frac{1}{2}, L+1; \frac{P_s}{P}\right) + \left(\frac{P_s}{P}\right)^{\frac{1}{2}} \frac{\Gamma(L-\frac{1}{2})}{\Gamma(\frac{1}{2})} \\ & \left. \Gamma(-\frac{1}{2})\Gamma(N+\frac{1}{2}) {}_2F_2\left(N+\frac{1}{2}, \frac{1}{2}; \frac{3}{2}-L, \frac{3}{2}; \frac{P_s}{P}\right) + \frac{\Gamma(L)\Gamma(\frac{1}{2})\Gamma(N)}{\Gamma(1)} \right] \end{aligned} \tag{3.20}$$

where ${}_pF_q(\cdot)$ is the generalized hypergeometric series and is defined as [42]

$${}_pF_q\left(a_1, \ldots, a_p; b_1, \ldots, b_q; x\right) = \sum_{n=0}^{\infty} \frac{(a_1)_n \cdots (a_p)_n}{(b_1)_n \cdots (b_q)_n} \frac{x^n}{n!}. \tag{3.21}$$

Equation (3.20) can be easily evaluated using software packages such as Maple, Mathematica, etc. Alternatively, eq. (3.19) can be evaluated numerically.

3.2 Optimum Combining

Let $\mathbf{R} = P\mathbf{R}_1$, where $\mathbf{R}_1 = \sum_{k=1}^{L} \mathbf{c}_k \mathbf{c}_k^H$. The interference covariance matrix $\mathbf{R}$ is defined in eq. (3.4). Each of $\mathbf{c}_k, k = 1, \ldots, L$, is an iid complex Gaussian vector with the same mean vector $\{\mathrm{E}[\mathbf{c}_k] = \mathbf{0}\}$ and the same covariance matrix $\left\{\mathbf{\Sigma} = \mathrm{E}\left[\mathbf{c}_k \mathbf{c}_k^H\right]\right\}$. The same parameters hold for $\mathbf{c}$. By definition, $\mathbf{\Sigma}$ is positive semidefinite and Hermitian. By assumption, it will be positive definite, hence, its inverse exists. When independent fading at each antenna element is assumed and $\sigma^2 = 1$, $\mathbf{\Sigma} = \mathbf{I}_N$, where $\mathbf{I}_N$ is an identity matrix of dimension N. When $\mathbf{\Sigma} > 0$, i.e. positive definite, and $L \geq N$, the matrix $\mathbf{R}_1$ (or $\mathbf{R}$) is positive definite with probability one [54]. Thus, $\mathbf{R}^{-1}$ exists in eq. (2.3). In multivariate statistics, the matrix $\mathbf{R}_1$ (apart from a constant factor) is known as the sample Hermitian covariance matrix [55].

The PDF of $\mathbf{R}_1$, i.e., the joint distribution of its distinct elements is [56]

$$f_{\mathbf{R}_1}(\mathbf{R}_1) = \begin{cases} \frac{|\mathbf{R}_1|^{L-N} |\mathbf{\Sigma}|^{-L} e^{-tr\left(\mathbf{\Sigma}^{-1}\mathbf{R}_1\right)}}{\tilde{\Gamma}_N(L)} & \mathbf{R}_1 > 0,\ \mathbf{\Sigma} > 0 \\ 0 & \text{otherwise,} \end{cases} \tag{3.22}$$

where $|\cdot|$ and $tr(\cdot)$ denote determinant and trace of a matrix, respectively. The complex multivariate gamma function

$$\tilde{\Gamma}_N(L) = \pi^{\frac{N(N-1)}{2}} \prod_{i=i}^{N} \Gamma(L - i + 1), \tag{3.23}$$

where $\Gamma(\cdot)$ is the standard gamma function. The distribution in eq. (3.22) is called the complex Wishart distribution with parameter $\mathbf{\Sigma}$ and L DOF. It is denoted as $CW_N(\mathbf{\Sigma}, L)$. The Wishart distribution is the multivariate generalization of the chi-square distribution [57]. When $N = 1$, $\mathbf{\Sigma} = \sigma^2$ and $\mathbf{R}_1$ is a scalar, the distribution in eq. (3.22), indeed, degenerates to a chi-square distribution with $2L$ DOF [40]. The PDF of $\mathbf{R}$ can be obtained by the transformation of the PDF given in eq. (3.22).

3.2.1 Distribution of the Maximum SIR μ

Using eq. (2.3), the maximum SIR at the array output can be computed [14]:

$$\begin{aligned} \mu &= P_s \mathbf{c}^H \mathbf{R}^{-1} \mathbf{c} \\ &= \frac{P_s}{P} \mathbf{c}^H \mathbf{R}_1^{-1} \mathbf{c} \\ &= \frac{P_s}{P} \nu, \end{aligned} \tag{3.24}$$

where the real scalar quantity $\nu = \mathbf{c}^H \mathbf{R}_1^{-1} \mathbf{c}$. Since $\mathbf{c}$ is complex Gaussian with mean $\mathbf{0}$, and covariance matrix $\mathbf{\Sigma}$ and is distributed independently of $\mathbf{R}_1$ which is $CW_N(\mathbf{\Sigma}, L)$, the PDF of ν is [49, 58, 59]

$$f_\nu(\nu) = \frac{\Gamma(L+1)}{\Gamma(N)\Gamma(L+1-N)} \frac{\nu^{N-1}}{(1+\nu)^{L+1}} \qquad \nu \geq 0,\ 1 \leq N \leq L. \tag{3.25}$$

The distribution in eq. (3.25) is a modified form of the central F distribution. In multivariate statistics, when the elements of $\mathbf{c}_k$ are real Gaussian with zero mean, σ^2 variance and the elements of $\mathbf{c}$ are real Gaussian with arbitrary mean, σ^2 variance, then ν (apart from a constant) is known as Hotelling's T^2 statistics [57]. And when $\mathbf{c}$ and $\mathbf{c}_k$ have the same mean vector $\mathbf{0}$ and the same covariance matrix $\mathbf{\Sigma}$, the distribution of ν is known as the *Null* distribution of the Hotelling's T^2 statistics [60]. When $\mathbf{c}$ has a non-zero mean vector, the distribution of ν is known as the *Non-Null* distribution of the Hotelling's T^2 statistics.

By using the transformation $\mu = \frac{P_s}{P}\nu$, the PDF of μ can easily be obtained:

$$f_\mu(\mu) = \frac{\Gamma(L+1)}{\Gamma(N)\Gamma(L+1-N)} \left(\frac{P_s}{P}\right)^{L+1-N} \frac{\mu^{N-1}}{(\frac{P_s}{P}+\mu)^{L+1}} \qquad \mu \geq 0,\ 1 \leq N \leq L. \tag{3.26}$$

It is important to note that the PDF of μ (or ν) does not depend on the form of covariance matrix $\mathbf{\Sigma}$. Both ρ and μ have the same modified form of the central F distribution, but with DOF. Unlike the distribution in eq. (3.11) which is valid for any $L, N \geq 1$, the distribution is eq. (3.26) is only valid for $1 \leq N \leq L$.

The mean of the maximum SIR μ can now be calculated [45]:

$$\begin{aligned}\bar{\mu} &= \mathrm{E}[\mu] \\ &= \frac{\Gamma(L+1)}{\Gamma(N)\Gamma(L+1-N)}\left(\frac{P_s}{P}\right)^{L+1-N}\int_0^{\infty}\frac{\mu^N}{(\frac{P_s}{P}+\mu)^{L+1}} \\ &= \frac{N}{L-N}\frac{P_s}{P}. \end{aligned} \tag{3.27}$$

3.2.2 Outage Probability of the Optimum Combiner

The outage probability with optimum combining (OC) can be derived in a similar fashion as the one shown with MRC and is

$$\begin{aligned}P_o &= \text{Probability}[\mu < \mu_p] \\ &= \int_0^{\mu_p} f_\mu(\mu)d\mu \\ &= \frac{\Gamma(L+1)}{\Gamma(N)\Gamma(L+1-N)}\left(\frac{P_s}{P}\right)^{L+1-N}\int_0^{\mu_p}\frac{\mu^{N-1}}{(\frac{P_s}{P}+\mu)^{L+1}}d\mu, \end{aligned} \tag{3.28}$$

where μ_p is the SIR protection ratio. Equation (3.28) can be evaluated in closed-form [53] and is

$$P_o = \frac{\Gamma(L+1)}{\Gamma(N+1)\Gamma(L+1-N)}\left(\frac{\mu_p P}{P_s}\right)^N {}_2F_1\left(L+1, N; N+1; -\frac{\mu_p P}{P_s}\right), \tag{3.29}$$

where ${}_2F_1(a, b; c; x)$ is the hypergeometric function and is defined in eq. (3.15).

3.2.3 BER of the Optimum Combiner

In deriving the BER with OC, we follow a similar approach to the one shown with MRC. Since the optimum combiner is a linear filter, the conditional BER, i.e., the BER computed for a given value of μ, is simply

$$P_{e|\mu} = \mathrm{Q}(\sqrt{2\mu}) = \frac{1}{2}\mathrm{erfc}(\sqrt{\mu}). \tag{3.30}$$

The unconditional BER, i.e., the one averaged over all the values of μ is

$$\begin{aligned}P_e &= \frac{1}{2}\int_0^{\infty}\mathrm{erfc}(\sqrt{\mu})f_\mu(\mu)d\mu \\ &= \frac{1}{2}\frac{\Gamma(L+1)}{\Gamma(N)\Gamma(L+1-N)}\left(\frac{P_s}{P}\right)^{L+1-N}\int_0^{\infty}\mathrm{erfc}(\sqrt{\mu})\frac{\mu^{N-1}}{(\frac{P_s}{P}+\mu)^{L+1}}d\mu. \end{aligned} \tag{3.31}$$

As shown in the Appendix B, eq. (3.31) can be evaluated as

$$
\begin{aligned}
P_e = & \frac{1}{2\sqrt{\pi}\Gamma(N)\Gamma(L+1-N)}\left[\left(\frac{P_s}{P}\right)^{L+1-N}\frac{\Gamma(N-L-\frac{1}{2})\Gamma(L+1)}{(N-L-1)}\right. \\
& {}_2F_2\left(L+1, L+1-N; L-N+\frac{3}{2}, L-N+2; \frac{P_s}{P}\right) + \left(\frac{P_s}{P}\right)^{\frac{1}{2}}\frac{\Gamma(L-N+\frac{1}{2})}{\Gamma(\frac{1}{2})} \\
& \Gamma(-\frac{1}{2})\Gamma(N+\frac{1}{2}){}_2F_2\left(N+\frac{1}{2}, \frac{1}{2}; N-L+\frac{1}{2}, \frac{3}{2}; \frac{P_s}{P}\right) \\
& \left. + \frac{\Gamma(L+1-N)\Gamma(\frac{1}{2})\Gamma(N)}{\Gamma(1)}\right], \qquad (3.32)
\end{aligned}
$$

where ${}_pF_q(\cdot)$ is the generalized hypergeometric series and is defined in eq. (3.21).

3.3 Effect of Fading Correlation on the Optimum Combiner

In order to gain a significant advantage from the use of antenna diversity there must be a sufficient degree of statistical independence in the fading of the signals received at several antenna elements [61]. In previous sections, we had assumed independent fading of the desired signal and interfering signals at each receive antenna element. In this section, we investigate the effect of fading correlation on the performance of the optimum combiner. We assume that the multipath reflections are uniformly distributed around the receive antenna elements.

Let the complex Gaussian channel coefficient $c_n = x_n + iy_n$, $n = 1, \ldots, N$, where x_n and y_n are the real and the imaginary parts, respectively. Both x_n and y_n have Gaussian distribution. The following relations hold:

$$
\begin{aligned}
& \mathrm{E}[x_n] = \mathrm{E}[y_n] = 0, \\
& \mathrm{E}[x_n^2] = \mathrm{E}[y_n^2] = \frac{1}{2}\mathrm{E}[|\, c_n \,|^2] = \frac{1}{2}\sigma^2, \\
& \mathrm{E}[x_m x_n] = \mathrm{E}[y_m y_n], \\
& \mathrm{E}[x_m y_n] = -\mathrm{E}[x_n y_m], \\
& \mathrm{E}[x_n y_n] = 0, \\
& \mathrm{E}[c_n c_m] = 0, \qquad (3.33)
\end{aligned}
$$

where $m, n = 1, \ldots, N$. From the above relations and the assumption that the multipath reflections are uniformly distributed around the receive antenna elements, the covariance matrix $\mathbf{\Sigma}$ has a special form [48, 37]:

$$\mathbf{\Sigma} = \sigma^2 \begin{bmatrix} 1 & \mathrm{J}_0(\beta) & \mathrm{J}_0(2\beta) & \ldots & \mathrm{J}_0((N-1)\beta) \\ \mathrm{J}_0(\beta) & 1 & \mathrm{J}_0(\beta) & \ldots & \mathrm{J}_0((N-2)\beta) \\ \mathrm{J}_0(2\beta) & \mathrm{J}_0(\beta) & 1 & \ldots & \mathrm{J}_0((N-3)\beta) \\ \vdots & \vdots & \vdots & \vdots & \vdots \\ \mathrm{J}_0((N-1)\beta) & \mathrm{J}_0((N-2)\beta) & \mathrm{J}_0((N-3)\beta) & \ldots & 1 \end{bmatrix}, \tag{3.34}$$

where $\mathrm{J}_0(\cdot)$ is the Bessel function of the first kind of order zero and $\beta = \frac{2\pi d}{\lambda}$. The spacing between the antenna elements is d and λ is the wavelength. It is clear from eq. (3.34) that the covariance matrix $\mathbf{\Sigma}$ is a function of the antenna element spacing d.

The important point to note is that in developing the expression of the PDF of μ, the assumption made was that the channel vectors $\mathbf{c}$, $\mathbf{c}_k$ have the same covariance matrix $\mathbf{\Sigma}$. No further assumptions on the form of $\mathbf{\Sigma}$ were necessary in obtaining the result in eq. (3.26). The implication of the independence of the PDF of μ from the specific form of $\mathbf{\Sigma}$ is that regardless of the antenna element spacing d, in this special case of non-independent fading, the performance of the optimum combiner is unaffected. This result is very significant. Usually, there is no direct line-of-sight (LOS) path present between the user and the base station. Therefore, the multipath reflections are uniformly distributed in the vicinity of the user. The above result makes OC possible even on a tiny portable unit without degradation in the performance.

The above result can be explained in a different manner as well. In the previous chapter, we showed that interference cancellation entails a loss of DOF, with a corresponding loss in the diversity performance. With $L \geq N$, all degrees of diversity are captured by interference. In effect, diversity is not playing a role. Hence, the spacing between the antenna elements becomes irrelevant. It is important to note that in

reaching the above conclusion, we have not considered the effects of mutual coupling between antenna elements.

3.4 Discussion of Results

In this section the results on the performance of MRC and OC studied in the previous sections are presented. We evaluate the system performance for the worst case scenario only, i.e., the mobile transmitting the desired signal is at the point in the cell farthest from the base station, and the interfering mobiles in the surrounding cells are as close as possible to the base station of the desired mobile. Furthermore, we consider only the six strongest interferers ($L = 6$), i.e., interferers from the first tier of cochannel cells. This is a reasonable assumption as the interference from the second tier of cochannel cells is much less than the first tier [62]. The variance σ^2 of the channel coefficients was assumed 1. The value of $\frac{P_s}{P}$ corresponding to the worst case scenario is determined from the given frequency reuse pattern. For a given frequency reuse pattern, there is a corresponding carrier-to-interference ratio (CIR). The relation between the CIR and the frequency reuse factor, for six equidistant cochannel interferers and a path loss exponent of four, is [3]

$$\begin{aligned} \text{CIR} &= \frac{a^4}{6} \\ &= \frac{(\sqrt{3\text{F}})^4}{6}, \end{aligned} \tag{3.35}$$

where a is the cochannel interference reduction factor and F is the frequency reuse factor. Table 3.1 summarizes the relation in eq. (3.35).

In Figures 3.1 and 3.2, the cumulative distribution function and the probability density function {eqs. (3.11), (3.26)} of array output SIR are plotted, respectively, with the number of antenna elements N as the parameter. These curves clearly show that SIR has a better chance to be high with an increase in the order of diversity N regardless of the combining method. Note that OC significantly decreases the value of

the cumulative distribution function, i.e., significantly increases the chances of higher SIR values, as compared to MRC. For $N = 1$, both MRC and OC provide identical results, as expected. This can be verified by plugging in $N = 1$ in equations (3.11) and (3.26). In Figure 3.3, the PDFs obtained by both the theory and Monte Carlo simulations are compared. They show a very good match.

In Figure 3.4, the mean SIRs {eqs. (3.12), (3.27)} are plotted as a function of the number of antenna elements N with frequency reuse factor F (or $\frac{P_s}{P}$) as the parameter. Optimum combining provides larger values of mean SIR as compared to MRC. The difference in the mean SIRs increases with an increase in N and F.

In Figure 3.5, the outage probability {eqs. (3.14), (3.29)} is shown as a function of the number of antenna elements N with frequency reuse factor F (or $\frac{P_s}{P}$) as the parameter. Clearly, the outage probability decreases with the increase in N for any F. Optimum combining shows a large decrease in the outage probability with respect to MRC. For an outage probability of 10^{-3} and corresponding BER of 10^{-6}, OC with $N = 6$ increases the system capacity by a factor of $\frac{7}{3}$. Figure 3.6 shows the probability of outage versus $\frac{P_s}{P}$ with N as the parameter. For a given $\frac{P_s}{P}$, OC decreases the outage probability as compared to MRC and this decrease becomes even greater as N increases. For a given outage probability, increasing N reduces the required $\frac{P_s}{P}$, subsequently increasing the number of users.

Figure 3.7 shows the BER performance {eqs. (3.20), (3.32)} for the worst case scenario versus the number of antenna elements N with frequency reuse factor F (or $\frac{P_s}{P}$) as the parameter. There is a significant (as large as two orders of magnitude) improvement in the performance (decrease in BER) of the optimum combiner as compared to the maximal ratio combiner. For a BER of 10^{-3} and $N = 3$, OC makes the frequency reuse factor F = 3 possible even for the worst case scenario. This corresponds to more than doubling of the system capacity. In Figure 3.8, the BER is plotted versus $\frac{P_s}{P}$ with N as the parameter. Again, for a given BER, increasing N

Table 3.1 Relation between F, CIR and $\frac{P_s}{P}$ in a Macrocellular System.

Frequency Reuse Factor F	CIR (dB) (Average Scenario)	CIR (dB) (Worst Scenario)	$\frac{P_s}{P}$ (Worst Scenario)
1	1.8	-7.8	1.0
3	11.3	4.3	16.15
4	13.8	7.9	37.0
7	18.7	14.4	165.25

reduces the required $\frac{P_s}{P}$, which in turn, leads to an increase in the system capacity. A further increase in the capacity is possible with OC. For example, for a BER of 10^{-3} and $N = 6$, OC requires 6 dB less $\frac{P_s}{P}$ than MRC.

Figure 3.9 shows the improvement, due to OC, versus the number of antenna elements N. The improvement is defined as the reduction in the required $\frac{P_s}{P}$, for a given BER, with OC as compared to MRC. For a given BER, the improvement with OC increases with increase in N.

In Figure 3.10, the improvement is plotted versus the average probability of bit error with N as the parameter. Again, the improvement increases with corresponding increase in N. Also, for a given N, the improvement increases with the decrease in the BER.

Figure 3.11 shows the diversity gain versus the number of antenna elements N. The diversity gain is defined as the reduction in the required $\frac{P_s}{P}$, for a given BER, with a corresponding increase in N. Optimum combining provides higher diversity gain than MRC and this difference in gain increases with N.

In a typical system, with shadow fading, randomly-located users, and less than 100% loading; there are only a few dominant interferers. This implies that gains with OC can be even larger than the ones shown here in this dissertation.

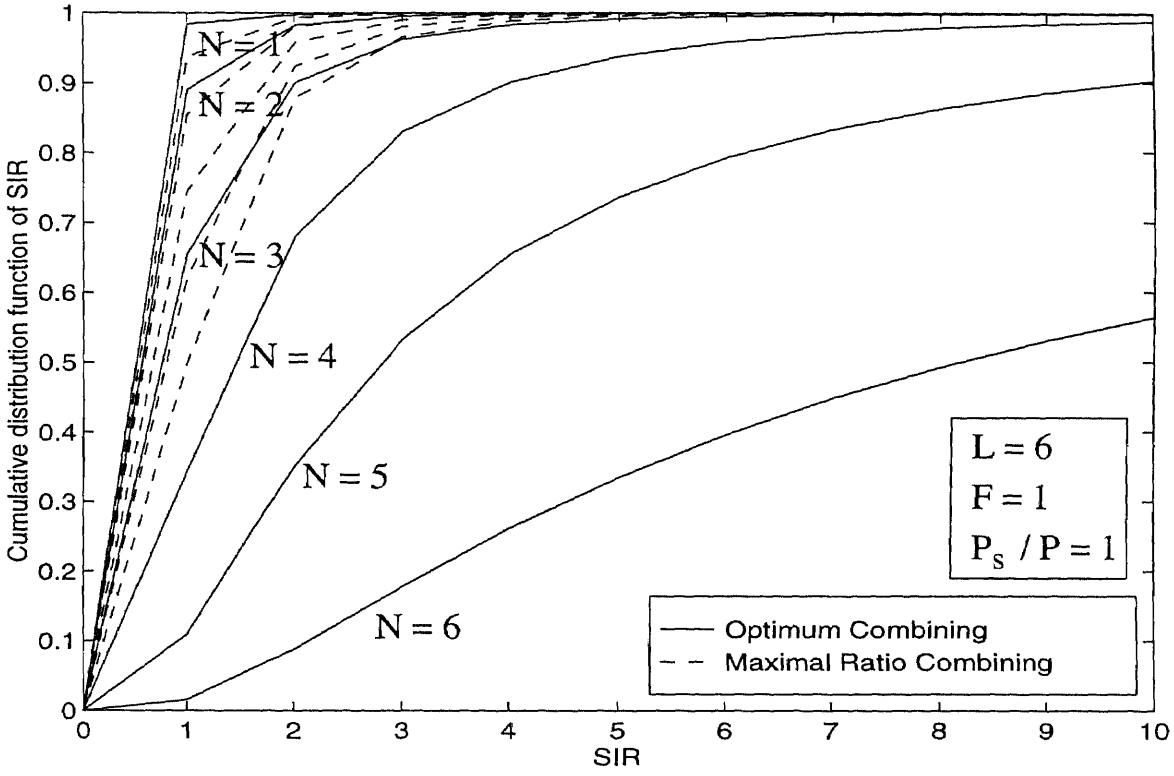

Figure 3.1 The effect of antenna diversity on the cumulative distribution function of SIR.

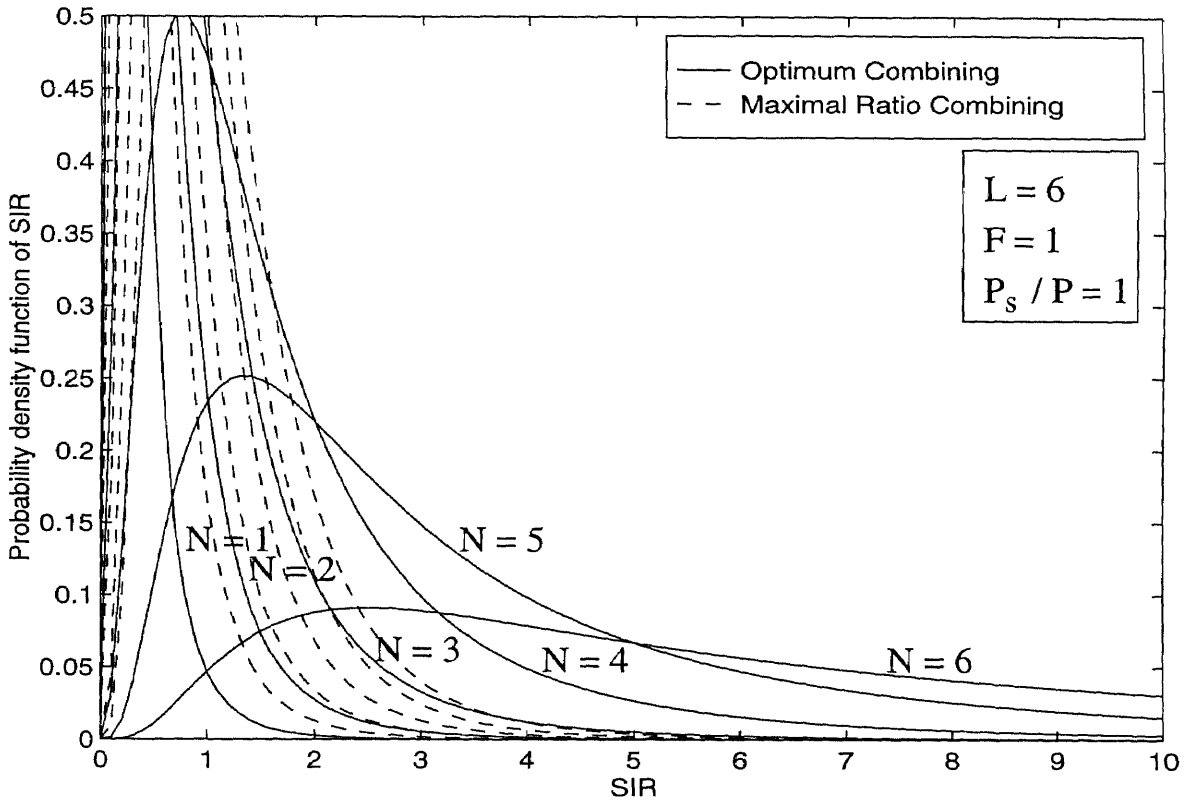

Figure 3.2 The effect of antenna diversity on the probability density function of SIR.

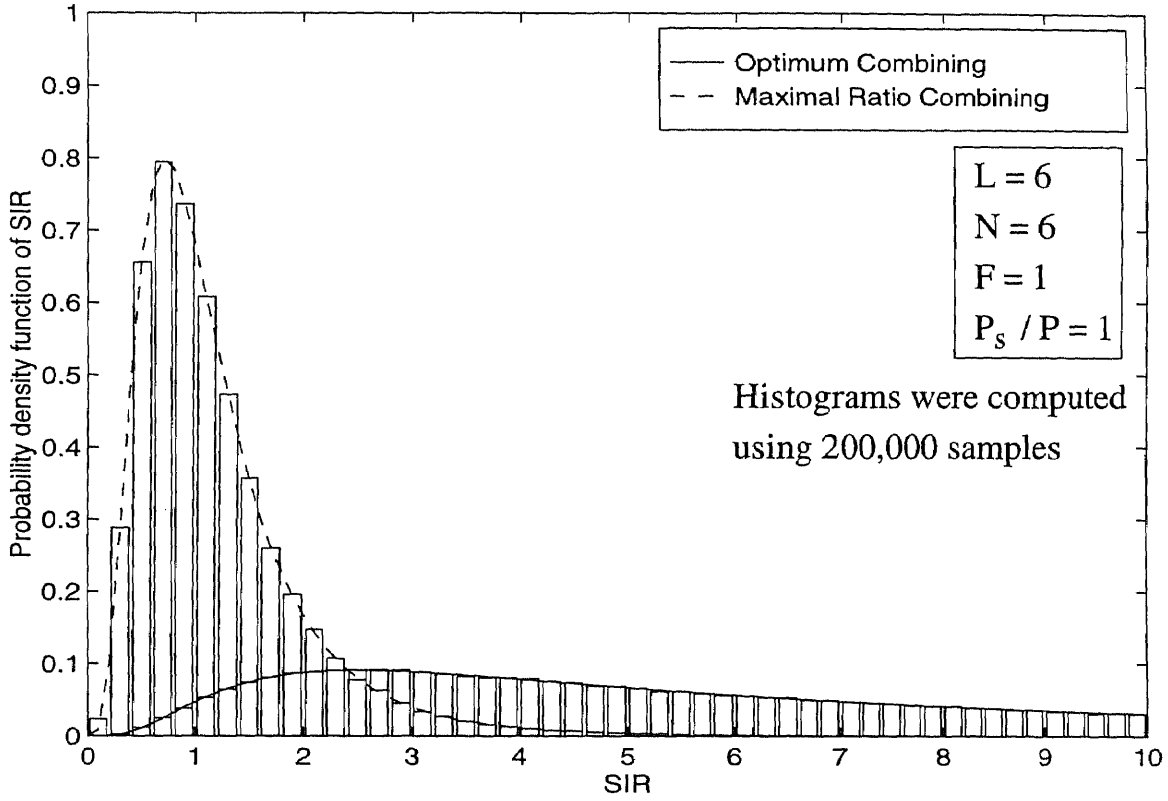

Figure 3.3 A comparison of the probability density functions using theory and simulation.

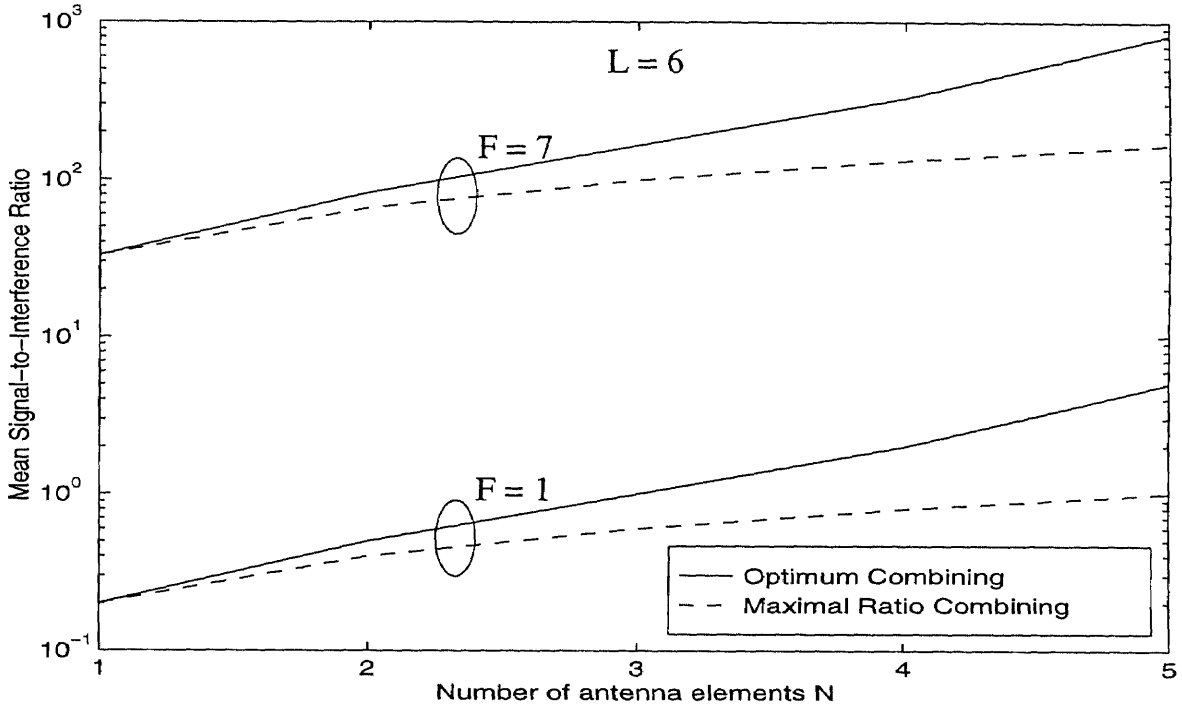

Figure 3.4 Mean SIR at the output of the antenna array versus the order of diversity N with Frequency reuse factor F as the parameter.

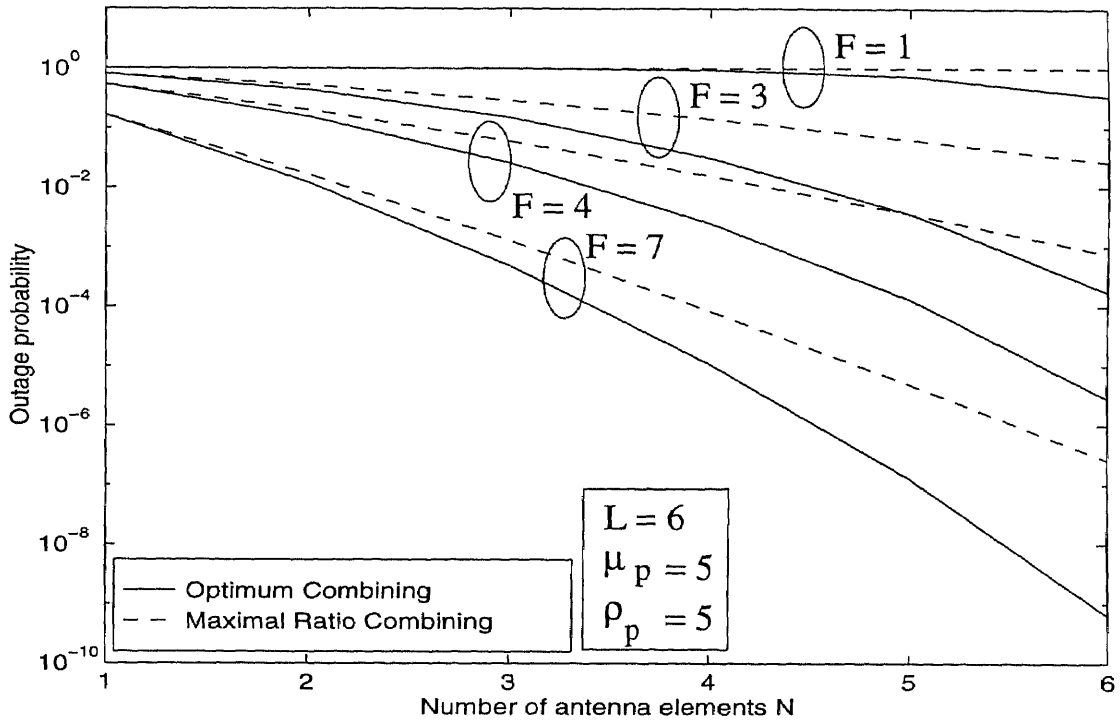

Figure 3.5 The outage probability versus the order of diversity N with Frequency reuse factor F as the parameter.

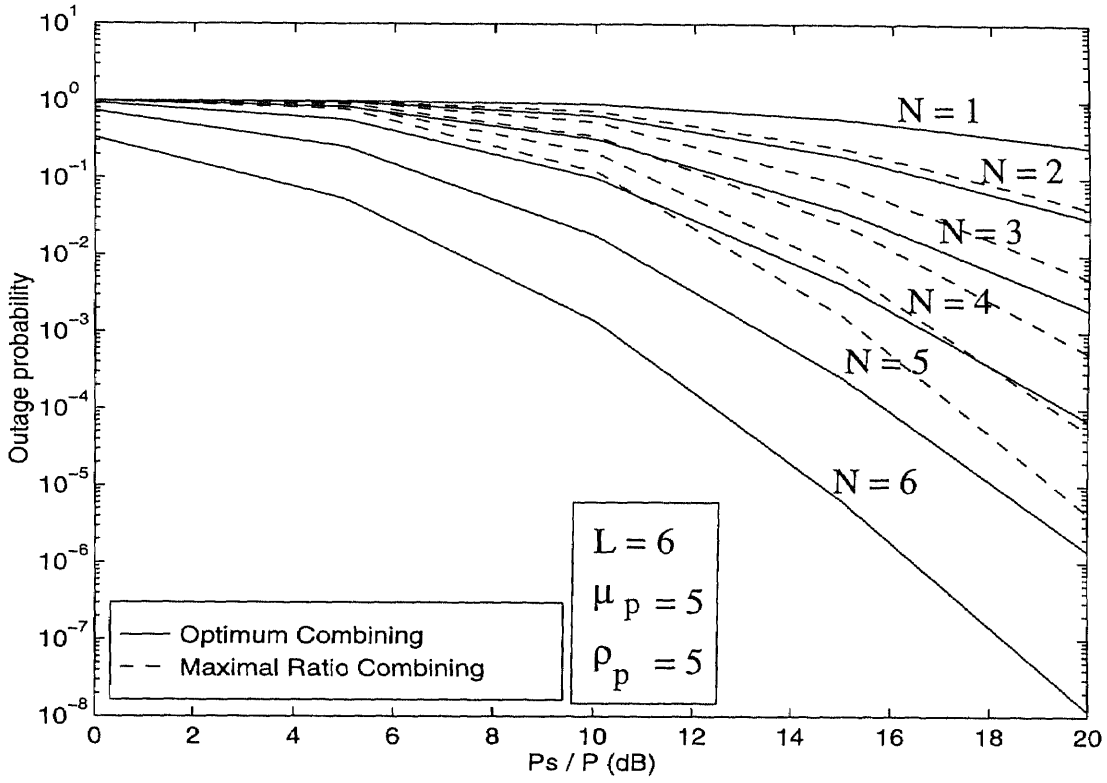

Figure 3.6 The outage probability versus $\frac{P_s}{P}$ with the order of diversity N as the parameter.

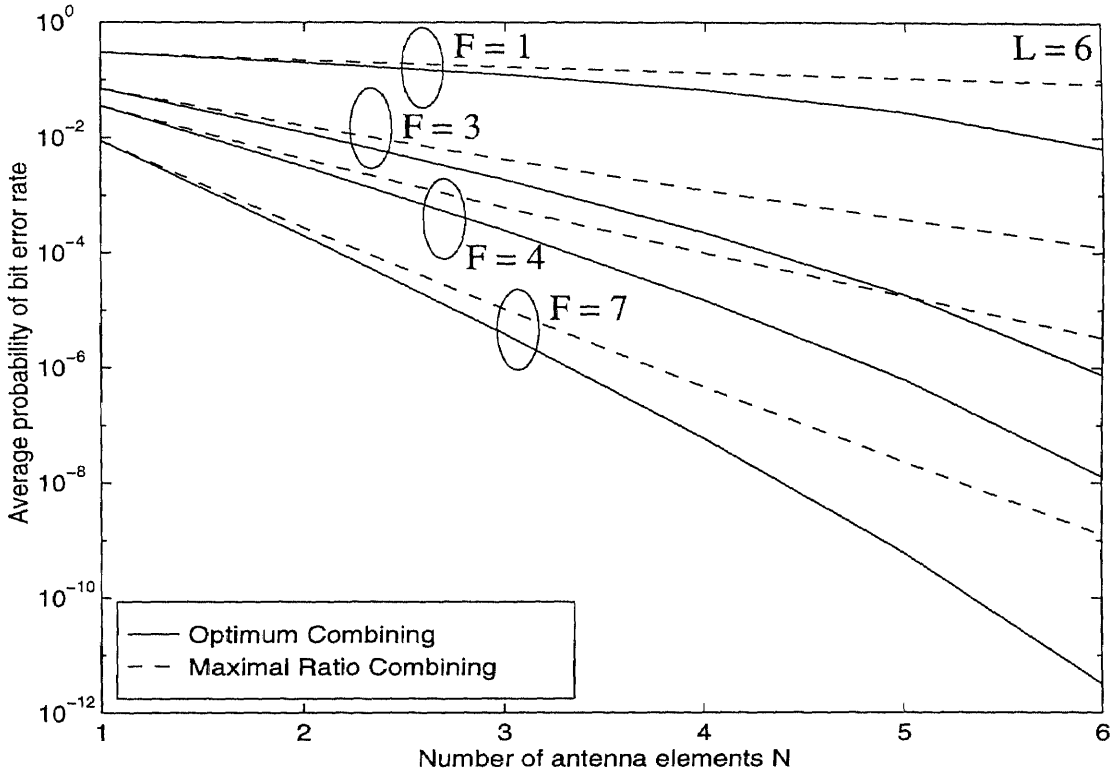

Figure 3.7 The average probability of bit error versus the order of diversity N with frequency reuse factor F as the parameter.

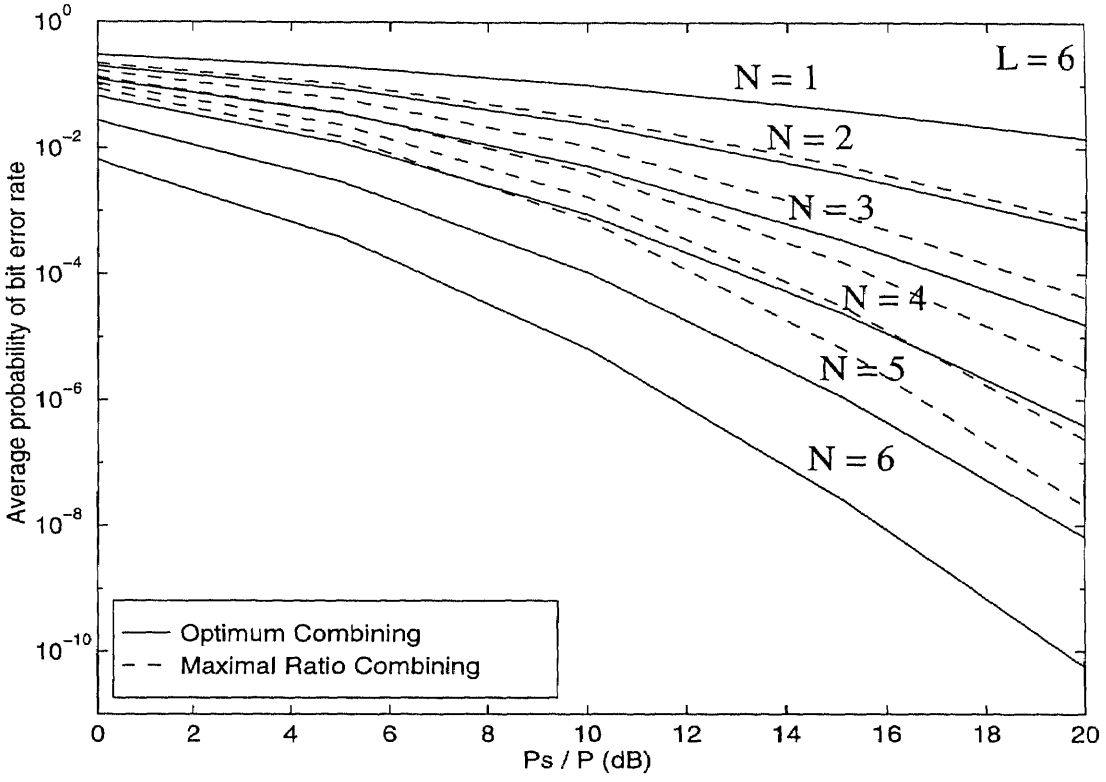

Figure 3.8 The average probability of bit error versus $\frac{P_s}{P}$ with the order of diversity N as the parameter.

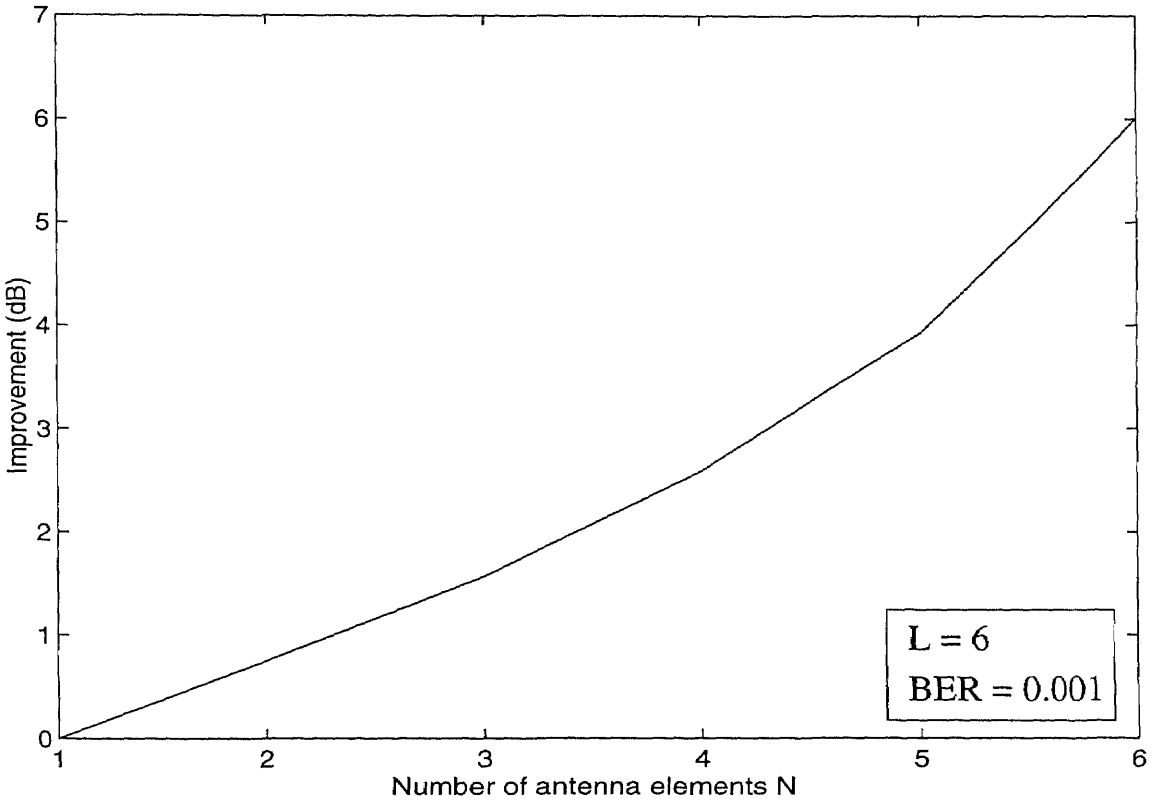

Figure 3.9 The improvement due to optimum combining versus the number of antenna elements N.

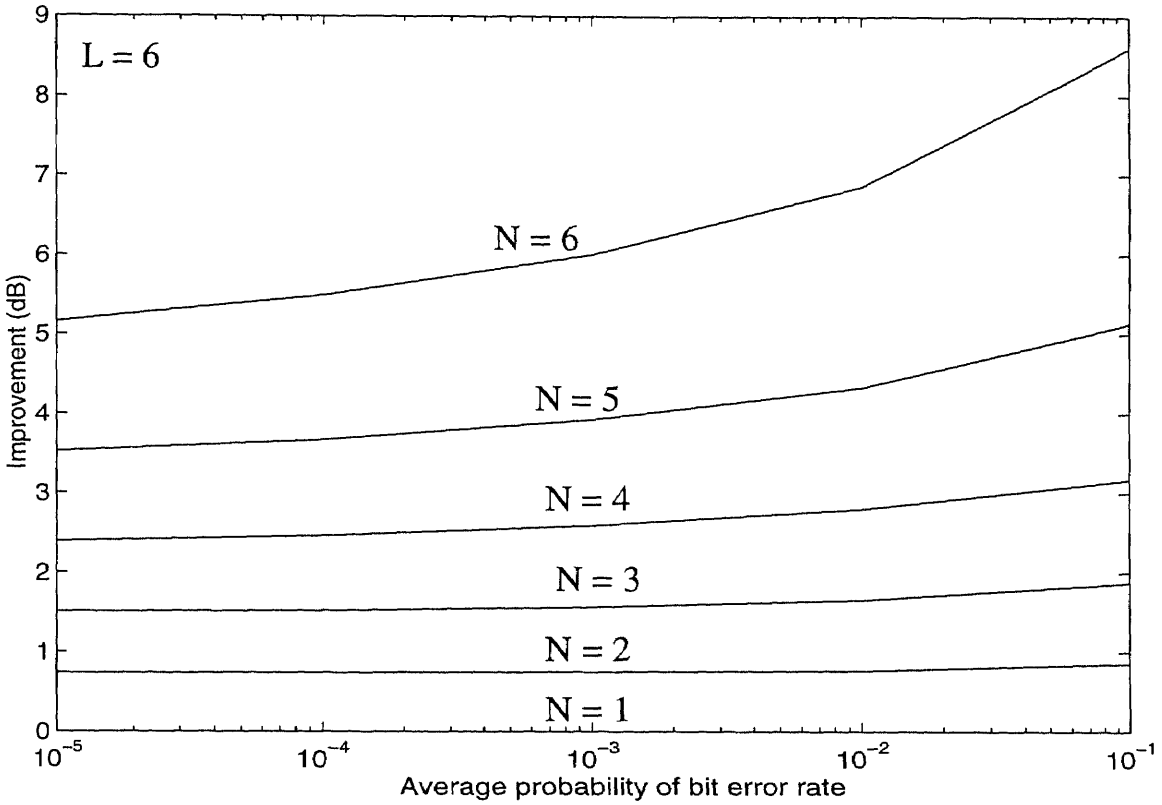

Figure 3.10 The improvement due to optimum combining versus the average probability of bit error.

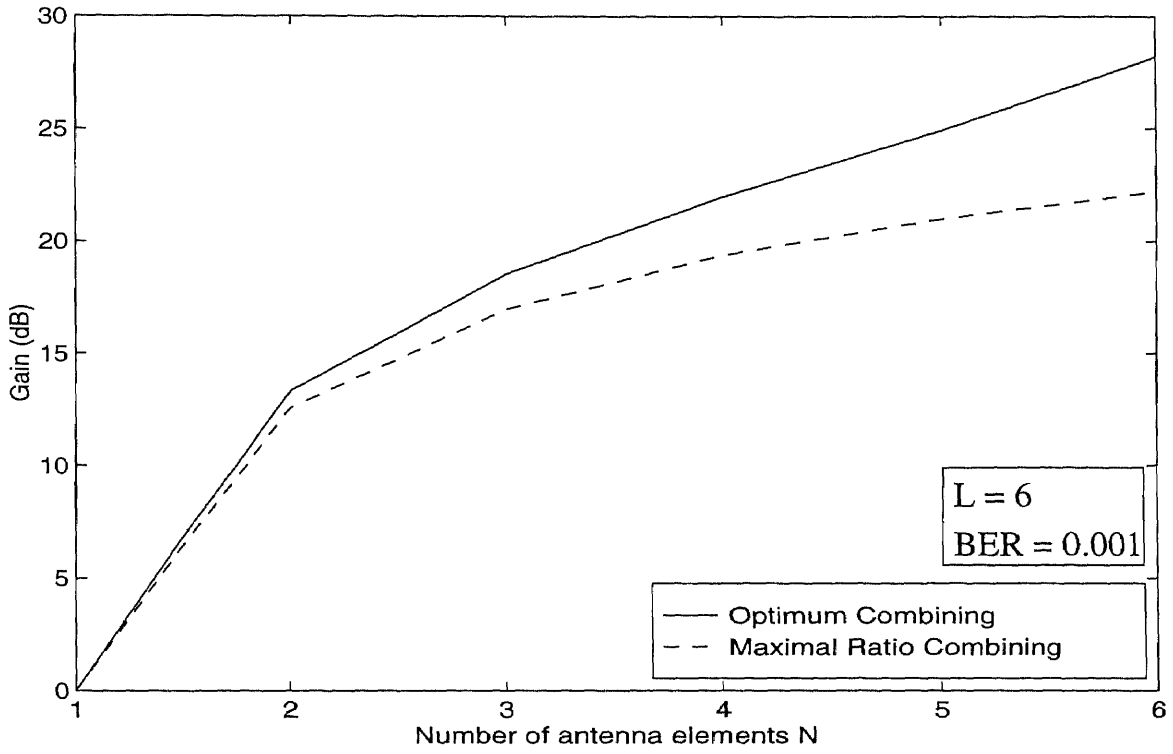

Figure 3.11 The diversity gain versus the number of antenna elements N.

CHAPTER 4

DIVERSITY COMBINING FOR DIGITAL MICROCELLULAR MOBILE RADIO COMMUNICATION SYSTEMS

In chapter 3, the performance of optimal combining (OC) and maximal ratio combining (MRC) was investigated for a macrocellular environment. That is, both the desired signal and cochannel interferers were assumed to be subject to Rayleigh fading. This is a reasonable assumption for medium to large cell systems. For microcellular systems, however, the validity of this assumption is in question. The key point in microcell interference modeling is that the desired and undesired signals should have different statistical characteristics [63]. One such interference model is Rician/Rayleigh model [63, 64]. The desired signal is assumed to have Rician statistics implying that a dominant multipath reflection or a line-of-sight (LOS) propagation exists within a cell. The interfering signals from cochannel cells are assumed to be subject to Rayleigh fading because of the absence of a LOS propagation.

In microcellular systems, due to small cell size, the path loss exponent can be as low as 2 (compared to the path loss exponent of 4 usually assumed in a macrocellular environment). This substantially reduces the received mean carrier-to-interference ratio (CIR). Therefore, the use of antenna arrays could be even more beneficial in a microcellular environment.

In this chapter, we derive expressions for the probability density function (PDF) of signal-to-interference ratio (SIR) at the output of the optimum combiner, the outage probability and the average probability of bit error rate (BER), under the Rician/Rayleigh model. We consider L ($L \geq N$) equal power cochannel interferers and N antenna elements. We also study MRC and derive similar expressions. The study is extended to the special case of the Rician/Rayleigh model, the Nonfading/Rayleigh model. That is, the desired signal is assumed nonfading.

4.1 Signal Model

The received signal vector, at the outputs of the separate antenna elements is given by

$$\mathbf{r}(t) = \sqrt{P_s}\mathbf{c}s(t) + \sqrt{P}\sum_{k=1}^{L}\mathbf{c}_k s_k(t), \tag{4.1}$$

where $s(t) \in \{-1, 1\}$ and $s_k(t) \in \{-1, 1\}$ are the desired and the k-th interfering signals, respectively, $\mathbf{c}$ and $\mathbf{c}_k$ are their respective channel propagation vectors. The desired signal is assumed to be Rician fading, whereas, the cochannel interferers are assumed to be Rayleigh fading.

The n-th, $n = 1, \ldots, N$, element of the desired signal propagation vector $\mathbf{c}$ consists of a fixed (specular) component and a random (scattered) component and is given by

$$c_n = \beta_n e^{-j\delta_n} + Se^{-j\Phi}, \tag{4.2}$$

where S and Φ are independent random variables, the first obeying the Rayleigh density function with mean square σ^2, and the second obeying the uniform density function between $[0, 2\pi]$. The amplitude and the phase of the fixed component at the n-th antenna element are β_n and δ_n, respectively. Therefore, the element c_n is a complex Gaussian random variable with mean $\beta_n e^{-j\delta_n}$ and variance σ^2. Due to independent fading at each antenna element, the c_n's are independent complex Gaussian random variables. Without loss of generality, we assume that $\beta_n = \beta$ for all $n = 1, \ldots, N$. The mean and the covariance matrix of the desired signal propagation vector $\mathbf{c}$ are $\{\mathrm{E}[\mathbf{c}] = \mathbf{M}\}$ and $\left\{\mathbf{\Sigma} = \mathrm{E}\left[(\mathbf{c} - \mathbf{M})(\mathbf{c} - \mathbf{M})^H\right]\right\}$. The mean vector $\mathbf{M} = \left[\beta e^{-j\delta_1}, \ldots, \beta e^{-j\delta_N}\right]^T$. Note that both $\mathbf{c}$ and $\mathbf{c}_k$ have the same covariance matrix $\mathbf{\Sigma}$.

Define the parameter K, called the Rice factor, as the ratio of the power associated with the LOS component and the power associated with the scattered component, i.e., $K = \frac{\beta^2}{\sigma^2}$. When $K = 0$, i.e., absence of LOS component, we have Rayleigh/Rayleigh model. The complete absence of fading is obtained with $K = \infty$

and we have the Nonfading/Rayleigh model. Thus, Rician fading includes Rayleigh fading and no fading as special cases.

4.2 Maximal Ratio Combining

The signal-to-interference ratio at the output of the maximal ratio combiner is

$$\rho = \frac{\mathbf{c}^H \mathbf{R}_s \mathbf{c}}{\mathbf{c}^H \mathbf{R} \mathbf{c}}, \tag{4.3}$$

where $\mathbf{R}_s$ and $\mathbf{R}$ are the covariance matrices of the desired signal and interferences, respectively. These covariance matrices are defined in eq. (3.4).

4.2.1 Distribution of SIR ρ

Equation (4.3) can be rewritten as

$$\begin{aligned} \rho &= \frac{P_s}{P} \frac{\mathbf{c}^H \mathbf{c} \mathbf{c}^H \mathbf{c}}{\sum_{k=1}^{L} \mathbf{c}^H \mathbf{c}_k \mathbf{c}_k^H \mathbf{c}} \\ &= \frac{P_s}{P} \frac{\| \mathbf{c} \|^2}{\sum_{k=1}^{L} b_k b_k^*}, \end{aligned} \tag{4.4}$$

where $b_k = \frac{\mathbf{c}^H \mathbf{c}_k}{\|\mathbf{c}\|}$. Since the elements of $\mathbf{c}_k$ are iid complex Gaussian with zero mean and σ^2 variance, the distribution of b_k for a given $\mathbf{c}$, is also complex Gaussian. As shown in chapter 3, the mean and the variance of b_k conditioned on $\mathbf{c}$ are 0 and σ^2, respectively. Also, b_k is distributed independently of $\mathbf{c}$.

Equation (4.4) can be written as

$$\begin{aligned} \rho &= \frac{P_s}{P} \frac{\| \mathbf{c} \|^2}{\sum_{k=1}^{L} | b_k |^2} \\ &= \frac{P_s}{P} \frac{\sum_{j=1}^{N} | f_j |^2}{\sum_{k=1}^{L} | b_k |^2} \\ &= \frac{P_s}{P} \zeta, \end{aligned} \tag{4.5}$$

where $\mathbf{c}^T = [f_1, \ldots, f_N]$ is the desired user's channel propagation vector and the superscript $\{T\}$ denotes transpose. Since each of f_j is a non-zero mean complex Gaussian random variable, $| f_j |^2$ is a non-central chi-square random variable with

two degrees of freedom (DOF). Each of $\mid b_k \mid^2$ is a chi-square random variable with two DOF. The quantity

$$\zeta = \frac{\sum_{j=1}^{N} \mid f_j \mid^2}{\sum_{k=1}^{L} \mid b_k \mid^2}, \tag{4.6}$$

is the ratio of two independent random variables, the numerator being non-central chi-square with $2N$ DOF and the denominator being central chi-square with $2L$ DOF. The distribution of ζ is therefore given by [49]:

$$\begin{aligned} f_\zeta(\zeta) &= e^{-\Omega}{}_1F_1\left(L+N; N; \Omega(1+\zeta^{-1})^{-1}\right) \\ &\quad \frac{\Gamma(L+N)}{\Gamma(L)\Gamma(N)} \frac{\zeta^{N-1}}{(1+\zeta)^{L+N}}, \qquad \zeta \geq 0,\ N \geq 1,\ L \geq 1, \end{aligned} \tag{4.7}$$

where $\Omega = \mathbf{M}\mathbf{\Sigma}^{-1}\mathbf{M}$ and ${}_1F_1(\cdot)$ is the Kummer's confluent hypergeometric function. The distribution in eq. (4.7) is a modified form of noncentral F distribution with the noncentrality parameter Ω. By using the transformation $\rho = \frac{P_s}{P}\zeta$, the PDF of the SIR ρ can easily be obtained and is

$$\begin{aligned} f_\rho(\rho) &= e^{-\Omega}{}_1F_1\left(L+N; N; \Omega\frac{\rho}{(\frac{P_s}{P}+\rho)}\right)\left(\frac{P_s}{P}\right)^L \\ &\quad \frac{\Gamma(L+N)}{\Gamma(L)\Gamma(N)} \frac{\rho^{N-1}}{(\frac{P_s}{P}+\rho)^{L+N}} \qquad \rho \geq 0,\ N \geq 1,\ L \geq 1. \end{aligned} \tag{4.8}$$

The PDF of ρ (or ζ) depends on the covariance matrix $\mathbf{\Sigma}$ only through the noncentrality parameter Ω. Since independent fading between antenna elements is assumed, i.e., $\mathbf{\Sigma} = \sigma^2\mathbf{I}_N$, the noncentrality parameter $\Omega = \frac{\mathbf{M}^H\mathbf{M}}{\sigma^2} = N\frac{\beta^2}{\sigma^2} = NK$, where K is the Rice factor. Using this value for Ω in eq. (4.8), the PDF of ρ becomes

$$\begin{aligned} f_\rho(\rho) &= e^{-NK}{}_1F_1\left(L+N; N; NK\frac{\rho}{(\frac{P_s}{P}+\rho)}\right)\left(\frac{P_s}{P}\right)^L \\ &\quad \frac{\Gamma(L+N)}{\Gamma(L)\Gamma(N)} \frac{\rho^{N-1}}{(\frac{P_s}{P}+\rho)^{L+N}} \qquad \rho \geq 0,\ N \geq 1,\ L \geq 1. \end{aligned} \tag{4.9}$$

When Rayleigh/Rayleigh model is assumed, i.e., $K = 0$, eq. (4.9) degenerates to eq. (3.11), as expected.

As shown in the Appendix E, the PDF of ρ under the Nonfading/Rayleigh model is given by

$$f_\rho(\rho) = \frac{1}{\Gamma(L)}\left(\frac{N^2 P_s \beta^4}{\kappa P}\right)^L \rho^{-L-1} e^{-\frac{N^2 P_s \beta^4}{\kappa \rho P}} \qquad \rho > 0,\ N \geq 1,\ L \geq 1, \tag{4.10}$$

where $\kappa = \mathbf{v}^H \mathbf{\Sigma} \mathbf{v}$ and $\mathbf{v}^T = [\beta e^{-j\delta_1}, \ldots, \beta e^{-j\delta_N}]$ is the desired signal's antenna array propagation vector.

4.2.2 Outage Probability

The outage probability for the maximal ratio combiner can now be evaluated:

$$\begin{aligned} P_o &= \text{Probability}\,[\rho < \rho_p] \\ &= \int_0^{\rho_p} f_\rho(\rho) d\rho \\ &= e^{-NK}\left(\frac{P_s}{P}\right)^L \frac{\Gamma(L+N)}{\Gamma(L)\Gamma(N)} \\ &\quad \int_0^{\rho_p} \frac{\rho^{N-1}}{(\frac{P_s}{P}+\rho)^{L+N}} {}_1F_1\left(L+N; N; NK\frac{\rho}{(\frac{P_s}{P}+\rho)}\right) d\rho, \end{aligned} \tag{4.11}$$

where ρ_p is the SIR protection ratio. A closed-form expression for the integral in eq. (4.11) is not known, however, it can be evaluated numerically.

The outage probability of the MRC under the Nonfading/Rayleigh model is given by [45]:

$$\begin{aligned} P_o &= \frac{1}{\Gamma(L)}\left(\frac{N^2 P_s \beta^4}{\kappa P}\right)^L \int_0^{\rho_p} \rho^{-L-1} e^{-\frac{N^2 P_s \beta^4}{\kappa \rho P}} d\rho \\ &= \frac{1}{\Gamma(L)}\left[\Gamma(L) - \Gamma(L,0) + \Gamma(L, \frac{N^2 P_s \beta^4}{\kappa \rho_p P})\right], \end{aligned} \tag{4.12}$$

where $\Gamma(a,x)$ is the complementary incomplete gamma function and is defined as [42]

$$\Gamma(a,x) = \int_x^\infty e^{-t} t^{a-1} dt, \qquad a > 0. \tag{4.13}$$

4.2.3 BER of the Maximal Ratio Combiner

The BER of the maximal ratio combiner is computed as

$$\begin{aligned} P_e &= \frac{1}{2}\int_0^\infty \text{erfc}(\sqrt{\rho}) f_\rho(\rho) d\rho \\ &= \frac{e^{-NK}}{2}\frac{\Gamma(L+N)}{\Gamma(L)\Gamma(N)}\left(\frac{P_s}{P}\right)^L \\ &\int_0^\infty \text{erfc}(\sqrt{\rho})\frac{\rho^{N-1}}{(\frac{P_s}{P}+\rho)^{L+N}} {}_1F_1\left(L+N; N; NK\frac{\rho}{(\frac{P_s}{P}+\rho)}\right) d\rho. \end{aligned} \tag{4.14}$$

A closed-form expression for the integral in eq. (4.14) is not known, however, it can be evaluated numerically.

As shown in the Appendix G, the BER of the maximal ratio combiner under the Nonfading/Rayleigh model is given by

$$\begin{aligned} P_e = \frac{1}{2\sqrt{\pi}\Gamma(L)}\Bigg[&\Gamma(L)\Gamma(\frac{1}{2}) + \left(\frac{N^2 P_s \beta^4}{\kappa P}\right)^L \frac{\Gamma(\frac{1}{2}-L)}{(-L)} \\ &{}_1F_2\left(L; L+1, L+\frac{1}{2}; \frac{N^2 P_s \beta^4}{\kappa P}\right) + \left(\frac{N^2 P_s \beta^4}{\kappa P}\right)^{\frac{1}{2}} \frac{\Gamma(-\frac{1}{2})\Gamma(L-\frac{1}{2})}{\Gamma(\frac{1}{2})} \\ &{}_1F_2\left(\frac{1}{2}; \frac{3}{2}, \frac{3}{2}-L; \frac{N^2 P_s \beta^4}{\kappa P}\right)\Bigg], \end{aligned} \tag{4.15}$$

where ${}_1F_2(\cdot)$ is the generalized hypergeometric series.

4.3 Optimum Combining

The SIR at the output of the optimum combiner is

$$\mu = \frac{P_s}{P}\mathbf{c}^H \mathbf{R}_1^{-1}\mathbf{c}, \tag{4.16}$$

where $\mathbf{R}_1 = \sum_{k=1}^{L} \mathbf{c}_k \mathbf{c}_k^H$.

4.3.1 Distribution of the Maximum SIR μ

Let $\nu = \mathbf{c}^H \mathbf{R}_1^{-1}\mathbf{c}$. The matrix $\mathbf{R}_1$ has a complex Wishart distribution $CW_N(\Sigma, L)$. The desired signal's channel vector $\mathbf{c}$ is complex Gaussian with the mean vector $\mathbf{M}$

and the same covariance matrix $\mathbf{\Sigma}$. The distribution of ν is, therefore, given as

$$\begin{aligned} f_\nu(\nu) &= e^{-\Omega}{}_1F_1\left(L+1; N; \Omega(1+\nu^{-1})^{-1}\right) \\ &\quad \frac{\Gamma(L+1)}{\Gamma(N)\Gamma(L+1-N)}\frac{\nu^{N-1}}{(1+\nu)^{L+1}} \qquad \nu \geq 0,\ 1 \leq N \leq L, \end{aligned} \tag{4.17}$$

where $\Omega = \mathbf{M}\mathbf{\Sigma}^{-1}\mathbf{M}$. The distribution in eq. (4.17) is a modified form of noncentral F distribution with the noncentrality parameter Ω. In multivariate statistics, when the elements of $\mathbf{c}$ and $\mathbf{R}_1$ are real Gaussian, then the distribution of $\nu = \mathbf{c}^H\mathbf{R}_1^{-1}\mathbf{c}$ is known as *Non-Null* distribution of the Hotelling's T^2 statistics. By using the transformation $\mu = \frac{P_s}{P}\nu$, the PDF of the SIR μ can easily be obtained and is

$$\begin{aligned} f_\mu(\mu) &= e^{-\Omega}{}_1F_1\left(L+1; N; \Omega\frac{\mu}{(\frac{P_s}{P}+\mu)}\right)\left(\frac{P_s}{P}\right)^{L+1-N} \\ &\quad \frac{\Gamma(L+1)}{\Gamma(N)\Gamma(L+1-N)}\frac{\mu^{N-1}}{(\frac{P_s}{P}+\mu)^{L+1}} \qquad \mu \geq 0,\ 1 \leq N \leq L. \end{aligned} \tag{4.18}$$

Since independent fading is assumed, the noncentrality parameter $\Omega = \frac{\mathbf{M}^H\mathbf{M}}{\sigma^2} = NK$. Using this value of Ω in eq. (4.18), we get

$$\begin{aligned} f_\mu(\mu) &= e^{-NK}{}_1F_1\left(L+1; N; NK\frac{\mu}{(\frac{P_s}{P}+\mu)}\right)\left(\frac{P_s}{P}\right)^{L+1-N} \\ &\quad \frac{\Gamma(L+1)}{\Gamma(N)\Gamma(L+1-N)}\frac{\mu^{N-1}}{(\frac{P_s}{P}+\mu)^{L+1}} \qquad \mu \geq 0,\ 1 \leq N \leq L. \end{aligned} \tag{4.19}$$

Note that both ρ and μ have the same modified form of non-central F distribution, but with different DOF.

When Rayleigh/Rayleigh model is assumed, i.e., $K = 0$, eq. (4.19) degenerates to eq. (3.26), as expected.

As shown in the Appendix F, the PDF of μ under the Nonfading/Rayleigh model is given by

$$f_\mu(\mu) = \frac{1}{\Gamma(L+1-N)}\left(\frac{P_s}{\eta P}\right)^{L+1-N} e^{-(\frac{P_s}{P}\frac{1}{\eta\mu})}\mu^{N-L-2} \qquad \mu > 0,\ 1 \leq N \leq L, \tag{4.20}$$

where $\eta = \left(\mathbf{v}^H\mathbf{\Sigma}^{-1}\mathbf{v}\right)^{-1}$.

4.3.2 Outage Probability

The outage probability of the optimum combiner can be calculated as

$$\begin{aligned} P_o &= \text{Probability}\,[\mu < \mu_p] \\ &= \int_0^{\mu_p} f_\mu(\mu)d\mu \\ &= e^{-NK}\left(\frac{P_s}{P}\right)^{L+1-N}\frac{\Gamma(L+1)}{\Gamma(N)\Gamma(L+1-N)} \\ &\quad \int_0^{\mu_p}\frac{\mu^{N-1}}{(\frac{P_s}{P}+\mu)^{L+1}}{}_1F_1\left(L+1;N;NK\frac{\mu}{(\frac{P_s}{P}+\mu)}\right)d\mu, \end{aligned} \tag{4.21}$$

where μ_p is the SIR protection ratio. A closed-form expression for the integral in eq. (4.21) is not known, however, it can be evaluated numerically.

The outage probability of the optimum combiner under the Nonfading/Rayleigh model is given by [45]

$$\begin{aligned} P_o &= \frac{1}{\Gamma(L+1-N)}\left(\frac{P_s}{\eta P}\right)^{L+1-N}\int_0^{\mu_p} e^{-(\frac{P_s}{P}\frac{1}{\eta\mu})}\mu^{N-L-2}d\mu \\ &= \frac{1}{\Gamma(L+1-N)}\left[\Gamma(L+1-N)-\Gamma(L+1-N,0)+\Gamma(L+1-N,\frac{P_s}{P\eta\mu_p})\right]. \end{aligned} \tag{4.22}$$

4.3.3 BER of the Optimum Combiner

The BER of the optimum combiner is computed as

$$\begin{aligned} P_e &= \frac{1}{2}\int_0^{\infty}\text{erfc}(\sqrt{\mu})f_\mu(\mu)d\mu \\ &= \frac{e^{-NK}}{2}\frac{\Gamma(L+1)}{\Gamma(N)\Gamma(L+1-N)}\left(\frac{P_s}{P}\right)^{L+1-N} \\ &\quad \int_0^{\infty}\text{erfc}(\sqrt{\mu})\frac{\mu^{N-1}}{(\frac{P_s}{P}+\mu)^{L+1}}{}_1F_1\left(L+1;N;NK\frac{\mu}{(\frac{P_s}{P}+\mu)}\right)d\mu. \end{aligned} \tag{4.23}$$

A closed-form expression for the integral in eq. (4.23) is not known, however, it can be evaluated numerically.

As shown in the Appendix H, the BER of the optimum combiner under the Nonfading/Rayleigh model is given by

$$P_e = \frac{1}{2\sqrt{\pi}\Gamma(L+1-N)}\left[\Gamma(L-N+1)\Gamma(\frac{1}{2}) + \left(\frac{P_s}{P\eta}\right)^{L+1-N}\frac{\Gamma(N-L-\frac{1}{2})}{(N-L-1)}\right.$$
$$ {}_1F_2\left(L+1-N; L-N+2, L-N+\frac{3}{2}; \frac{P_s}{P\eta}\right) + \left(\frac{P_s}{P\eta}\right)^{\frac{1}{2}}\frac{\Gamma(-\frac{1}{2})\Gamma(L-N+\frac{1}{2})}{\Gamma(\frac{1}{2})}$$
$$\left. {}_1F_2\left(\frac{1}{2}; \frac{3}{2}, N-L+\frac{1}{2}; \frac{P_s}{P\eta}\right)\right], \tag{4.24}$$

where ${}_1F_2(\cdot)$ is the generalized hypergeometric series.

4.4 Performance Analysis

This section presents results on the performance of diversity combining techniques investigated in the earlier sections. The performance is evaluated for the worst case scenario. The number of cochannel interferers is $L = 6$. The relationship between CIR and $\frac{P_s}{P}$ is CIR $= \frac{P_s(K+1)}{6P}$, CIR $= \frac{P_s}{6P}$, CIR $= \frac{P_s\beta^2}{6P\sigma^2}$, for Rician/Rayleigh, Rayleigh/Rayleigh and Nonfading/Rayleigh models, respectively. The Rice factor K was assumed to be 5. Table 4.1 shows relationships between frequency reuse factor F, CIR and $\frac{P_s}{P}$ for a dual path loss exponent.

In Figures 4.1 and 4.2, the cumulative distribution function and the probability density function {eqs. (4.9), (4.19)} of the array output SIR are plotted, respectively, with the order of diversity N as the parameter. Again, these curves clearly show that SIR has a better chance to be high with an increase in the order of diversity N regardless of the combining method. Also, OC significantly increases the chances of higher SIR values, as compared to MRC.

In Figure 4.3, the outage probability {eqs. (4.11), (4.21)} is shown as a function of the number of antenna elements N. Clearly, the outage probability decreases as N increases. For a given N, increasing the Rice factor K, decreases the outage probability as expected. Optimum combining shows a large decrease in the outage

probability with respect to MRC. For a given N, the difference in the outage probabilities with OC and MRC, increases with an increase in K. Figure 4.4 shows the probability of outage versus CIR. For a given CIR, OC decreases the outage probability as compared to MRC and this decrease becomes even greater as K increases. In Figure 4.5, the outage probability is shown as a function of the Rice factor K. Figure 4.6 shows the outage probability versus signal-to-interference protection ratio.

Figure 4.7 shows the BER performance {eqs. (4.14), (4.23)} versus the number of antenna elements N. There is a significant improvement in the performance (decrease in BER) of the optimum combiner as compared to the maximal ratio combiner with increase in N. For a given N, the difference in BERs of the optimum combiner and the maximal ratio combiner increases with an increase in K. In Figure 4.8, the BER is plotted versus CIR. For a given BER, OC reduces the required CIR as compared to MRC, which in turn, can lead to an increase in the system capacity. In Figure 4.9, the BER is shown as a function of the Rice factor K.

Figure 4.10 shows the improvement, due to OC, versus the order of diversity N. The improvement is defined as the reduction in the required $\frac{P_s}{P}$, for a given BER, with OC as compared to MRC. For a given BER, the improvement with OC increases with increase in N. Note that the value of the Rice factor K plays no significant role.

Figure 4.11 shows the diversity gain versus the order of diversity N. The diversity gain is defined as the reduction in the required $\frac{P_s}{P}$, for a given BER, with a corresponding increase in N. Optimum combining provides higher diversity gain than MRC and this difference in gain increases with N. It is clear from the figure that as K increases, i.e., the fading gets less severe, the diversity gain decreases as expected.

Table 4.1 Relation between F, CIR and $\frac{P_e}{P}$ in a Microcellular System.

F	CIR (dB) (Average)	CIR (dB) (Worst)	Rician/ Rayleigh $\frac{P_e}{P}$ (Worst)	Rayleigh/ Rayleigh $\frac{P_e}{P}$ (Worst)	Nonfading/ Rayleigh $\frac{P_e}{P}$ (Worst)
1	-3.01	-7.78	0.16	1.0	1.0
3	1.76	-1.76	0.66	4.0	4.0
4	3.01	0.05	1.01	6.07	6.07
7	5.44	3.30	2.14	12.83	12.83

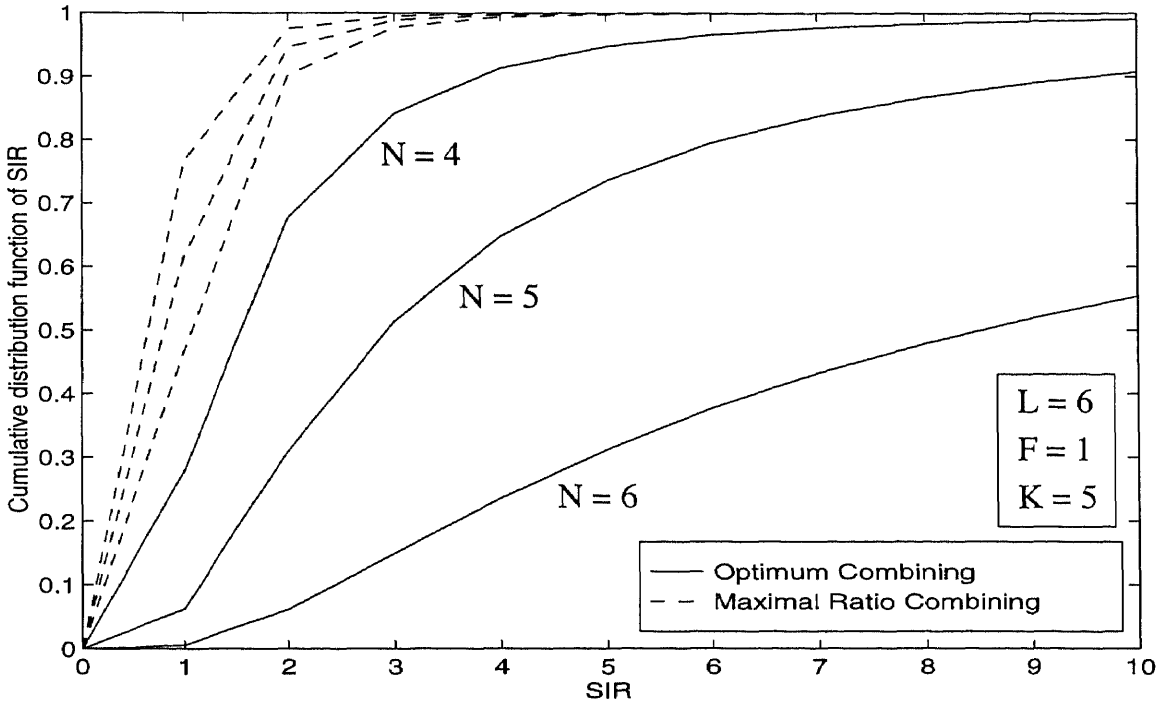

Figure 4.1 The influence of the order of diversity N on the cumulative distribution function of SIR.

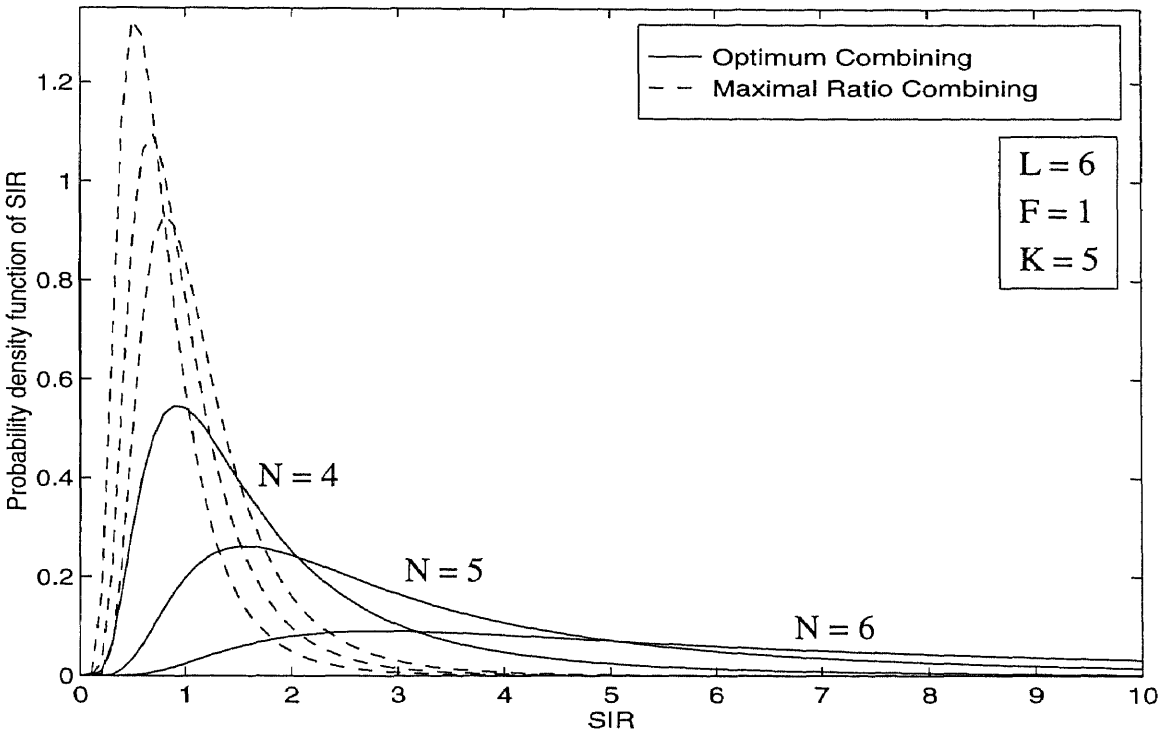

Figure 4.2 The influence of the order of diversity N on the probability density function of SIR.

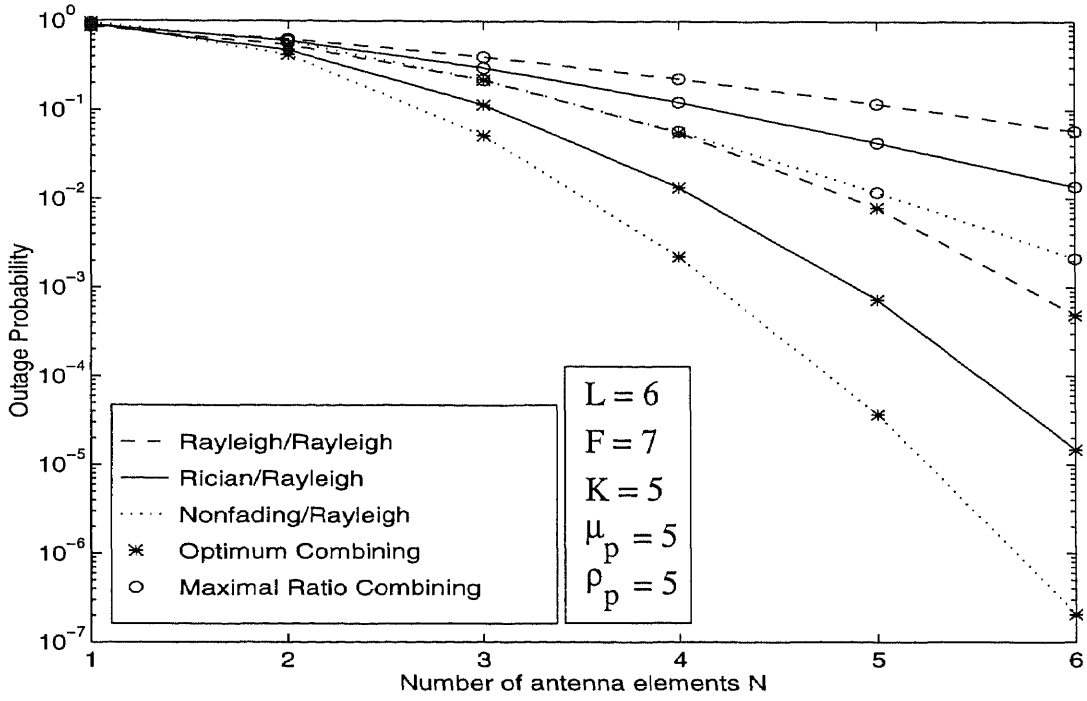

Figure 4.3 The outage probability versus the number of antenna elements N.

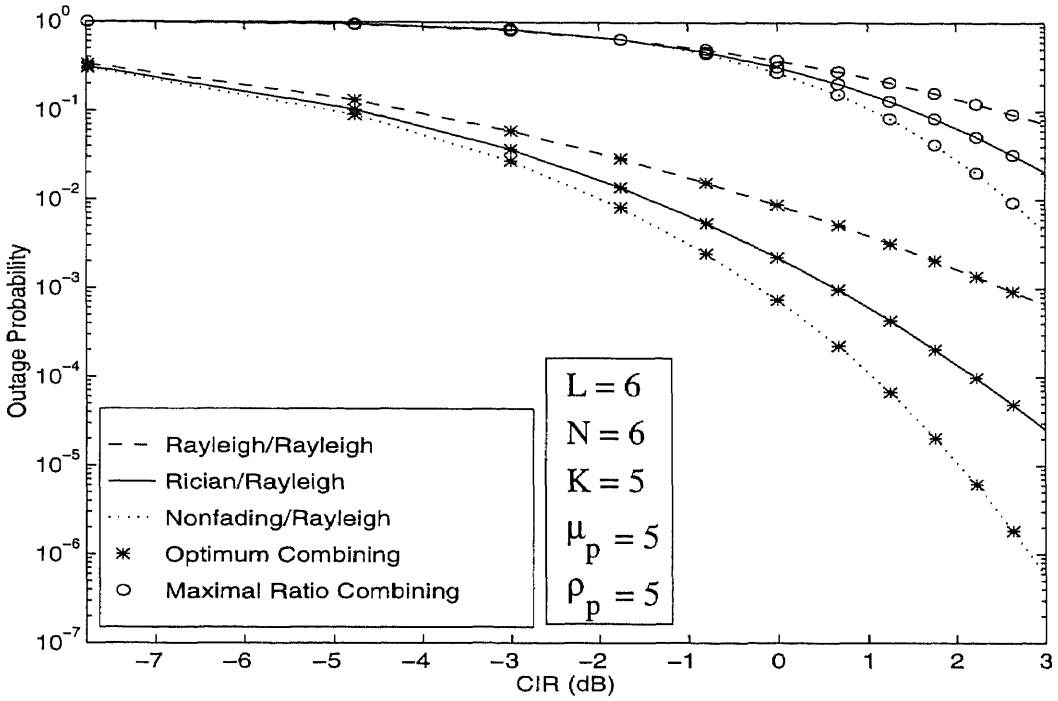

Figure 4.4 The outage probability versus carrier-to-interference ratio.

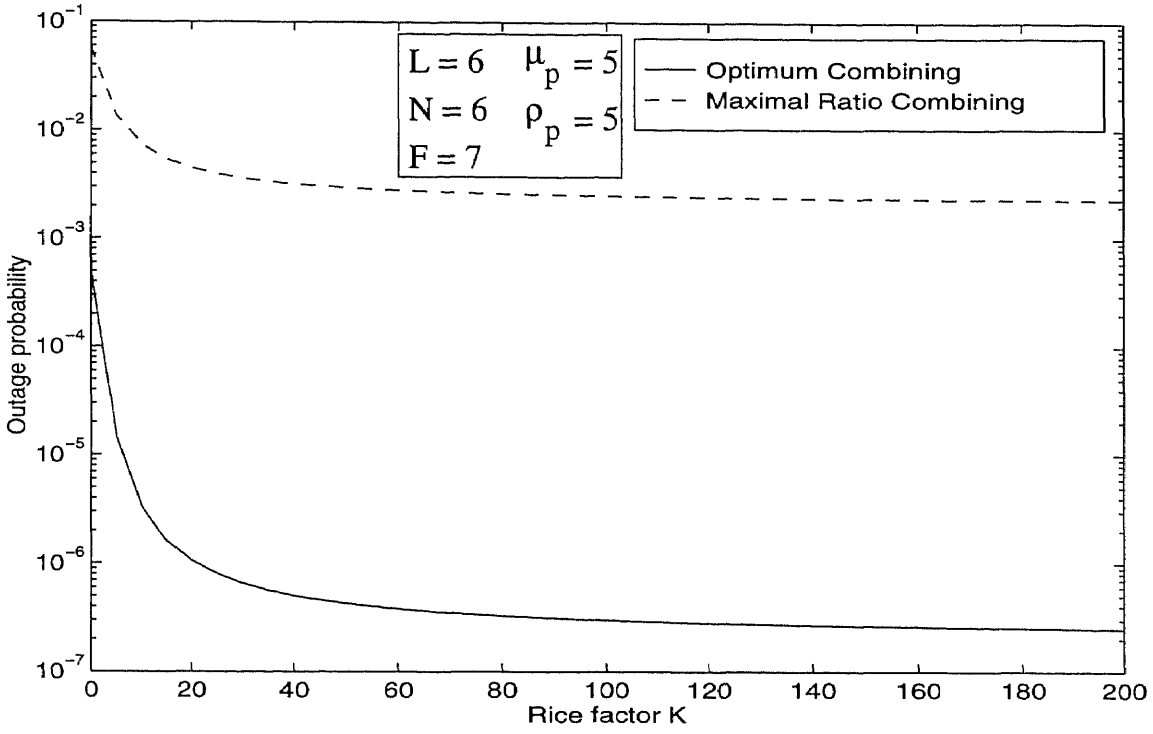

Figure 4.5 The outage probability versus the Rice factor K.

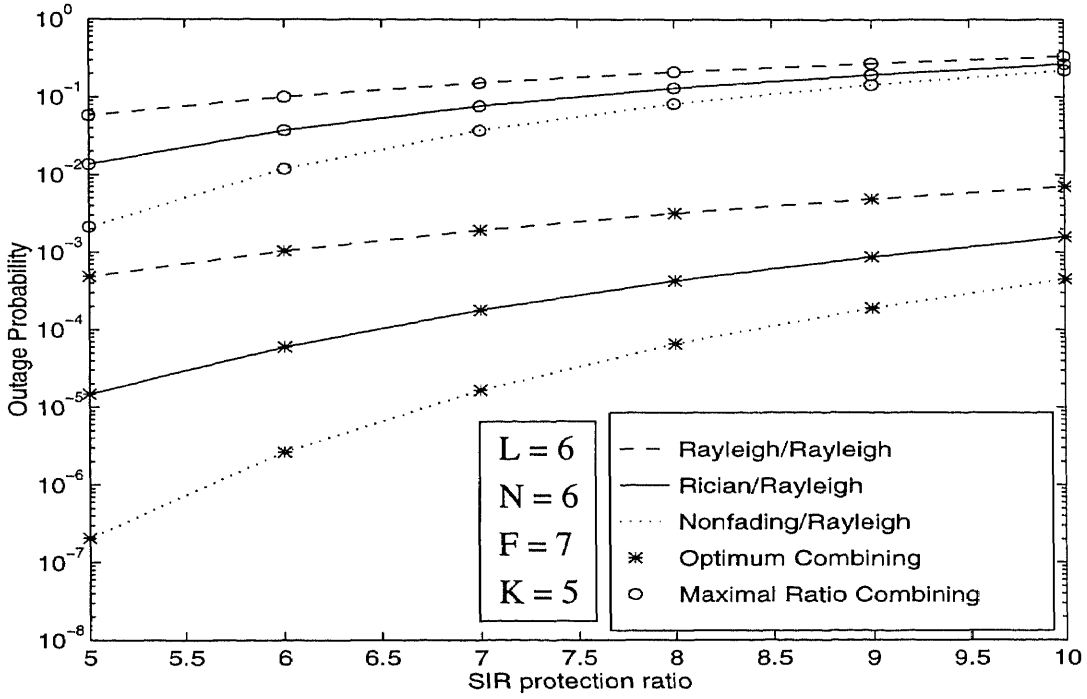

Figure 4.6 The outage probability versus signal-to-interference protection ratio.

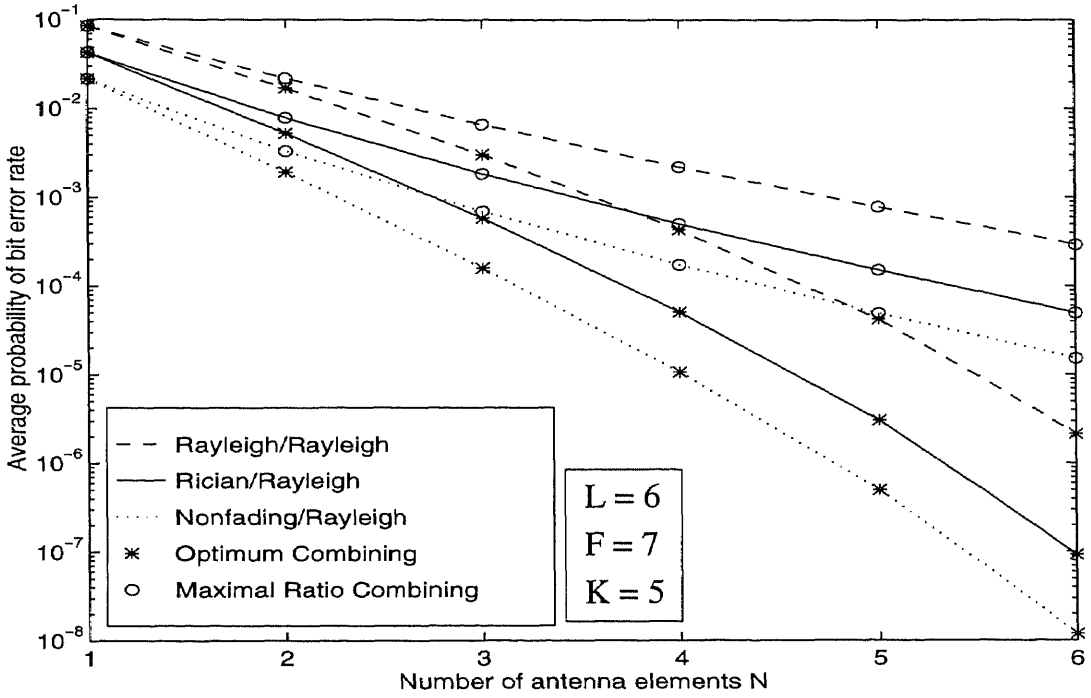

Figure 4.7 The average probability of bit error versus the number of antenna elements N.

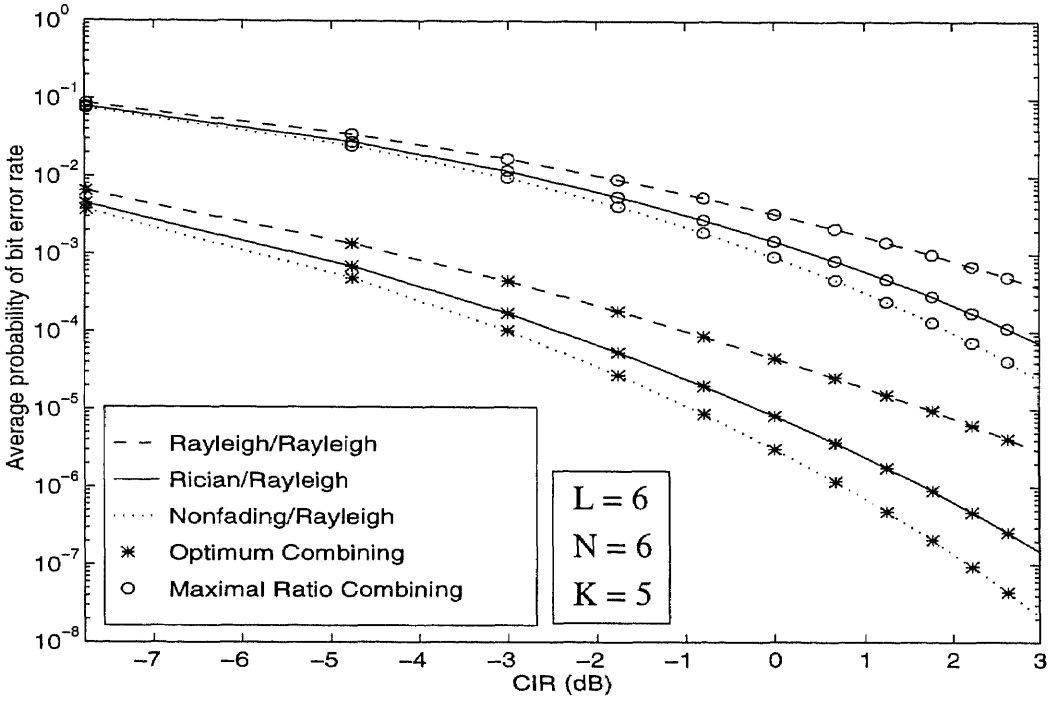

Figure 4.8 The average probability of bit error versus carrier-to-interference ratio.

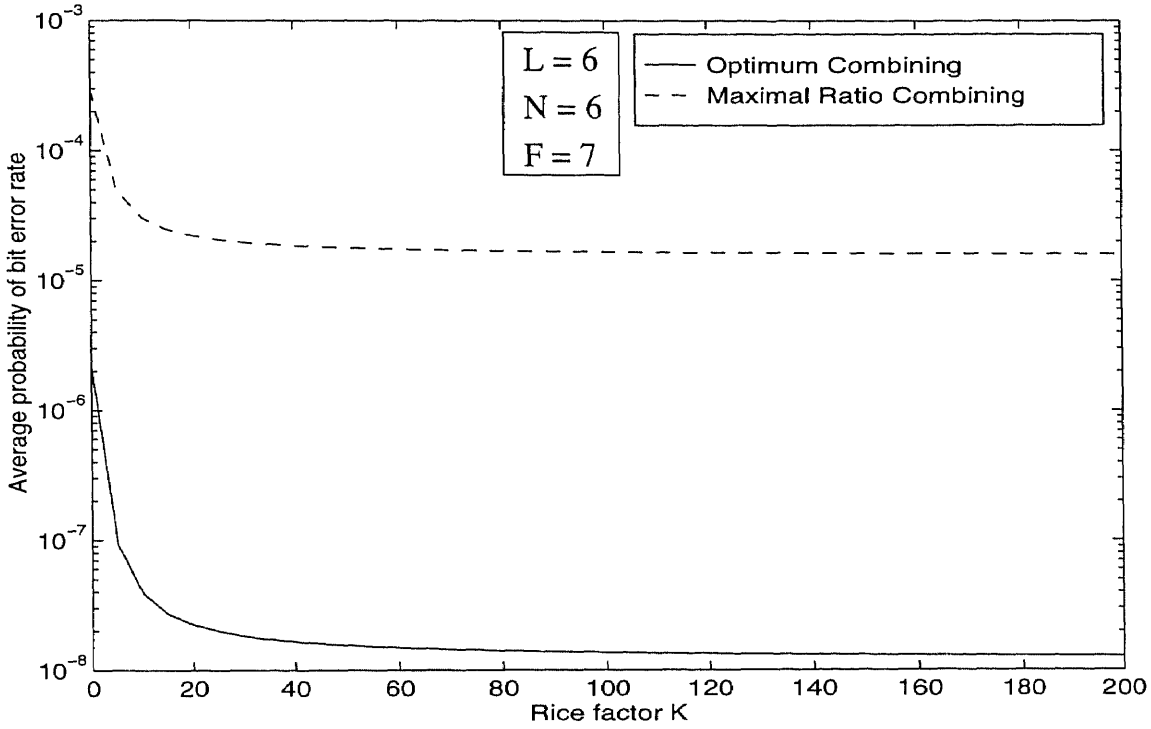

Figure 4.9 The average probability of bit error versus the Rice factor K.

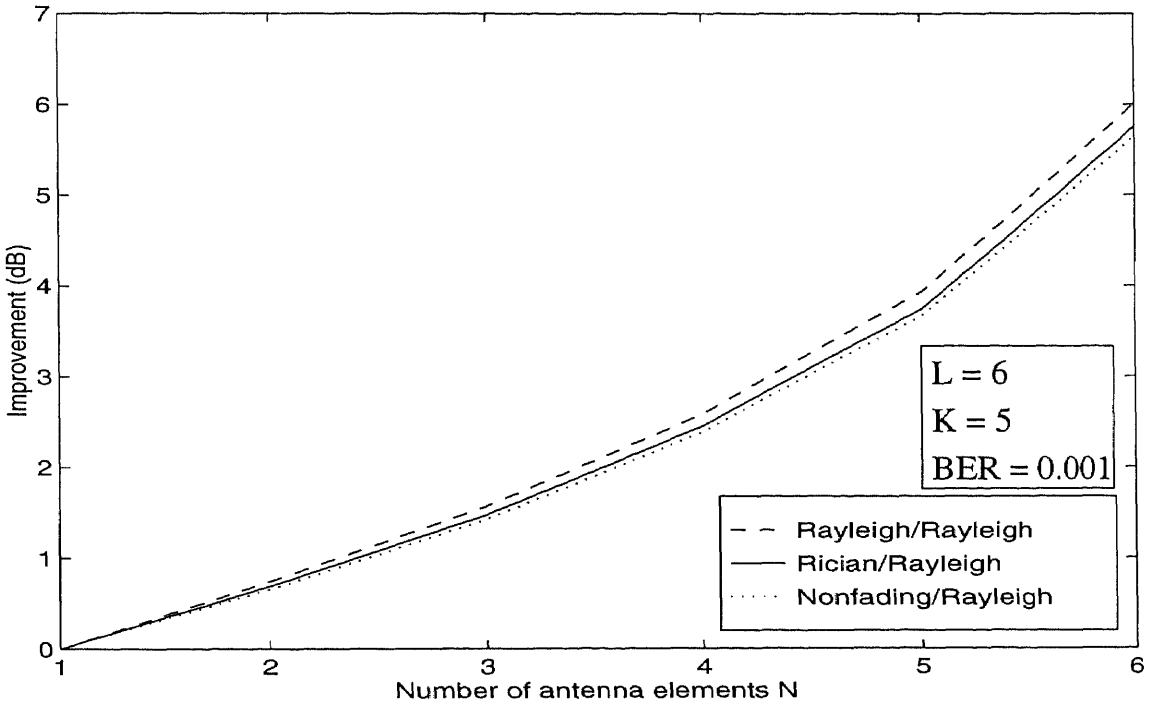

Figure 4.10 The improvement due to optimum combining versus the order of diversity N.

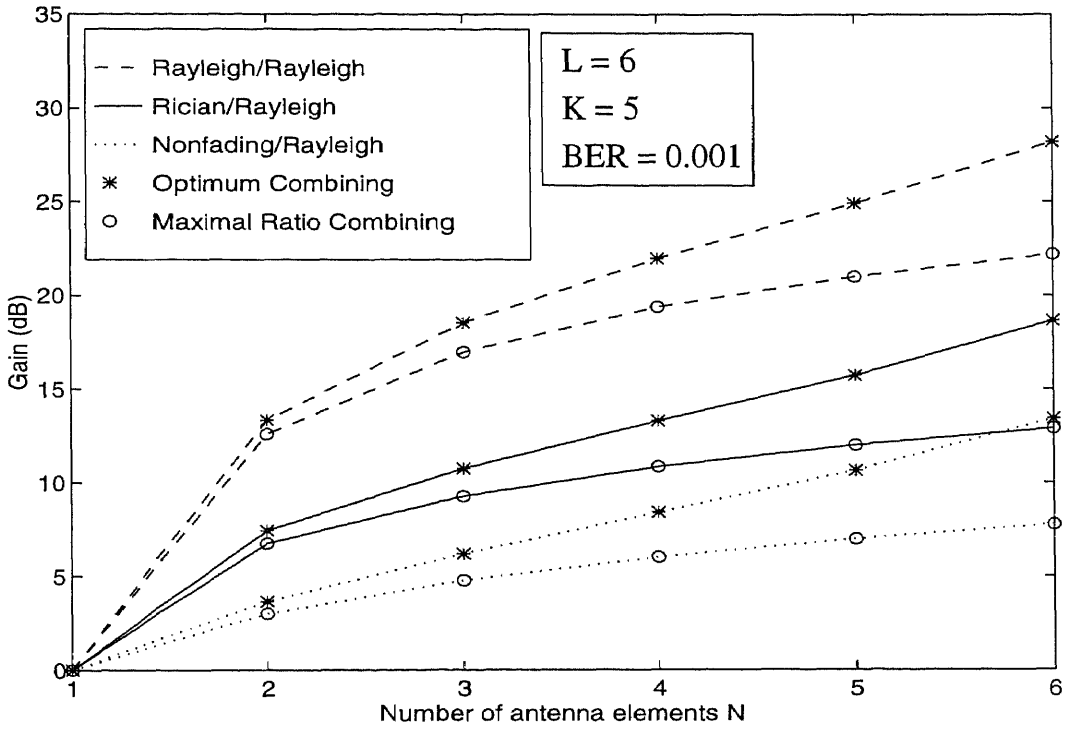

Figure 4.11 The diversity gain versus the order of diversity N.

CHAPTER 5

SPACE-TIME NARROWBAND INTERFERENCE SUPPRESSION IN DS-CDMA COMMUNICATION FOR PCS (SINGLE USER)

The need to suppress narrowband signals in direct-sequence code division multiple access (DS-CDMA) systems arises in applications where narrowband signals are overlaid with wideband signals to increase spectral efficiency. This concept has been proposed for both the personal communication systems (PCS) band and the cellular band. The co-existence of these two different systems within the same frequency spectrum, will cause interference to both systems. In this work we are concerned with the interference caused by the narrowband signal to the DS-CDMA signal.

The conventional approach to rejecting narrowband interference has been to sample the received signal at the chip interval, and to exploit the high correlation between the interference samples prior to spread spectrum demodulation. This method essentially places a notch at the narrowband interference frequency. The notch, however, also removes a portion of the DS-CDMA signal. As the bandwidth of the interference increases, the notch widens and the DS-CDMA signal loss becomes more significant. A number of authors have explored the performance of DS-CDMA overlay system [30, 31] with a narrowband BPSK signal as an interference.

In this chapter we study space-time processing for narrowband interference suppression. Space-time (ST) processing provides degrees of freedom (DOF) for both interference cancellation and diversity combining. The performance of ST receiver architectures, cascade and joint, is evaluated for suppressing a narrowband interference overlaid with a DS-CDMA signal in a frequency-selective slowly fading Rayleigh channel. Analytical expressions are obtained for asymptotic efficiency, the probability density function (PDF) of the output signal-to-interference-plus-noise ratio (SINR), the average probability of bit error rate (BER) and its upper bound, associated with each architecture.

5.1 System Configuration

Consider the uplink (mobile to base) of a coherent mobile communication system. The lowpass equivalent of the transmitted DS-CDMA signal is given by

$$s(t) = \sqrt{P}d(t)u(t), \tag{5.1}$$

where P is the signal power, $d(t) \in \{-1, 1\}$ is the data bit with duration T_b, and $u(t)$ is the signature waveform with chip duration T_c. The signature sequence $u(t)$ is assumed such that

$$\int_0^{T_b} u(t - iT_c)u(t - jT_c)\, dt = \begin{cases} T_b & i = j \\ 0 & i \neq j, \end{cases} \tag{5.2}$$

where $0 \leq i, j \leq (L-1)$ and $L = \frac{T_b}{T_c}$ is the processing gain. Normalizing T_c to unity, we have $L = T_b$. For a DS-CDMA signal with chip duration T_c, the spread spectrum bandwidth is approximately $B_s = 2/T_c$.

The time-variant frequency-selective Rayleigh fading channel is modeled as a tap-delay line with tap spacing T_c and tap coefficients $\{c_m(t)\}$. The complex lowpass equivalent channel impulse response is given by [35]

$$h(\tau, t) = \sum_{m=0}^{M-1} c_m(t)\ \delta(t - \tau - mT_c), \tag{5.3}$$

where $M = \lfloor \frac{T_m}{T_c} \rfloor + 1$ is the number of resolvable paths and $\delta(\cdot)$ denotes the Dirac impulse function. The notation $\lfloor \cdot \rfloor$ denotes the integer part. The total multipath delay spread T_m of the channel is assumed to be much smaller than the bit duration T_b. The channel coefficients $\{c_m(t)\}$ are modeled as zero-mean, complex-valued, stationary, mutually independent Gaussian random processes. The magnitude and the phase of $\{c_m(t)\}$ are Rayleigh distributed and uniformly distributed between $[0, 2\pi]$, respectively. The channel is characterized by slow fading such that $\{c_m(t)\} = \{c_m\}$ during the processing interval.

The narrowband interference is assumed to be a non-fading BPSK signal, and is defined by its equivalent lowpass representation as

$$J(t) = \sqrt{J}b(t)e^{j(2\pi\nu t + \vartheta)}, \tag{5.4}$$

where ν is the offset of the interference carrier frequency from the carrier frequency of DS-CDMA signal. The parameters J and ϑ denote the received interference power and phase, respectively. The information sequence $b(t) \in \{-1, 1\}$ has bit rate $1/T_i$, where T_i is the bit duration. The ratio of the interference bandwidth to the DS-CDMA bandwidth is given by

$$p = \frac{B_i}{B_s} = \frac{T_c}{T_i}. \tag{5.5}$$

The ratio of the offset of the interference carrier frequency to half of the DS-CDMA bandwidth is defined by

$$q = \frac{\nu}{(\frac{B_s}{2})} = \nu T_c. \tag{5.6}$$

The base station uses an N antenna element uniform linear array, with array elements assumed sufficiently separated such that spatial diversity (independent fading at each receive antenna element) is achieved with respect to the DS-CDMA signal. The equivalent baseband received signal at the n-th antenna can be written as

$$x_n(t) = \sqrt{P} \sum_{m=0}^{M-1} c_{nm} d(t - mT_c) u(t - mT_c) + \xi_n(t) + v_n(t), \tag{5.7}$$

where $\{c_{nm}\}$, $n = 1, \ldots, N$, $m = 0, \ldots, M-1$, represent the complex-valued tap coefficients of the fading channels as seen by DS-CDMA user. Samples of $\{c_{nm}\}$ are statistically independent between paths m, and between antennas n. The quantity $\xi_n(t)$ is the narrowband interference at the n-th antenna element and is given by

$$\xi_n(t) = \sqrt{J} b(t) e^{j(2\pi\nu t + \vartheta)} e^{j\phi_n}, \tag{5.8}$$

where ϕ_n is the electrical angle of the interference at the n-th antenna element. The additive noise $v_n(t)$ is modeled as complex white Gaussian with zero mean and variance σ^2. We assume perfect code synchronization.

A demodulator is used at each antenna element to collect the energy of the received signal from all independent paths and to despread the signal. The demodulator consists of an M tap-delay line and matched filters. The tap-delay line

compensates for the delay propagation in the channel, providing the time alignment for demodulation with the signature sequence $u(t)$. The general configuration at the base station is shown in Figure 5.1. The demodulator is shown in Figure 5.2. The output at the m-th tap correlator at the n-th antenna for the l-th symbol is given by

$$\begin{aligned} y_{nm}(l) &= \int_{lT_b}^{(l+1)T_b} x_n(t+mT_c)\, u(t)\, dt \\ &= \int_{lT_b}^{(l+1)T_b} \left\{ \sqrt{P} \sum_{i=0}^{M-1} c_{ni} d(t+mT_c - iT_c) u(t+mT_c - iT_c) \right\} u(t) dt \\ &\quad \int_{lT_b}^{(l+1)T_b} \xi_n(t+mT_c) u(t) dt + \int_{lT_b}^{(l+1)T_b} v_n(t+mT_c) u(t) dt \\ &= \sqrt{P} L d(l) c_{nm} + \xi_{nm}(l) + \eta_{nm}(l), \end{aligned} \tag{5.9}$$

where $\xi_{nm}(l)$ and $\eta_{nm}(l)$ are narrowband interference and noise at the output of the matched filter. The last line in eq. (5.9) follows from the assumption made in eq. (5.2).

5.2 Spatial Processing

In this section we consider spatial processing only, i.e., all the terms except for $m = 0$ vanishes in eqs. (5.7), (5.9). In other words, we consider flat Rayleigh fading at each antenna element. Define an N dimensional array vector $\mathbf{y}(l)$ for the l-th symbol at the output of the matched filter as

$$\mathbf{y}(l) = \sqrt{P} L d(l) \mathbf{c} + \boldsymbol{\Upsilon}(l) + \boldsymbol{\Psi}(l), \tag{5.10}$$

where $\mathbf{c} = [c_1, \ldots, c_N]^T$, is the vector of DS-CDMA user's channel coefficients. The terms $\boldsymbol{\Upsilon}(l) = [\xi_1(l), \ldots, \xi_N(l)]^T$ and $\boldsymbol{\Psi}(l) = [\eta_1(l), \ldots, \eta_N(l)]^T$ are interference and noise spatial vectors at the output of the correlators, respectively.

5.2.1 Distribution of SINR

The maximum SINR at the output of the antenna array is [14]

$$\mu = PL^2 \mathbf{c}^H \mathbf{R}_{ni}^{-1} \mathbf{c}, \tag{5.11}$$

where $\mathbf{R}_{ni} = \boldsymbol{\Upsilon}\boldsymbol{\Upsilon}^H + (\sigma^2 L)\mathbf{I}_N$, is the interference-plus-noise covariance matrix at the output of the matched filter and $\mathbf{I}_N$ is the identity matrix of dimension N. Using unitary transformation Q in eq. (5.11), we get

$$\mu = PL^2 \mathbf{c}^H Q \Lambda^{-1} Q^H \mathbf{c}, \tag{5.12}$$

where Λ is a diagonal matrix with eigenvalues $\{\lambda_1, \ldots, \lambda_N\}$ of the matrix $\mathbf{R}_{ni}$. Let $\mathbf{s} = Q^H \mathbf{c}$. Due to the unitary transformation Q, the elements of $\mathbf{s}$ have the same distribution as that of the elements of $\mathbf{c}$. Equation (5.12) can be rewritten as

$$\mu = PL^2 \sum_{l=1}^{N} \frac{|s_l|^2}{\lambda_l}, \tag{5.13}$$

where $\mathbf{s}^T = [s_1, \ldots, s_N]$. Since the elements of $\mathbf{c}$ have Rayleigh distributed amplitudes, each of $\{|s_l|^2\}$ is a chi-square random variable with two DOF. The eigenvalues $\{\lambda_l\}$ of $\mathbf{R}_{ni}$ are

$$\lambda_l = \begin{cases} JNL + \sigma^2 L & l = 1 \\ \sigma^2 L & l = 2, \ldots, N. \end{cases}$$

Due to the mutual independence of the terms in eq. (5.13), the characteristic function of μ is [40]

$$\phi_\mu(jw) = \frac{1}{\left(1 - jw\frac{P_s}{JN+\sigma^2}\right)\left(1 - jw\frac{P_s}{\sigma^2}\right)^{N-1}}, \tag{5.14}$$

where $P_s = PLE\left[|c_n|^2\right], n = 1, \ldots, N$, is the mean desired signal power per antenna. E denotes expectation. Define $h = \frac{P_s}{\sigma^2}$ as the mean signal-to-noise ratio (SNR) per antenna element. The PDF of μ can now be obtained by applying the inverse Fourier transformation to eq. (5.14) and is [41]

$$f_\mu(\mu) = \frac{(JN + \sigma^2)\mu^{N-1} e^{\frac{-(JN+\sigma^2)\mu}{P_s}} {}_1F_1\left(N-1; N; \frac{JN\mu}{P_s}\right)}{\sigma^2 \Gamma(N) h^N}, \ \mu \geq 0, \ N > 1, \tag{5.15}$$

where ${}_1F_1(\cdot)$ is the Kummer's confluent hypergeometric function and $\Gamma(\cdot)$ is the gamma function.

5.2.2 Asymptotic Efficiency of the Spatial Combiner

An alternative to the BER as a figure of merit that has been used to characterize the performance of a communication system is the ratio of SNRs with and without the presence of interference [40]. This desirable figure of merit is the asymptotic efficiency. The asymptotic efficiency is defined as the ratio $\zeta = \frac{\gamma_{\text{eff}}}{\gamma_o}$, where γ_{eff} is measured in the presence of the interference, and γ_o is observed with the interference absent, in the region of low noise power. The asymptotic efficiency represents the performance loss due to the presence of interference. Obviously, $\gamma_{\text{eff}} \leq \gamma_o$. Using eq. (5.13),

$$\begin{aligned} \gamma_{\text{eff}} &= \mathrm{E}[\mu] \\ &= \frac{P_s}{JN+\sigma^2} + \frac{(N-1)P_s}{\sigma^2}, \end{aligned} \tag{5.16}$$

where E denotes expectation. Without interference, $\gamma_o = \frac{NP_s}{\sigma^2}$. Hence the asymptotic efficiency of the spatial processor is given by

$$\begin{aligned} \zeta &= \lim_{\sigma^2 \to 0} \left(\frac{\sigma^2}{N(JN+\sigma^2)} + \frac{N-1}{N} \right) \\ &= 1 - \frac{1}{N}. \end{aligned} \tag{5.17}$$

This relation clearly illustrates the loss of one DOF incurred by the interference cancellation process.

5.3 Cascade Space-Time Processing

The cascade ST receiver consists of a temporal processor using the outputs of the spatial processor as shown in Figure 5.3. Using eq. (5.9), define the N-dimensional array vector at the output f the m-th tap matched filter for the l-th symbol as $\mathbf{y}_m^T(l) = [y_{1m}(l), \ldots, y_{Nm}(l)]$.

The optimum weight vector, which maximizes SINR, is given by

$$\mathbf{f}_m = \mathbf{R}_m^{-1}\mathbf{r}_m, \tag{5.18}$$

where

$$\begin{aligned} \mathbf{r}_m &= \mathrm{E}[\mathbf{y}_m(l)d(l)] \\ &= \sqrt{P}L\mathbf{c}_m \end{aligned} \tag{5.19}$$

is the cross-correlation vector and

$$\mathbf{R}_m = \mathrm{E}\left[\{\mathbf{y}_m(l) - d(l)\mathbf{r}_m\}\{\mathbf{y}_m(l) - d(l)\mathbf{r}_m\}^H\right] \tag{5.20}$$

is the array interference-plus-noise covariance matrix at the output of the m-th correlator. $\mathbf{c}_m^T = [c_{1m}, \ldots, c_{Nm}]$ is the vector of channel coefficients at the m-th tap delay. Following spatial processing with the spatial weight vector $\mathbf{f}_m$, the spatial output at the m-th tap-delay line is $z_m(l) = \mathbf{f}_m^H\mathbf{y}_m(l)$.

Let $\mathbf{z}^T(l) = [z_0(l), \ldots, z_{M-1}(l)]$ be a vector that consists of the M outputs of the spatial combiners. The vector $\mathbf{z}(l)$ is fed into the temporal combiner. Define the output of the ST combiner as $\rho(l) = \mathbf{g}^H\mathbf{z}(l)$, where $\mathbf{g}$ is the temporal weight vector. We consider two ways to combine the elements of $\mathbf{z}(l)$: (1) straight combiner, i.e., $\mathbf{g} = \mathbf{1}$ and (2) optimum combiner in which $\mathbf{g}$ is derived in a similar fashion as the optimum spatial weight vector $\mathbf{f}_m$.

5.3.1 Straight Temporal Combiner ($\mathbf{g} = \mathbf{1}$)

Due to mutual independence of the spatial outputs $\{z_m(l)\}$, the SINR at the output of the cascade ST is $\mu = \sum_{m=0}^{M-1}\mu_m$, where μ_m is the SINR associated with each of the spatial combiner. Each $\{\mu_m\}$ has the characteristic function and the PDF given by eqs. (5.14), (5.15), respectively. Since μ_m's are mutually independent, we have:

$$\begin{aligned} \phi_\mu(jw) &= [\phi_{\mu_m}(jw)]^M \\ &= \frac{1}{\left(1 - jw\frac{P_s}{JN+\sigma^2}\right)^M \left(1 - jw\frac{P_s}{\sigma^2}\right)^{(N-1)M}}, \end{aligned} \tag{5.21}$$

where $P_s = PLE[|c_{nm}|^2], n = 1,\ldots,N, m = 0,\ldots,M-1$. The PDF of μ can now be obtained and is given by

$$f_\mu(\mu) = \frac{(JN+\sigma^2)^M \mu^{NM-1} e^{\frac{-(JN+\sigma^2)\mu}{P_s}} {}_1F_1\left((N-1)M; NM; \frac{JN\mu}{P_s}\right)}{(\sigma^2)^M \Gamma(NM) h^{NM}}, \mu \geq 0, N > 1. \tag{5.22}$$

5.3.2 Asymptotic Efficiency of Cascade Space-Time Processor

The asymptotic efficiency of the cascade optimum space/straight temporal (COSST) processor can be evaluated as

$$\begin{aligned} \gamma_{\text{eff}} &= \mathrm{E}[\mu] \\ &= \sum_{m=0}^{M-1} \mathrm{E}[\mu_m] \\ &= \frac{P_s M}{JN+\sigma^2} + \frac{(N-1)MP_s}{\sigma^2}. \end{aligned} \tag{5.23}$$

and $\gamma_o = \frac{NMP_s}{\sigma^2}$. Hence the asymptotic efficiency of the COSST processor is given by

$$\begin{aligned} \zeta &= \lim_{\sigma^2 \to 0} \left(\frac{\sigma^2}{N(JN+\sigma^2)} + \frac{(N-1)M}{NM} \right) \\ &= 1 - \frac{1}{N}. \end{aligned} \tag{5.24}$$

This relation illustrates the loss of M DOF, out of a total of NM, incurred by the interference cancellation process.

5.3.3 Optimum Temporal Combiner

The vector $\mathbf{z}(l)$, fed into the temporal combiner, can be expressed as

$$\mathbf{z}(l) = \sqrt{P} L d(l) \mathbf{B} + \boldsymbol{\Upsilon}_t + \boldsymbol{\Psi}_t, \tag{5.25}$$

where $\mathbf{B}^T = \left[\mathbf{f}_0^H \mathbf{c}_0, \ldots, \mathbf{f}_{M-1}^H \mathbf{c}_{M-1}\right]$, $\boldsymbol{\Upsilon}_t^T = \left[\mathbf{f}_0^H \boldsymbol{\Upsilon}_0, \ldots, \mathbf{f}_{M-1}^H \boldsymbol{\Upsilon}_{M-1}\right]$ is the interference vector and $\boldsymbol{\Psi}_t^T = \left[\mathbf{f}_0^H \boldsymbol{\Psi}_0, \ldots, \mathbf{f}_{M-1}^H \boldsymbol{\Psi}_{M-1}\right]$ is the noise vector.

The optimum temporal weight vector $\mathbf{g}$, which maximizes SINR, is given by

$$\mathbf{g} = \mathbf{R}_t^{-1} \mathbf{r}_t, \tag{5.26}$$

where

$$\begin{aligned} \mathbf{r}_t &= \mathrm{E}[\mathbf{z}(l)d(l)] \\ &= \sqrt{P}L\mathbf{B} \end{aligned} \tag{5.27}$$

is the cross-correlation vector and

$$\mathbf{R}_t = \mathrm{E}\left[\{\mathbf{z}(l) - d(l)\mathbf{r}_t\}\{\mathbf{z}(l) - d(l)\mathbf{r}_t\}^H\right] \tag{5.28}$$

is the interference-plus-noise covariance matrix at the input of the temporal combiner. Hence, the SINR at the output of cascade optimum space/optimum temporal (COSOT) processor is given by

$$\mu = \frac{PL^2\mathrm{E}\left[\left|\mathbf{g}^H\mathbf{B}\right|^2\right]}{\mathrm{E}\left[\left|\mathbf{g}^H\boldsymbol{\Upsilon}_t\right|^2\right] + \mathrm{E}\left[\left|\mathbf{g}^H\boldsymbol{\Psi}_t\right|^2\right]}. \tag{5.29}$$

The expectation is taken with respect to the noise over a time interval during which the channel is considered constant (due to slow fading assumption). Thus, μ is modeled as a random variable parameterized by the channel coefficients $\{c_{nm}\}$. Unfortunately, the PDF of μ is not known.

5.4 Joint Space-Time Processing

With the joint ST combiner, processing is carried out simultaneously in the ST domains. The configuration of the joint ST is shown in Figure 5.4. Define the NM-dimensional stacked vector for the l-th symbol after the spread spectrum demodulation as

$$\mathbf{Y}(l) = \left[\mathbf{y}_0^T(l), \ldots, \mathbf{y}_{(M-1)}^T(l)\right]^T = \sqrt{P}Ld(l)\mathbf{C} + \boldsymbol{\Upsilon}(l) + \boldsymbol{\Psi}(l), \tag{5.30}$$

where $\mathbf{C}^T = \left[\mathbf{c}_0^T, \ldots, \mathbf{c}_{M-1}^T\right]$ is the vector of channel coefficients. The interference and noise vectors are $\boldsymbol{\Upsilon}^T(l) = \left[\boldsymbol{\Upsilon}_0^T(l), \ldots, \boldsymbol{\Upsilon}_{M-1}^T(l)\right]$ and $\boldsymbol{\Psi}^T(l) = \left[\boldsymbol{\Psi}_0^T(l), \ldots, \boldsymbol{\Psi}_{M-1}^T(l)\right]$, respectively.

Using similar procedure as shown before, the maximum SINR at the output of the joint ST combiner can be shown to be given by

$$\mu_{jd} = PL^2 \sum_{l=1}^{NM} \frac{|s_l|^2}{\lambda_l}, \tag{5.31}$$

where $\mathbf{s}^T = [s_1, \ldots, s_{NM}]$, $\{\lambda_l\}$ are the eigenvalues of $\mathbf{R} = \boldsymbol{\Upsilon}\boldsymbol{\Upsilon}^H + (\sigma^2 L)\mathbf{I}_{NM}$ and $\mathbf{I}_{NM}$ is the identity matrix of dimension NM. Each of $\{|s_l|^2\}$ is a chi-square random variable with two degrees of freedom. The eigenvalues $\{\lambda_l\}$ of $\mathbf{R}$ are

$$\lambda_l = \begin{cases} \lambda_l & l = 1, \ldots, r \\ \sigma^2 L & l = r+1, \ldots, NM, \end{cases}$$

where $1 \leq r \leq M$. The value of r depends on the bandwidth (BW) of the narrowband interference, which in turn determines the number of principal eigenvalues (eigenvalues containing most of the interference power) of $\mathbf{R}$. The number of principal eigenvalues can be predicted by the Landau-Pollak theorem and is $r \approx p(M-1)+1$, where $p = \frac{T_c}{T_i}$ and M is the number of taps in the temporal processor. Clearly, when the interference BW is very small compared to DS-CDMA signal BW, $r = 1$, whereas when the interference BW is same as DS-CDMA BW, $r = M$. Also, when $M = 1$, i.e., spatial processing only, $r = 1$ regardless of the value of p, demonstrating the robustness of spatial processor with respect to interference BW.

5.4.1 Distribution of SINR for Joint ST Combiner

The characteristic function of μ is given by

$$\phi_\mu(jw) = \left(\prod_{l=1}^{r} \frac{1}{(1 - jw\gamma_l)} \right) \frac{1}{(1 - jw\gamma_o)^{NM-r}}, \tag{5.32}$$

where $\gamma_l = \frac{LP_s}{\lambda_l}$ and $\gamma_o = \frac{P_s}{\sigma^2}$. The PDF of μ can now be obtained:

$$f_\mu(\mu) = \frac{\gamma_o^{-(NM-r)} \mu^{(NM-r)}}{\Gamma(NM-r+1)} \sum_{l=1}^{r} \frac{\pi_l e^{\frac{-\mu}{\gamma_l}} {}_1F_1\left(NM-r; NM-r+1; \left(\frac{1}{\gamma_l} - \frac{1}{\gamma_o}\right)\mu\right)}{\gamma_l}, \tag{5.33}$$

where $\pi_l = \prod_{k=1, k\neq l}^{r} \frac{\gamma_l}{\gamma_l - \gamma_k}$. Here, it was assumed that $\{\lambda_l, l = 1, \ldots, r\}$ are distinct. If they are equal, the characteristic function and the PDF of μ can easily be derived using eqs. (5.21), (5.22).

5.4.2 Asymptotic Efficiency of Joint Space-Time Combiner

Following a similar procedure as shown in previous sections, the asymptotic efficiency of the joint ST combiner can be shown to be:

$$\zeta = 1 - \frac{r}{NM}, \qquad 1 \leq r \leq M. \tag{5.34}$$

Interestingly, when the interference BW equals DS-CDMA BW, i.e., $r = M$, the asymptotic efficiencies of the COSST combiner and joint domain optimum combiner are identical.

5.5 Average Probability of Bit Error Rate Calculations

In this section we calculate the BER for the spatial optimum combiner, COSST combiner and joint ST optimum combiner. The sum of residual interference and noise at the output of the ST combiner (array) is assumed Gaussian.

The BER is simply

$$\begin{aligned} P_e &= \int_0^\infty \frac{1}{2}\mathrm{erfc}(\sqrt{\mu}) f_\mu(\mu) d\mu \\ &= \frac{1}{2} - \frac{1}{2}\int_0^\infty \mathrm{erf}(\sqrt{\mu}) f_\mu(\mu) d\mu, \end{aligned} \tag{5.35}$$

where $\mathrm{erf}(\cdot)$ and $\mathrm{erfc}(\cdot)$ are the error and the complementary error functions, respectively and $f_\mu(\mu)$ is the PDF of μ.

5.5.1 BER of the Spatial Combiner

As shown in Appendix C, the BER for the spatial combiner is:

$$P_e = \frac{1}{2} - \frac{(JN+\sigma^2)\Gamma(N+\frac{1}{2})P_s^{N+\frac{1}{2}} F_2\left(N+\frac{1}{2}, 1, N-1; \frac{3}{2}, N; \frac{P_s}{JN+\sigma^2+P_s}, \frac{JN}{JN+\sigma^2+P_s}\right)}{\sqrt{\pi}\sigma^2\Gamma(N)h^N(JN+\sigma^2+P_s)^{N+\frac{1}{2}}}, \tag{5.36}$$

where $F_2(\cdot)$ is Appell's hypergeometric function of two variables.

5.5.2 BER of the COSST

As shown in Appendix C, the BER for the COSST is:

$$P_e = \frac{1}{2} - \frac{(JN+\sigma^2)^M \Gamma(NM+\frac{1}{2})}{\sqrt{\pi}(\sigma^2)^M \Gamma(NM) h^{NM} (\frac{JN+\sigma^2+P_s}{P_s})^{NM+\frac{1}{2}}} F_2\left(NM+\frac{1}{2}, 1, (N-1)M; \frac{3}{2}, NM; \frac{P_s}{JN+\sigma^2+P_s}, \frac{JN}{JN+\sigma^2+P_s}\right). \quad (5.37)$$

5.5.3 BER of the Joint ST Combiner

As shown in Appendix C, the BER for the joint ST combiner is:

$$P_e = \frac{1}{2} - \sum_{l=1}^{r} \frac{\Gamma(NM-r+\frac{3}{2})\pi_l}{\sqrt{\pi}\Gamma(NM-r+1)\gamma_o{}^{(NM-r)}\gamma_l(1+\frac{1}{\gamma_l})^{NM-r+\frac{3}{2}}} F_2\left(NM-r+\frac{3}{2}, 1, NM-r; \frac{3}{2}, NM-r+1; \frac{\gamma_l}{\gamma_l+1}, \frac{1-\frac{\gamma_l}{\gamma_o}}{\gamma_l+1}\right) \quad (5.38)$$

Equations (5.36), (5.37) and (5.38), though exact, do not offer any meaningful insight. Hence, meaningful upper bounds of these BERs are derived.

5.6 Upper Bound on the BERs of the Space-Time Receivers

In this section, we derive upper bounds on the BERs derived in the previous sections.

5.6.1 Upper Bound on the BER of the Spatial Combiner

Using the bound [46] $\text{erfc}(\sqrt{\mu}) < e^{-u}$ in eq. (5.35), we get

$$P_e < \frac{1}{2}\int_0^\infty e^{-\mu} f_\mu(\mu) d\mu = \frac{1}{2}\int_0^\infty \frac{(JN+\sigma^2)\mu^{N-1} e^{-\left(\frac{JN+\sigma^2}{P_s}+1\right)\mu} {}_1F_1\left(N-1; N; \frac{JN\mu}{P_s}\right)}{\sigma^2\Gamma(N)h^N}, \quad (5.39)$$

Using the identity [43]

$$\int_0^\infty e^{-st} t^{a-1} {}_1F_1(c; a; xt) dt = \frac{\Gamma(a)}{s^a}\left(1-\frac{x}{s}\right)^{-c} \quad (5.40)$$

in eq. (5.39), we get

$$P_e < \frac{(JN+\sigma^2)}{2(JN+\sigma^2+P_s)(1+\frac{P_s}{\sigma^2})^{N-1}}. \tag{5.41}$$

This expression provides useful insight into a few special cases. When there is no interference, i.e., $J = 0$, $P_e < \frac{1}{2(1+h)^N}$. This is the upper bound for the BER of an N-th order space diversity receiver employing maximal ratio combining (MRC) without interference, as expected. When the interference power is infinite, i.e., $J \to \infty$, the expression becomes $P_e < \frac{1}{2(1+h)^{N-1}}$. This is the upper bound for the BER of an $(N-1)$-th order diversity MRC receiver without interference. This implies that the presence of interference with infinite power in the channel, results in the loss of one diversity path. This result was previously mentioned in the case of a Rayleigh fading interference.

5.6.2 Upper Bound on the BER of COSST

Following a similar procedure as shown above, the upper bound on the BER of COSST can be shown to be given by

$$P_e < \frac{(JN+\sigma^2)^M}{2(JN+\sigma^2+P_s)^M(1+\frac{P_s}{\sigma^2})^{(N-1)M}}. \tag{5.42}$$

Clearly, the COSST combiner, without interference, performs as an NM-th order diversity receiver, whereas presence of an interference with infinite power, results in a loss of M DOF.

5.6.3 Upper Bound on the BER of Joint ST Processor

Following a similar procedure as shown above, the upper bound on the BER of joint ST combiner can be shown to be given by

$$\begin{aligned} P_e &< \frac{1}{2}\sum_{l=1}^{r}\frac{\pi_l}{(1+\gamma_l)(1+\gamma_o)^{NM-r}} \\ &= \frac{1}{2}\frac{1}{(1+\gamma_1)(1+\gamma_2)\ldots(1+\gamma_r)(1+\gamma_o)^{NM-r}}. \end{aligned} \tag{5.43}$$

Without interference, the joint processor performs as an NM-th order diversity receiver. With interference of infinite power, it performs as an $(NM - r)$-th order diversity receiver. The number of principal eigenvalues r depends on the BW of the narrowband interference. When the BW of the narrowband interference approaches the BW of the DS-CDMA signal, i.e., $r = M$, the joint processor and the COSST processor show similar performance.

5.7 Discussion of Results

This section presents both analytical and simulation results on the performance of the ST combining schemes studied in the previous sections. The channel was modeled with $M = 4$ taps. The data symbols were modulated by Gold sequence of length $L = 31$ and $T_b = T_i = LT_c = 31$. The interference-to-signal ratio prior to spread spectrum demodulation (at the input of the correlators) is $J/S = 25$ dB, where the signal power $S = P\beta$, and $\beta = \mathrm{E}\{\mid c_{nm} \mid^2\}$. The number of antennas $N = 2$ and the offset of the interference carrier frequency $\nu = \frac{1}{LT_c} = \frac{1}{31}$.

In Figure 5.5, the BER is plotted as a function of the average total SNR $= NM\frac{P_s}{\sigma_2}$. Covariance matrices and cross-correlation vectors used for optimum combining (OC) were estimated from blocks of 50 samples. The simulation results shown are averages of 4000 Monte Carlo runs. The COSST simulations provide a good match to the theoretical BER curve. In this case the ratio of the number of samples used to estimate the covariance matrix and the signal dimension is $\frac{50}{2}$ (OC is carried out only in the spatial domain with two antennas). Notice that the COSST and the COSOT show similar performance. For the joint ST case the simulation curve indicates slightly higher BER's than predicted by theory. This is explained by the covariance matrix estimation errors. In this case the ratio of the number of samples used to estimate the covariance matrix and the signal dimension is $\frac{50}{8}$ $(NM = 8)$. The effect of the number of samples used to estimate the covariance

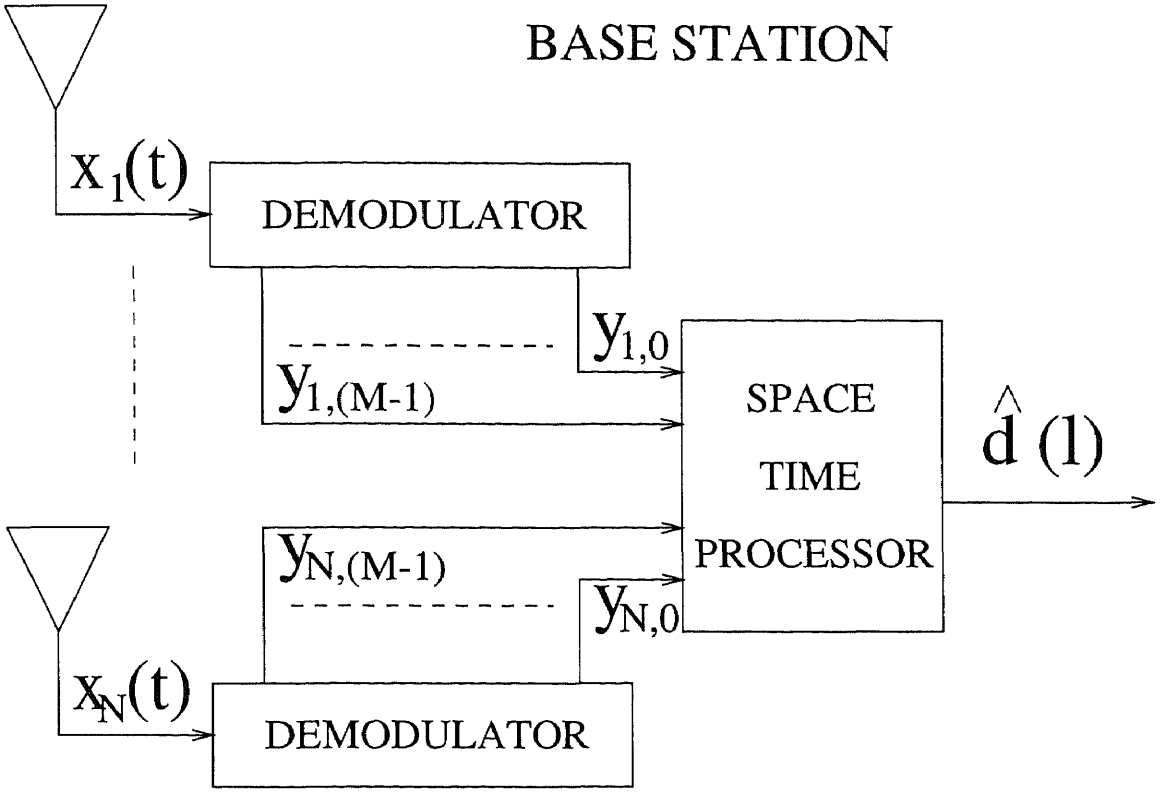

Figure 5.1 General configuration of space-time receiver.

matrix is illustrated in Figure 5.6 where the joint ST simulations were generated using 50 and 100 samples estimates. A closer match between theory and simulations is clearly evident when the number of samples used to estimate the covariance matrix is increased.

In Figure 5.7, the BER of the overlay system is shown as a function of the ratio p of the interference BW to the DS-CDMA signal BW. The performance of the COSST and the COSOT combiners is not affected by the interference BW as mentioned in the previous section. The performance of the joint ST combiner approaches that of the COSST when the $p = 1$, as indicated by the asymptotic efficiency expression derived in the earlier section.

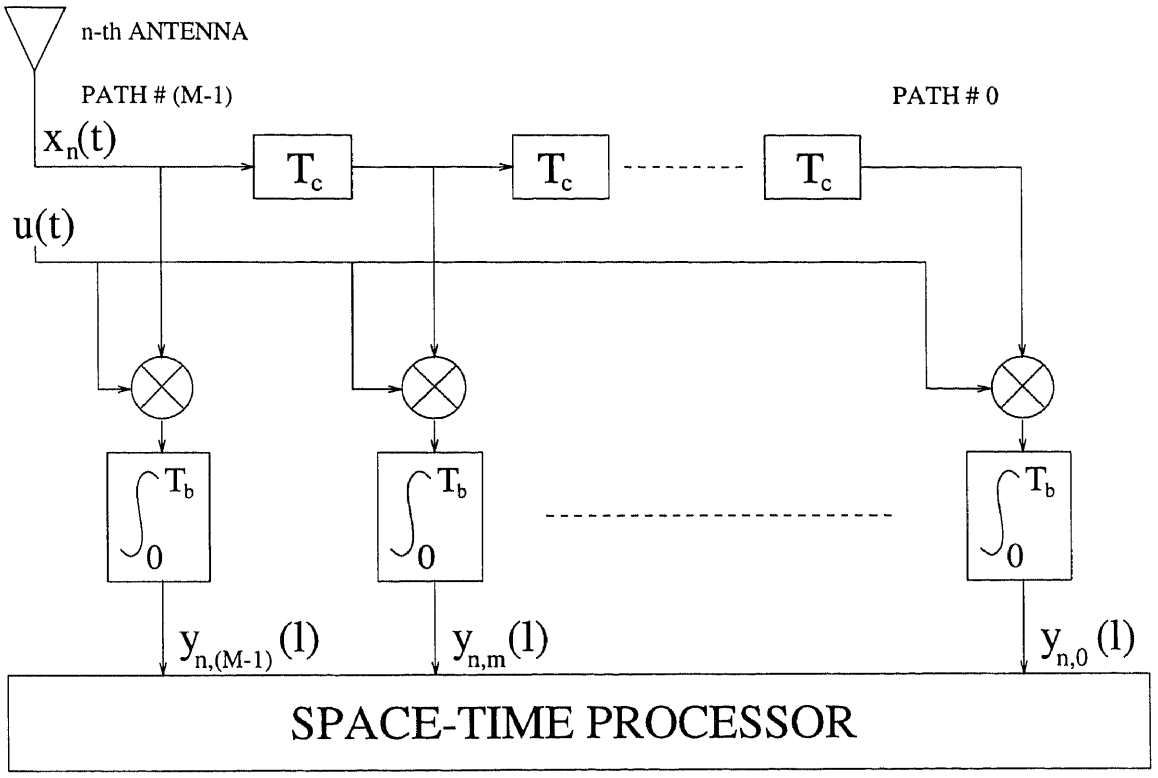

Figure 5.2 Demodulator.

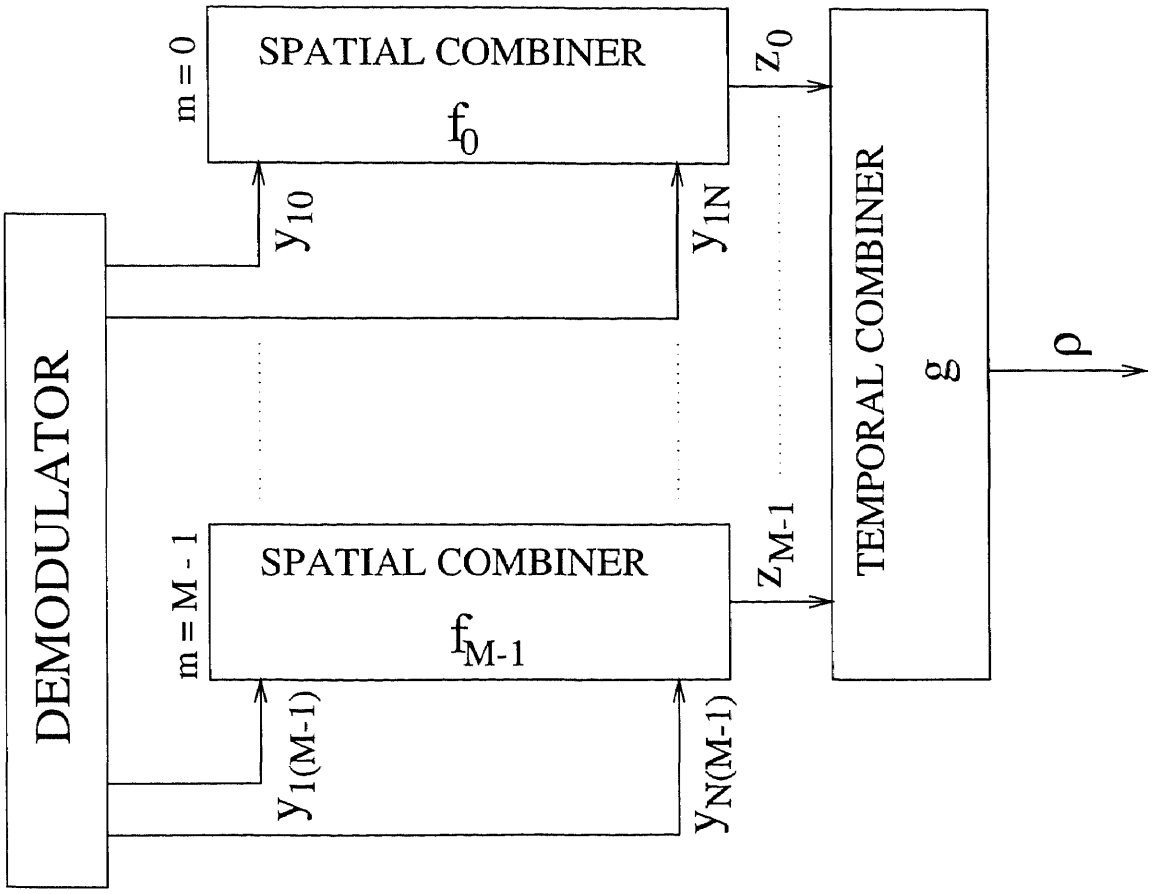

Figure 5.3 Configuration of cascade space-time processing.

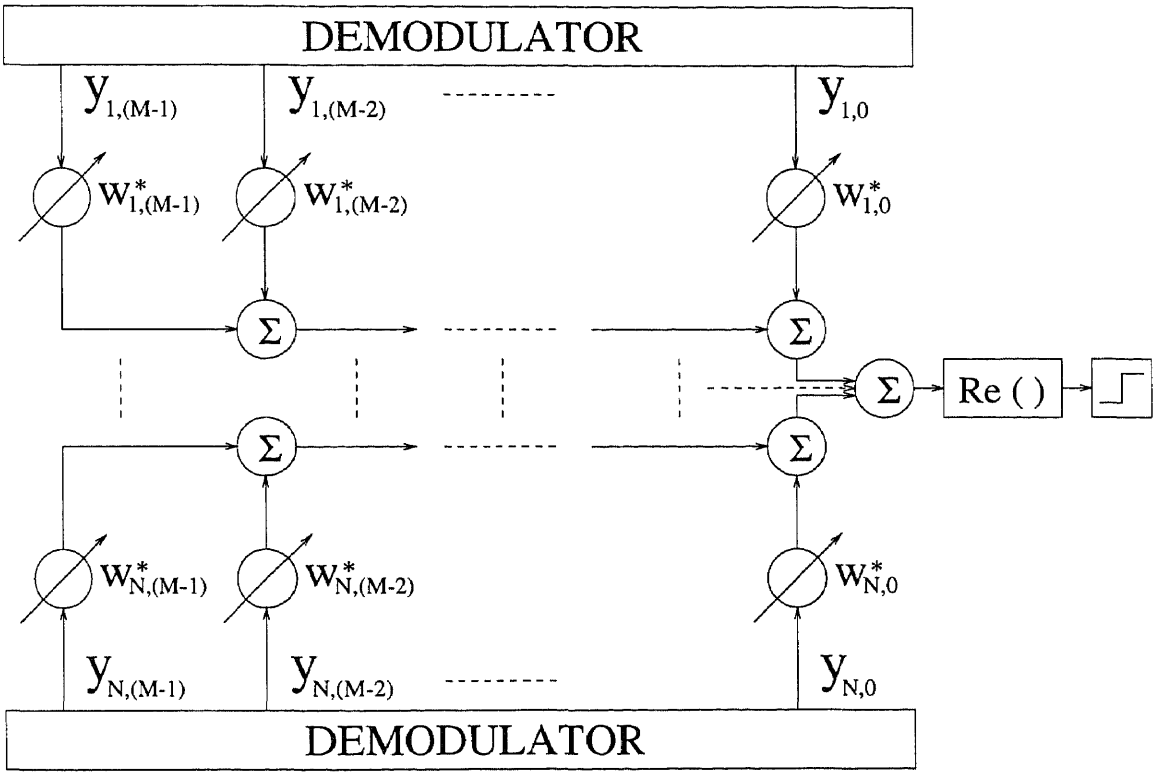

Figure 5.4 Configuration of joint space-time processing.

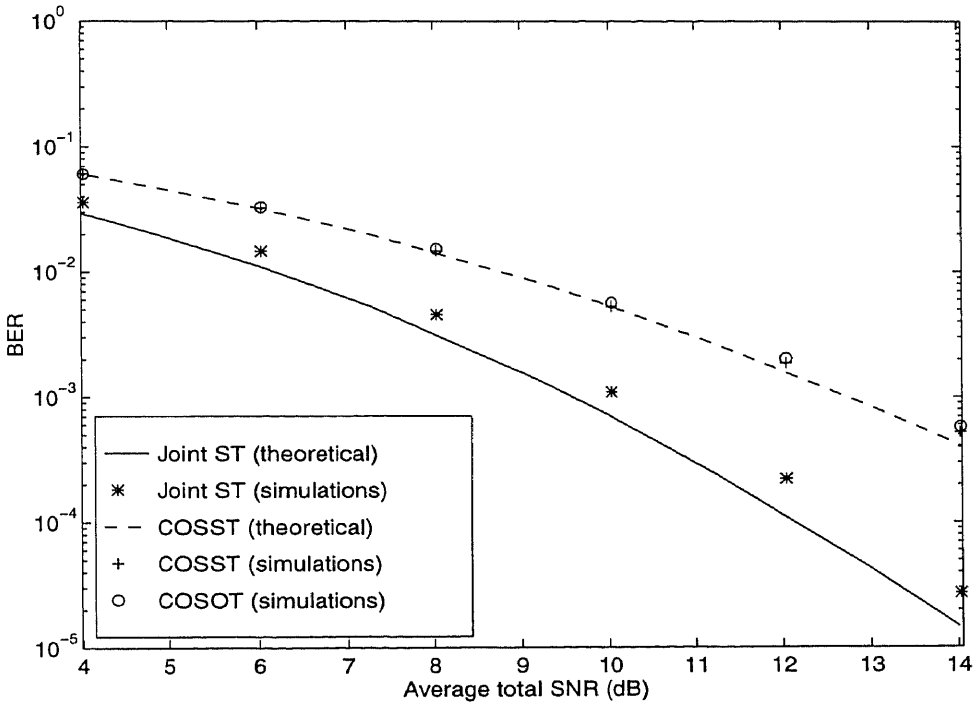

Figure 5.5 BER of space-time receiver for DS-CDMA overlay system.

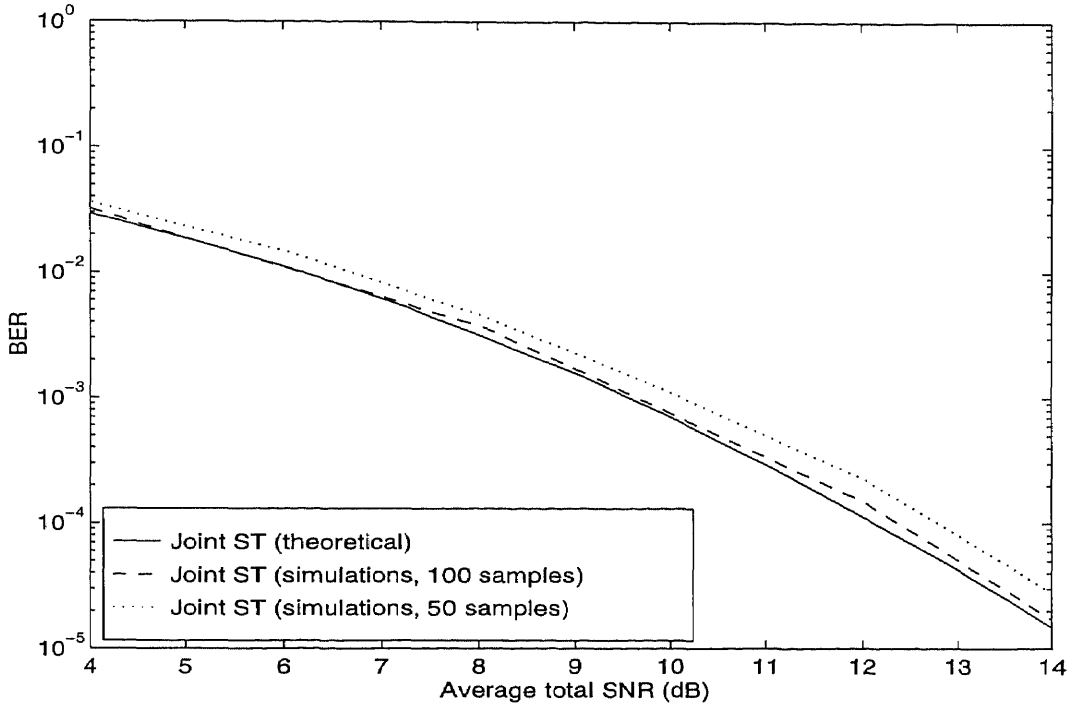

Figure 5.6 BER of the joint space-time optimum combiner.

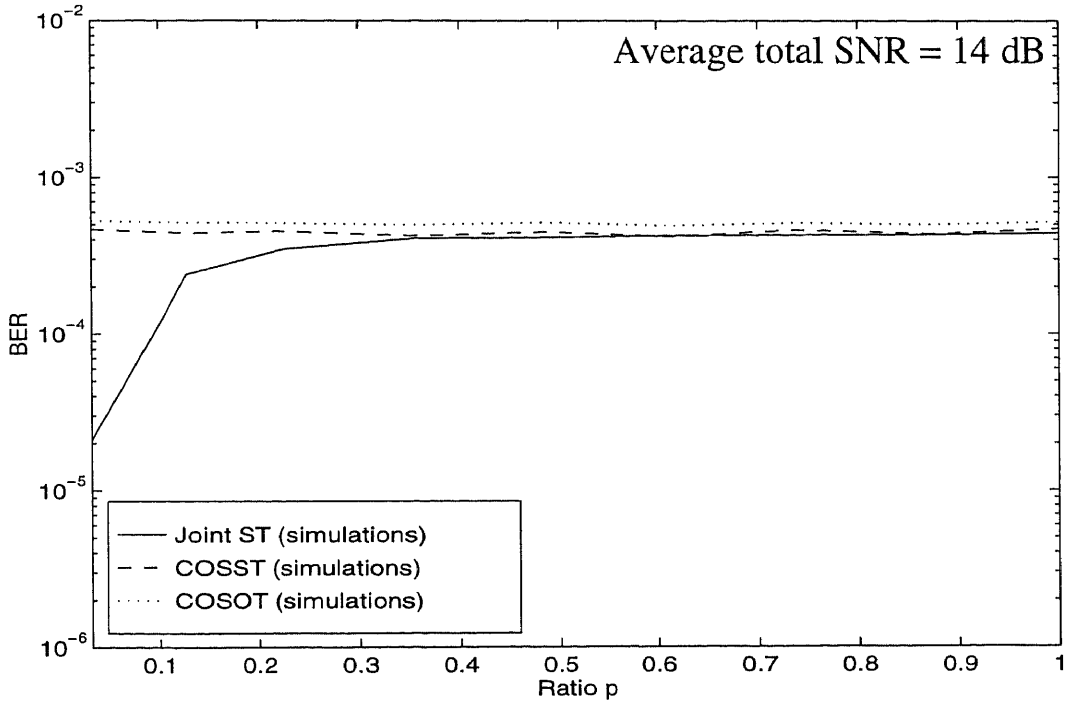

Figure 5.7 Performance of the space-time receiver as a function of ratio p.

CHAPTER 6

SPACE-TIME NARROWBAND INTERFERENCE SUPPRESSION IN DS-CDMA COMMUNICATION FOR PCS (MULTIPLE USERS)

In the previous chapter, the performance of various space-time (ST) receiver architectures was evaluated for a single user direct-sequence code division multiple access (DS-CDMA) system overlaying a narrowband waveform. In this chapter, we evaluate the performance of these receivers for a multiuser asynchronous DS-CDMA overlay system. We further study the average probability of bit error rate (BER), and how this performance is influenced by various parameters.

6.1 Signal Model

Consider a cell site with K active users. The transmitted signal for the kth DS-CDMA user is given by

$$S_k(t) = \sqrt{2P_k}\, d_k(t)\, u_k(t)\, \cos(2\pi f_o t + \theta_k), \tag{6.1}$$

where P_k is the average power of the signal, $d_k(t) \in \{-1, 1\}$ is a random binary sequence representing data, $u_k(t) \in \{-1, 1\}$ is the signature sequence, f_o is the carrier frequency, and θ_k is the random phase introduced by the BPSK modulator uniformly distributed between $[0, 2\pi]$. The processing gain is $D = T_b/T_c$, where T_b is the bit duration and T_c is the chip duration. For a DS-CDMA signal with chip duration T_c, the spread spectrum bandwidth is approximately $B_s = 2/T_c$.

The narrowband interference is assumed to be a non-fading BPSK signal given by

$$J(t) = \sqrt{2J}\, b(t)\, \cos(2\pi(f_o + \nu)t + \vartheta), \tag{6.2}$$

where ν is the offset of the interference carrier frequency from the DS-CDMA signal carrier frequency and parameters J and ϑ denote the received interference power and phase, respectively. The information sequence $b(t) \in \{-1, 1\}$ has bit rate $1/T_i$,

where T_i is the bit duration. The interference bandwidth $B_i = 2/T_i$ and $B_i \ll B_s$. The ratio of the interference bandwidth to the DS-CDMA bandwidth is given by $p = \frac{B_i}{B_s} = \frac{T_c}{T_i}$. The ratio of the offset of the interference carrier frequency to half of the DS-CDMA bandwidth is defined by $q = \frac{2\nu}{B_s} = \nu T_c$.

The base station uses an N-element uniform linear array, with array elements sufficiently separated such that spatial diversity (independent fading at each receive antenna) is achieved with respect to the DS-CDMA signals. The general configuration at the base station is shown in Figure 5.1. The signal received from the desired user is denoted $S_1(t)$, while signals received from the other users are considered cochannel interferences with respect to the desired user. The equivalent baseband received signal at the n-th antenna can be written as

$$\begin{aligned} x_n(t) &= \sqrt{P} \sum_{m=0}^{M-1} c_{nm}^{(1)}\, d_1(t - mT_c - \tau_1)\, u_1(t - mT_c - \tau_1) \\ &\quad + \sqrt{P} \sum_{k=2}^{K} \sum_{m=0}^{M-1} c_{nm}^{(k)}\, d_k(t - mT_c - \tau_k)\, u_k(t - mT_c - \tau_k) \\ &\quad + \xi_n(t) + v_n(t), \end{aligned} \tag{6.3}$$

where $\{c_{nm}^{(k)}\}$, $k = 1, \ldots, K$, $m = 0, \ldots, (M-1)$, $n = 1, \ldots, N$ represent the complex-valued tap coefficients of the fading channels as seen by each of the DS-CDMA users. The number of resolvable paths is M. Samples of $\{c_{nm}^{(k)}\}$ are statistically independent between users k, between paths m, and between antenna elements n. The fact that all $\{P_k = P\}$ implies that the base station provides adaptive power control such that received signals from all K users have the same average power (to overcome the so called near-far problem). The received signals are assumed asynchronous, with τ_k denoting the delay of the k-th user uniformly distributed between $[0, T_b]$. Without loss of generality, we set $\tau_1 = 0$. The quantity $\xi_n(t)$ is the narrowband interference at the n-th antenna and is given by eq. (5.8). The additive noise $v_n(t)$ is modeled as complex white Gaussian with zero mean and variance σ^2. We assume perfect code synchronization.

The received signal at each antenna passes through the tap-delay line and is fed into the correlators for spread spectrum demodulation. The tap-delay line compensates for the delay propagation in the channel, providing the time alignment for demodulation with the desired user's signature $u_1(t)$. The output at the m-th tap correlator at the n-th antenna for the l-th symbol is given by

$$\begin{aligned} y_{nm}(l) &= \int_{lT_b}^{(l+1)T_b} x_n(t+mT_c)\, u_1(t)\, dt \\ &= \int_{lT_b}^{(l+1)T_b} \left\{ \sqrt{P} \sum_{i=0}^{M-1} c_{ni}^{(1)}\, d_1(t+mT_c-iT_c)\, u_1(t+mT_c-iT_c) \right\} u_1(t)dt \\ &+ \int_{lT_b}^{(l+1)T_b} \\ &\quad \left\{ \sqrt{P} \sum_{k=2}^{K} \sum_{i=0}^{M-1} c_{ni}^{(k)} d_k(t+mT_c-iT_c-\tau_k) u_k(t+mT_c-iT_c-\tau_k) \right\} u_1(t)dt \\ &+ \int_{lT_b}^{(l+1)T_b} \xi_n(t+mT_c)u_1(t)dt + \int_{lT_b}^{(l+1)T_b} v_n(t+mT_c)u_1(t)dt. \end{aligned} \tag{6.4}$$

As shown in the Appendix I, $y_{nm}(l)$ can be written explicitly in terms of the contributions of the desired user, cochannel interferences, narrowband interference and noise:

$$\begin{aligned} y_{nm}(l) &= \sqrt{P}d_1(l)B_{nm(0)}^{(1)} + \sqrt{P}d_1(l+1)B_{nm(1)}^{(1)} + \sqrt{P}d_1(l-1)B_{nm(-1)}^{(1)} \\ &+ \sum_{k=2}^{K} \left\{ \sqrt{P}d_k(l)B_{nm(0)}^{(k)} + \sqrt{P}d_k(l+1)B_{nm(1)}^{(k)} + \sqrt{P}d_k(l-1)B_{nm(-1)}^{(k)} \right\} \\ &+ \xi_{nm}(l) + \eta_{nm}(l), \end{aligned} \tag{6.5}$$

where $B_{nm(\alpha)}^{(1)}$, $\alpha = 0, 1, -1$, represents the aggregate cross-correlation with the desired user signature waveform $u_1(t)$ of all paths and symbols d_1, as seen at the m-th tap delay and at the n-th antenna. $B_{nm(\alpha)}^{(1)}$ consists of contributions of the current symbol $d_1(l)$, as well as the previous and the next symbols. Similarly, $B_{nm(\alpha)}^{(k)}$ represent contributions of the cochannel interferences $d_k(l+\alpha)$, $k = 2, \ldots, K$, to the output of the cross-correlation with $u_1(t)$. The term $\xi_{nm}(l)$ is the narrowband interference at the output of the matched filter. The quantity $\eta_{nm}(l)$ is the noise

at the output of the matched filter. Subsequent to the slow fading model assumed, coefficients $\{B^{(k)}_{nm(\alpha)}\}$ are constant during the processing interval.

6.2 Space-Time Optimum Combining

We consider two approaches to ST optimum combining (OC): cascade ST and joint ST. The cascade ST processor consists of a temporal processor using the outputs of the spatial processor as shown in Figure 5.3. The joint ST processor is applied simultaneously to all the signals in the array/tap-delay line structure.

6.2.1 Spatial Combiner

Spatial processing combines the signals following spread spectrum demodulation, i.e., it combines the signals y_{nm} for each m. Define the N-dimensional array vector at the output of the m-th tap matched filter for the l-th symbol as $\mathbf{y}^T_m(l) = [y_{1m}(l), \ldots, y_{Nm}(l)]$. As can be seen from eq. (6.5), this output consists of the desired user signal, interference and noise, and can be written as

$$\mathbf{y}_m(l) = \sqrt{P} d_1(l) \mathbf{B}^{(1)}_{m(0)} + \boldsymbol{\Upsilon}_m(l) + \boldsymbol{\Psi}_m(l), \tag{6.6}$$

where $\mathbf{B}^{(1)}_{m(0)} = \left[B^{(1)}_{1m(0)}, \ldots, B^{(1)}_{Nm(0)}\right]^T$. The quantity $\boldsymbol{\Psi}_m(l) = [\eta_{1m}(l), \ldots, \eta_{Nm}(l)]^T$ is the noise array vector. The interference array vector, which consists of self-interference, cochannel interferences, and narrowband interference, can be expressed as

$$\boldsymbol{\Upsilon}_m(l) = \sum_{k=1}^{K} \sum_{\substack{\alpha=-1 \\ \alpha \neq 0 \text{ if } k=1}}^{1} \sqrt{P} d_k(l+\alpha) \mathbf{B}^{(k)}_{m(\alpha)} + \boldsymbol{\Xi}_m(l), \tag{6.7}$$

where $\boldsymbol{\Xi}_m(l) = [\xi_{1m}(l), \ldots, \xi_{Nm}(l)]^T$ is the narrowband interference vector. The reason α is not equal to 0 when k equals 1 is because it is the desired term. Following spatial processing with the spatial weight vector $\mathbf{f}_m$, the spatial output at the m-th tap-delay line is $z_m(l) = \mathbf{f}^H_m \mathbf{y}_m(l)$. Due to the independence between successive symbols of the same user, as well as mutual independence between DS-CDMA users,

the narrowband interference, and the noise, the cross-correlation of the array vector and the desired signal at the m-th tap-delay is given by

$$\mathbf{r}_m = \mathrm{E}\left[\mathbf{y}_m(l)d_1(l)\right] = \sqrt{P}\mathbf{B}^{(1)}_{m(0)}. \tag{6.8}$$

The cross-correlation vector $\mathbf{r}_m$ can be estimated using a training sequence or previous bit estimates $\widehat{d_1}(l)$:

$$\widehat{\mathbf{r}}_m = \frac{1}{L}\sum_{i=1}^{L}\mathbf{y}_m(i)\widehat{d_1}(i), \tag{6.9}$$

where L is the number of samples used in the estimation. The optimum weight vector, which maximizes the signal-to-interference-plus-noise ratio (SINR) at the output of the spatial combiner is given by

$$\mathbf{f}_m = \mathbf{R}_m^{-1}\mathbf{r}_m, \tag{6.10}$$

where $\mathbf{R}_m$ is the interference-plus-noise covariance matrix at the output of the m-th correlator and is defined as:

$$\mathbf{R}_m = \mathrm{E}\left[\left\{\mathbf{y}_m(l) - d_1(l)\mathbf{r}_m\right\}\left\{\mathbf{y}_m(l) - d_1(l)\mathbf{r}_m\right\}^H\right]. \tag{6.11}$$

The covariance matrix can be estimated similar to the cross-correlation vector:

$$\widehat{\mathbf{R}}_m = \frac{1}{L}\sum_{i=1}^{L}\left[\mathbf{y}_m(i) - \widehat{d_1}(i)\widehat{\mathbf{r}_m}\right]\left[\mathbf{y}_m(i) - \widehat{d_1}(i)\widehat{\mathbf{r}_m}\right]^H. \tag{6.12}$$

$\widehat{\mathbf{R}}_m$ is the maximum likelihood estimate of $\mathbf{R}_m$ and is the time-averaged sample covariance matrix. When the statistics are estimated from the data samples, the solution is not necessarily optimal and is affected by the quality of the estimates. In [65], it has been shown that at least $L = 2N$ samples of data is required in order to obtain a solution within 3 dB of the optimal SINR, i.e., when the covariance matrix is known priori. The number of data samples $L \geq N$ will guarantee the existence of the inverse of the sample covariance matrix $\widehat{\mathbf{R}}_m$ [57].

6.2.2 Space-Time Combiner

Let $\mathbf{z}(l) = [z_0(l), \ldots, z_{M-1}(l)]$ be a vector that consists of the M outputs of the spatial combiners. The vector $\mathbf{z}(l)$ is fed into the temporal combiner. It can be expressed as

$$\mathbf{z}(l) = \sqrt{P} d_1(l)\mathbf{U} + \boldsymbol{\Upsilon}_t + \boldsymbol{\Psi}_t, \tag{6.13}$$

where $\mathbf{U}^T = \left[\mathbf{f}_0^H \mathbf{B}_{0(0)}^{(1)}, \ldots, \mathbf{f}_{M-1}^H \mathbf{B}_{(M-1)(0)}^{(1)}\right]$. The interference and noise vectors are $\boldsymbol{\Upsilon}_t^T = \left[\mathbf{f}_0^H \boldsymbol{\Upsilon}_0, \ldots, \mathbf{f}_{M-1}^H \boldsymbol{\Upsilon}_{(M-1)}\right]$ and $\boldsymbol{\Psi}_t^T = \left[\mathbf{f}_0^H \boldsymbol{\Psi}_0, \ldots, \mathbf{f}_{M-1}^H \boldsymbol{\Psi}_{(M-1)}\right]$, respectively. The output of the cascade ST combiner is $\rho(l) = \mathbf{g}^H \mathbf{z}(l)$, where $\mathbf{g}$ is the temporal weight vector. Assuming mutual independence of the terms in eq. (6.13), the cascade ST cross-correlation vector is given by

$$\mathbf{r}_t = \mathrm{E}\left[\mathbf{z}(l) d_1(l)\right] = \sqrt{P}\mathbf{U}. \tag{6.14}$$

The optimum weight vector, which maximizes SINR at the output of the temporal processor is given by

$$\mathbf{g} = \mathbf{R}_t^{-1} \mathbf{r}_t, \tag{6.15}$$

where $\mathbf{R}_t$ is the interference-plus-noise covariance matrix at the input of the temporal combiner and is defined as:

$$\mathbf{R}_t = \mathrm{E}\left[\left\{\mathbf{z}(l) - d_1(l)\mathbf{r}_t\right\}\left\{\mathbf{z}(l) - d_1(l)\mathbf{r}_t\right\}^H\right]. \tag{6.16}$$

The SINR at the output of the cascade ST combiner is given by

$$\mu = \frac{P\mathrm{E}\left[\left|\mathbf{g}^H\mathbf{U}\right|^2\right]}{\mathrm{E}\left[\left|\mathbf{g}^H\boldsymbol{\Upsilon}_t\right|^2\right] + \mathrm{E}\left[\left|\mathbf{g}^H\boldsymbol{\Psi}_t\right|^2\right]}, \tag{6.17}$$

where P is the desired signal power and E denotes expectation. The expectation is taken with respect to the noise over a time interval during which the channel is considered constant. Thus, μ is a random variable parameterized by the channel $B_{nm(\alpha)}^{(k)}$. When the number of active users K is large and power control is incorporated, then according to the central limit theorem, the sum of the residual interference (self, cochannel, and narrowband) and noise can be approximated by a

Gaussian random variable. Thus, BER conditioned on μ (a specific set of fading channels, under the above Gaussian assumption) is given by

$$P_{e|\mu} = \mathrm{Q}(\sqrt{2\mu}), \tag{6.18}$$

where $\mathrm{Q}(\cdot)$ is the area under the tail of the Gaussian probability density function and is given by eq. (3.17). The unconditional BER, i.e., the one averaged over all fading channels, is then given by

$$P_e = \int_0^\infty \mathrm{Q}(\sqrt{2\mu})\ f_\mu(\mu)\ d\mu, \tag{6.19}$$

where $f_\mu(\mu)$ is the probability density function of μ.

6.2.3 Joint Space-Time Combiner

With the joint domain combiner, processing is carried out simultaneously in the space-time domains. To formulate the joint space-time optimum weight vector, define the NM-dimensional stacked vector for the l-th symbol after the spread spectrum demodulation as

$$\mathbf{Y}(l) = \left[\mathbf{y}_0^T(l), \ldots, \mathbf{y}_{(M-1)}^T(l)\right]^T = \sqrt{P} d_1(l)\mathbf{B}_0 + \boldsymbol{\Upsilon}(l) + \boldsymbol{\Psi}(l), \tag{6.20}$$

where $\mathbf{B}_0^T = \left[\mathbf{B}_{0(0)}^{(1)T}, \ldots, \mathbf{B}_{(M-1),(0)}^{(1)T}\right]$. The interference and noise vectors are $\boldsymbol{\Upsilon}^T(l) = \left[\boldsymbol{\Upsilon}_0^T(l), \ldots, \boldsymbol{\Upsilon}_{(M-1)}^T(l)\right]$ and $\boldsymbol{\Psi}^T(l) = \left[\boldsymbol{\Psi}_0^T(l), \ldots, \boldsymbol{\Psi}_{(M-1)}^T(l)\right]$, respectively. The joint domain cross-correlation vector and interference-plus-noise covariance matrix are given by

$$\mathbf{r} = \mathrm{E}[\mathbf{Y}(l) d_1(l)] = \sqrt{P}\mathbf{B}_0 \tag{6.21}$$

and

$$\mathbf{R} = \mathrm{E}\left[\{\mathbf{Y}(l) - d_1(l)\mathbf{r}\}\{\mathbf{Y}(l) - d_1(l)\mathbf{r}\}^H\right], \tag{6.22}$$

respectively. The joint domain optimum weight vector, which maximizes the SINR, is given by

$$\mathbf{w} = \mathbf{R}^{-1}\mathbf{r}. \tag{6.23}$$

The SINR at the output of the joint ST optimum combiner is given by

$$\mu = \frac{P\mathrm{E}\left[\left|\mathbf{w}^H\mathbf{B}_0\right|^2\right]}{\mathrm{E}\left[\left|\mathbf{w}^H\boldsymbol{\Upsilon}\right|^2\right] + \mathrm{E}\left[\left|\mathbf{w}^H\boldsymbol{\Psi}\right|^2\right]}. \tag{6.24}$$

6.3 Numerical Results

This section presents numerical results on the performance of the ST combining schemes studied in the previous section. The channel was modeled with $M = 4$ taps. The data symbols were modulated by Gold sequences of length $D = 127$. The narrowband interference-to-signal ratio at the input of the correlators is $J/S = 25$ dB, where the signal power $S = P\beta$, and $\beta = \mathrm{E}\left[\mid c_{nm}^{(k)} \mid^2\right]$. Covariance matrices and cross-correlation vectors were estimated from blocks of 31 symbols using relations similar to those in eqs. (6.12) and (6.9), respectively. Curves shown are averages of 2000 Monte Carlo runs.

Figure 6.1 shows the BER performance of the DS-CDMA system as a function of the average total signal-to-noise ratio $\bar{\gamma}_b$ for $N = 2$. The average total signal-to-noise ratio is $\bar{\gamma}_b = NM\bar{\gamma}_c$, where $\bar{\gamma}_c$ is the average signal-to-noise ratio per path and is given by $\bar{\gamma}_c = \frac{P}{\sigma^2}\beta$. Clearly, the joint ST processor outperforms the cascade version. The difference in performance between the cascade and the joint processors is a consequence of the number of DOF available to each configurations. The cascade configuration has $(N + M - 2)$ DOF, with respect to interference cancellation, while joint configuration has $(NM - 1)$. Since the number of cochannel interferences $K \gg NM$, each additional DOF provides increased performance. Note that as $\bar{\gamma}_b$ increases, the performance of both configurations becomes interference limited.

In Figure 6.2, the asymptotic ($\sigma^2 \rightarrow 0$) BER of the system is shown as a function of the ratio p of the interference bandwidth to the DS-CDMA signal bandwidth. The performance of cascade ST processor is invariant with respect to

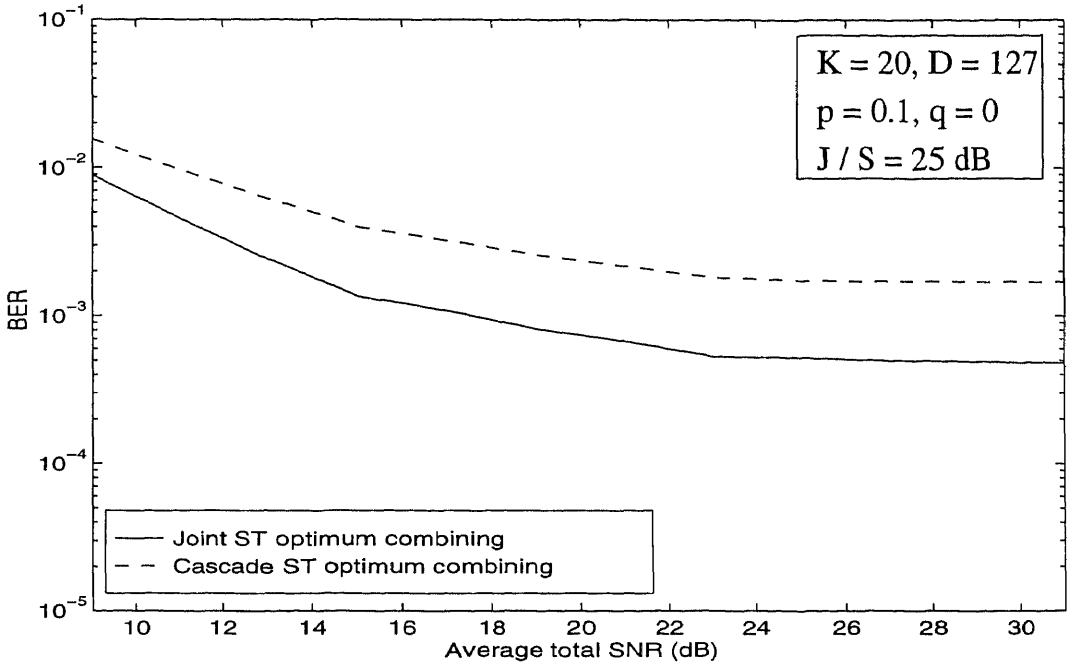

Figure 6.1 Performance of space-time receivers for DS-CDMA overlay system.

interference bandwidth and serves as the upper bound for the joint ST processor when the interference bandwidth approaches DS-CDMA signal bandwidth.

Figure 6.3 demonstrates the asymptotic BER performance of the ST configurations as a function of the ratio q of the offset of the interference carrier frequency to the half DS-CDMA signal bandwidth. The performance of the ST processors is very robust to the change in q. When $q = 1$ the narrowband interference is outside the DS-CDMA frequency band.

In Figure 6.4, the asymptotic BER of the DS-CDMA system as a function of the number of active users K is shown for different values of J/S. It is seen that for large J/S and for a given BER, the joint ST receiver can support many more users than can the cascade ST receiver. When $J/S \leq 10$ dB and the number of active users L is large, both configurations show similar performance.

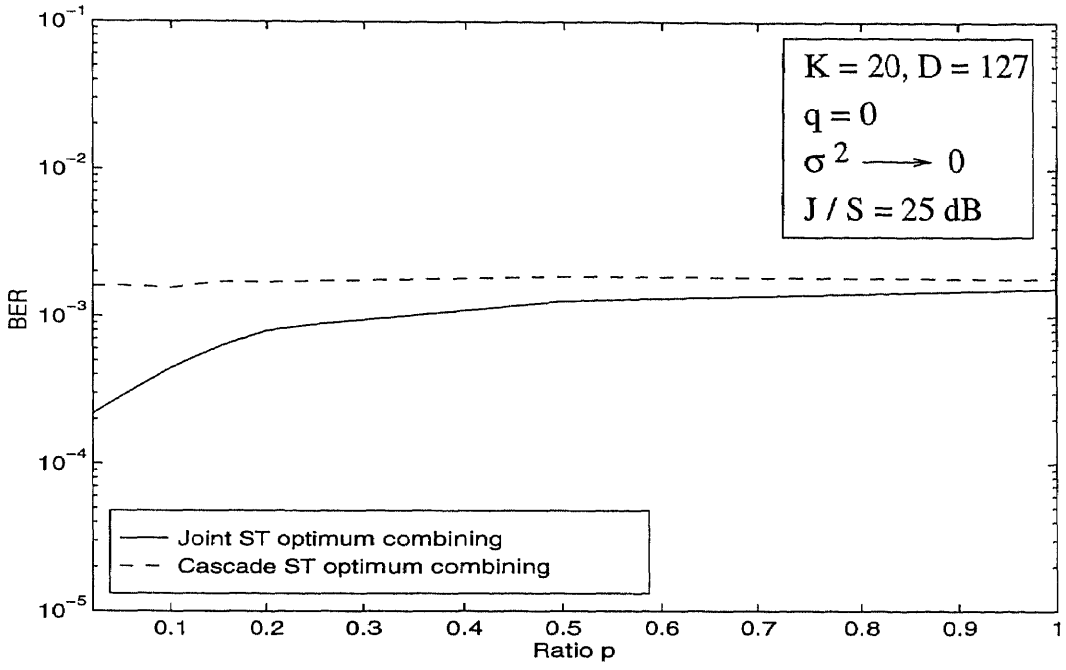

Figure 6.2 Performance of space-time receivers as a function of ratio p.

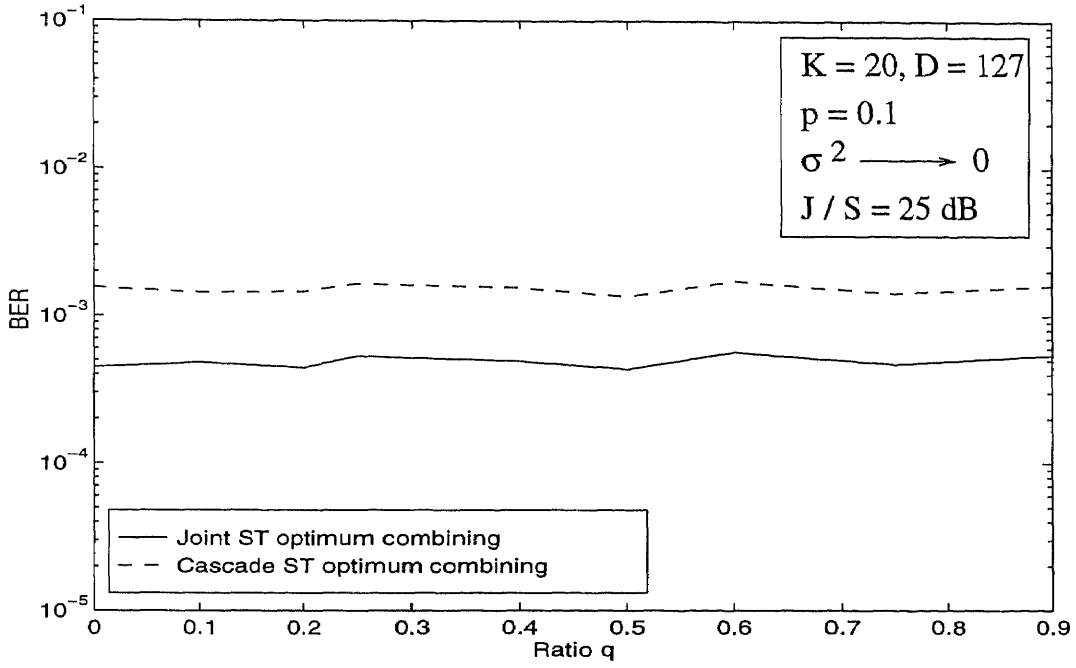

Figure 6.3 Performance of space-time receivers as a function of ratio q.

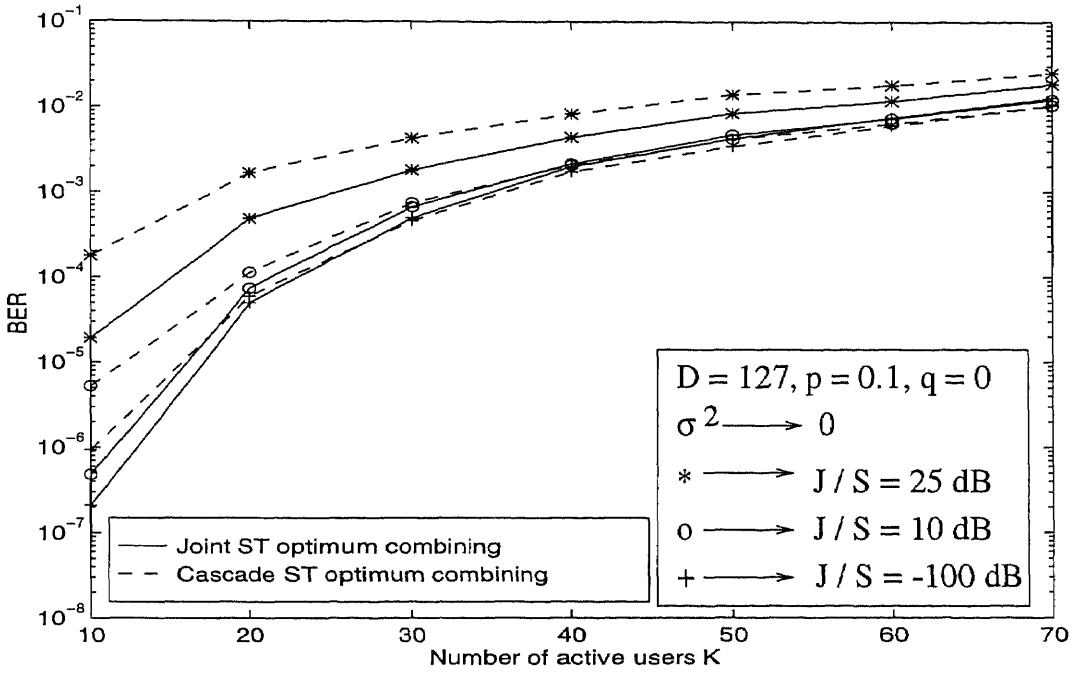

Figure 6.4 Performance of space-time receivers as a function of number of active users K.

CHAPTER 7
CONCLUSIONS

In this dissertation, we studied space-time processing for digital mobile radio communication systems. The application of spatial processing, to increase the capacity of both macrocellular as well as microcellular systems, has been investigated. The performance of space-time processing is evaluated for CDMA overlay scenarios for personal communication systems.

In chapter 2, we studied optimum combining (OC) for macrocellular systems. The performance of optimum combining was evaluated for L ($L < N$) Rayleigh fading cochannel interferers, where N is the number of antenna elements. We derived an expression for the probability density function (PDF) of the signal-to-interference-plus-noise ratio (SINR) at the output of the optimum combiner. Expressions for the average probability of bit error rate (BER) were developed. Meaningful upper bounds on these BER expressions were also derived. Results, with optimum combining, indicate that the interference cancellation entails a loss of degrees of freedom (DOF), with a corresponding loss in the diversity performance.

In chapter 3, we studied and compared the performance of both maximal ratio combining (MRC) and OC for macrocellular systems. We considered L ($L \geq N$) Rayleigh fading cochannel interferers. We derived expressions for the PDFs of signal-to-interference ratio (SIR) at the output of an antenna array using both MRC and OC. Closed-form expressions for the BER and the outage probability with both MRC and OC were developed. These closed-form expressions provide a convenient tool for system analysis and a substitute for time consuming Monte Carlo simulations. Results showed that with OC there is an improvement in the performance as compared to MRC with only a few antenna elements even when the number of interferers L is greater than the number of antenna elements N. This improvement, however, becomes significant as the number of antenna elements

increases. We studied independent as well as non-independent fading at the antenna elements. For the special case of non-independent fading in which the multipath reflections are assumed to be uniformly distributed around the receive antenna elements, we showed that the performance of the optimum combiner is not affected by the spacing between the antenna elements. This result is of significant importance since it makes OC possible even on a tiny portable unit without degradation in the performance.

In chapter 4, we studied and compared the performance of both MRC and OC for microcellular systems. The use of antenna arrays could be even more beneficial in a microcellular environment due to small received mean carrier-to-interference ratio. The desired signal is assumed to have Rician statistics, whereas, the cochannel interferers are assumed to have Rayleigh statistics. This is the so called Rician/Rayleigh model. We derived expressions for the PDFs of the SIR at the output of an antenna array using both MRC and OC. Expressions for the BER and the outage probability with both MRC and OC were developed. Similar expressions were developed for the special case of the Rician/Rayleigh model, the Nonfading/Rayleigh model. That is, the desired signal is assumed nonfading. Again, OC showed significant performance improvement as compared to MRC.

We conclude that OC is a cost effective alternative to increase both the performance and the capacity of digital cellular mobile radio communication systems.

In chapter 5, we studied space-time processing for narrowband interference suppression in DS-CDMA communication for PCS. The need to suppress narrowband signals in direct sequence code division multiple access (DS-CDMA) systems arises in applications where narrowband signals are overlaid with wideband signals to increase spectral efficiency. Spatial and temporal processing provides DOF for both interference cancellation and diversity combining. The performance of space-time receiver architectures, cascade and joint, was evaluated for suppressing a narrowband

interference overlaid with a DS-CDMA signal in a frequency-selective slowly fading Rayleigh channel. Analytical expressions were obtained for asymptotic efficiency, PDF of output SINR, BER and its upper bound, associated with each architecture. Results indicate that the cascade space-time processor serves as an upper bound on the performance of the joint space-time processor.

In chapter 6, the performance of space-time receiver architectures is evaluated for a multiuser asynchronous DS-CDMA overlay system. The performance is evaluated in terms of the BER, and how this performance is influenced by various parameters is also examined. The joint space-time processor provides superior performance compared to that of the cascade space-time processor and the performance of both configurations becomes interference limited in the region of high signal-to-noise ratio (SNR). The performance of cascade processor is unaffected by the bandwidth of the narrowband interference and serves as an upper bound on the performance of the joint processor when the narrowband interference bandwidth approaches the bandwidth of the DS-CDMA signal.

We conclude that the space-time combining schemes can be implemented to enhance both the performance and the capacity of a CDMA system overlaying narrowband waveforms for PCS.

APPENDIX A

DERIVATION OF BER FOR MRC

In this section, we derive the BER expression given in eq. (3.20) Rewriting the expression for the BER, we have

$$\begin{aligned} P_e &= \frac{1}{2}\int_0^\infty \mathrm{erfc}(\sqrt{\rho}) f_\rho(\rho) d\rho \\ &= \frac{1}{2}\frac{\Gamma(L+N)}{\Gamma(L)\Gamma(N)}\left(\frac{P_s}{P}\right)^L \int_0^\infty \mathrm{erfc}(\sqrt{\rho})\frac{\rho^{N-1}}{(\frac{P_s}{P}+\rho)^{L+N}} d\rho. \end{aligned} \tag{A.1}$$

Using the identity [42]

$$\mathrm{erfc}(\sqrt{\rho}) = \frac{\rho^{-\frac{1}{4}}}{\sqrt{\pi}} e^{-\frac{\rho}{2}} \mathrm{W}_{-\frac{1}{4},\frac{1}{4}}(\rho), \tag{A.2}$$

in eq. (A.1), we get

$$P_e = \frac{1}{2\sqrt{\pi}}\frac{\Gamma(L+N)}{\Gamma(L)\Gamma(N)}\left(\frac{P_s}{P}\right)^L \int_0^\infty \frac{\rho^{N-\frac{5}{4}}}{(\frac{P_s}{P}+\rho)^{L+N}} e^{-\frac{\rho}{2}} \mathrm{W}_{-\frac{1}{4},\frac{1}{4}}(\rho) d\rho, \tag{A.3}$$

where $\mathrm{W}_{p,q}(\cdot)$ is the Whittaker function of the second kind and is defined as

$$\mathrm{W}_{p,q}(x) = \frac{x^p e^{-\frac{x}{2}}}{\Gamma(q-p+\frac{1}{2})}\int_0^\infty e^{-t} t^{(q-p-\frac{1}{2})}(1+\frac{t}{x})^{(q+p-\frac{1}{2})} dt, \quad q-p+\frac{1}{2} > 0. \tag{A.4}$$

Equation (A.3) can be evaluated in a closed form [45] and is

$$P_e = \frac{1}{2\sqrt{\pi}\Gamma(L)\Gamma(N)}\left(\frac{P_s}{P}\right)^{\frac{-1}{4}} \mathrm{G}_{2,3}^{3,1}\left(\frac{P_s}{P}\,\middle|\, \begin{matrix} -N+\frac{5}{4}, \frac{5}{4} \\ L+\frac{1}{4}, \frac{3}{4}, \frac{1}{4} \end{matrix}\right), \tag{A.5}$$

where $\mathrm{G}_{p,q}^{m,n}(\cdot)$ is the Meijer's G-function and is defined as [45]

$$\mathrm{G}_{p,q}^{m,n}\left(x\,\middle|\, \begin{matrix} a_1,\ldots,a_p \\ b_1,\ldots,b_q \end{matrix}\right) = \frac{1}{2\pi i}\int_C \frac{\prod_{j=1}^m \Gamma(b_j-s)\prod_{j=1}^n \Gamma(1-a_j+s)}{\prod_{j=m+1}^q \Gamma(1-b_j+s)\prod_{j=n+1}^p \Gamma(a_j-s)} x^s ds, \tag{A.6}$$

where C is a curve separating the poles of $\prod_{j=1}^m \Gamma(b_j-s)$ from those of $\prod_{j=1}^n \Gamma(1-a_j+s)$, $1 \le q$, $0 \le n \le p \le q$, $0 \le m \le q$; $x \neq 0$ and $\mid x \mid < 1$ if $q = p$; $x \neq 0$ if $q > p$. See [66] for more definitions and evaluation of the G-function.

Using the identity [45]

$$G_{p,q}^{q,1}\left(x \,\middle|\, \begin{matrix} a_1,\ldots,a_p \\ b_1,\ldots,b_q \end{matrix}\right) = x^{a_1-1} \\ \mathrm{E}\left(1-a_1+b_1,\ldots,1-a_1+b_q : 1-a_1+a_2,\ldots,1-a_1+a_p : x\right), \quad \text{(A.7)}$$

in eq. (A.5), we get

$$P_e = \frac{1}{2\sqrt{\pi}\Gamma(L)\Gamma(N)}\left(\frac{P_s}{P}\right)^{-N} \mathrm{E}\left(L+N, N+\frac{1}{2}, N : N+1 : \frac{P_s}{P}\right), \quad \text{(A.8)}$$

where $\mathrm{E}(\cdot)$ is the MacRobert's E-function and is defined as [45]

$$\begin{aligned} \mathrm{E}\left(a_1,\ldots,a_p : b_1,\ldots,b_q : x\right) &= \sum_{r=1}^{p} \frac{\hat{\prod}_{s=1}^{p}\Gamma(a_s-a_r)}{\prod_{t=1}^{q}\Gamma(b_t-a_r)}\Gamma(a_r)x^{a_r} \\ &\quad {}_{q+1}F_{p-1}(a_r, a_r-b_1+1,\ldots,a_r-b_q+1; \\ &\quad a_r-a_1+1,\ldots,*,\ldots,a_r-a_p+1;(-1)^{p-q}x), \end{aligned} \quad \text{(A.9)}$$

where ${}_pF_q(\cdot)$ is the generalized hypergeometric series and is as defined in eq. (3.21). The $\hat{}$ in $\hat{\prod}$ denotes the omission of the term when $s=r$. Also, the $*$ in ${}_pF_q(\cdot)$ indicates omission of the term (a_r-a_r+1). Equation (A.9) is valid for $p \geq q+1$.

Using the identity of eq. (A.9) in eq. (A.8), we get

$$\begin{aligned} P_e &= \frac{1}{2\sqrt{\pi}\Gamma(L)\Gamma(N)}\left(\frac{P_s}{P}\right)^{-N}\left[\left(\frac{P_s}{P}\right)^{L+N}\frac{\Gamma(\frac{1}{2}-L)\Gamma(-L)\Gamma(L+N)}{\Gamma(1-L)}\right. \\ &\quad {}_2F_2\left(L+N, L; L+\frac{1}{2}, L+1; \frac{P_s}{P}\right) + \left(\frac{P_s}{P}\right)^{N+\frac{1}{2}}\frac{\Gamma(L-\frac{1}{2})}{\Gamma(\frac{1}{2})} \\ &\quad \Gamma(-\tfrac{1}{2})\Gamma(N+\tfrac{1}{2}){}_2F_2\left(N+\frac{1}{2}, \frac{1}{2}; \frac{3}{2}-L, \frac{3}{2}; \frac{P_s}{P}\right) + \left(\frac{P_s}{P}\right)^{N}\frac{\Gamma(L)\Gamma(\frac{1}{2})}{\Gamma(1)} \\ &\quad \left.\Gamma(N){}_2F_2\left(N, 0; 1-L, \frac{1}{2}; \frac{P_s}{P}\right)\right] \end{aligned}$$

$$= \frac{1}{2\sqrt{\pi}\Gamma(L)\Gamma(N)}\left[\left(\frac{P_s}{P}\right)^L \Gamma(\tfrac{1}{2}-L)\Gamma(L+N)\right.$$
$$(-L)$$
$${}_2F_2\left(L+N, L; L+\frac{1}{2}, L+1; \frac{P_s}{P}\right) + \left(\frac{P_s}{P}\right)^{\frac{1}{2}} \frac{\Gamma(L-\frac{1}{2})}{\Gamma(\frac{1}{2})}$$
$$\left.\Gamma(-\frac{1}{2})\Gamma(N+\frac{1}{2}){}_2F_2\left(N+\frac{1}{2}, \frac{1}{2}; \frac{3}{2}-L, \frac{3}{2}; \frac{P_s}{P}\right) + \frac{\Gamma(L)\Gamma(\frac{1}{2})\Gamma(N)}{\Gamma(1)}\right], \tag{A.10}$$

where we have used the fact that ${}_2F_2\left(N, 0; 1-L, \frac{1}{2}; \frac{P_s}{P}\right) = 1$.

APPENDIX B

DERIVATION OF BER FOR OPTIMUM COMBINER

In this section, we derive the BER expression given in eq. (3.32). In deriving this BER expression, we follow similar steps as the ones shown with MRC. Rewriting the expression for the average probability of bit error, we have

$$P_e = \frac{1}{2}\frac{\Gamma(L+1)}{\Gamma(N)\Gamma(L+1-N)}\left(\frac{P_s}{P}\right)^{L+1-N}\int_0^\infty \mathrm{erfc}(\sqrt{\mu})\frac{\mu^{N-1}}{(\frac{P_s}{P}+\mu)^{L+1}}d\mu. \quad \text{(B.1)}$$

Using the identity of eq. (A.2) in eq. (B.1) we get

$$P_e = \frac{1}{2\sqrt{\pi}}\frac{\Gamma(L+1)}{\Gamma(N)\Gamma(L+1-N)}\left(\frac{P_s}{P}\right)^{L+1-N}\int_0^\infty \frac{\mu^{N-\frac{5}{4}}}{(\frac{P_s}{P}+\mu)^{L+1}}e^{-\frac{\mu}{2}}\mathrm{W}_{-\frac{1}{4},\frac{1}{4}}(\mu)d\mu. \quad \text{(B.2)}$$

Equation (B.2) can be evaluated in a closed form [45] and is

$$P_e = \frac{1}{2\sqrt{\pi}\Gamma(N)\Gamma(L+1-N)}\left(\frac{P_s}{P}\right)^{\frac{-1}{4}}\mathrm{G}_{2,3}^{3,1}\left(\frac{P_s}{P}\middle|\begin{matrix}-N+\frac{5}{4},\frac{5}{4}\\ L-N+\frac{5}{4},\frac{3}{4},\frac{1}{4}\end{matrix}\right). \quad \text{(B.3)}$$

Using the identity of eq. (A.7) in eq. (B.3) we get

$$P_e = \frac{1}{2\sqrt{\pi}\Gamma(N)\Gamma(L+1-N)}\left(\frac{P_s}{P}\right)^{-N}\mathrm{E}\left(L+1,N+\frac{1}{2},N:N+1:\frac{P_s}{P}\right). \quad \text{(B.4)}$$

Using the identity of eq. (A.9) in eq. (B.4) we get

$$\begin{aligned}P_e \;=\; & \frac{1}{2\sqrt{\pi}\Gamma(N)\Gamma(L+1-N)}\left(\frac{P_s}{P}\right)^{-N}\left[\left(\frac{P_s}{P}\right)^{L+1}\frac{\Gamma(N-L-\frac{1}{2})\Gamma(N-L-1)}{\Gamma(N-L)}\right.\\
& \Gamma(L+1){}_2F_2\left(L+1,L+1-N;L-N+\frac{3}{2},L-N+2;\frac{P_s}{P}\right)+\left(\frac{P_s}{P}\right)^{N+\frac{1}{2}}\\
& \frac{\Gamma(L-N+\frac{1}{2})\Gamma(-\frac{1}{2})\Gamma(N+\frac{1}{2})}{\Gamma(\frac{1}{2})}{}_2F_2\left(N+\frac{1}{2},\frac{1}{2};N-L+\frac{1}{2},\frac{3}{2};\frac{P_s}{P}\right)\\
& \left.+\left(\frac{P_s}{P}\right)^{N}\frac{\Gamma(L+1-N)\Gamma(\frac{1}{2})\Gamma(N)}{\Gamma(1)}\,{}_2F_2\left(N,0;N-L,\frac{1}{2};\frac{P_s}{P}\right)\right]\end{aligned}$$

$$= \frac{1}{2\sqrt{\pi}\Gamma(N)\Gamma(L+1-N)}\left[\left(\frac{P_s}{P}\right)^{L+1-N}\frac{\Gamma(N-L-\frac{1}{2})\Gamma(L+1)}{(N-L-1)}\right.$$
$${}_2F_2\left(L+1, L+1-N; L-N+\frac{3}{2}, L-N+2; \frac{P_s}{P}\right) + \left(\frac{P_s}{P}\right)^{\frac{1}{2}}$$
$$\frac{\Gamma(L-N+\frac{1}{2})\Gamma(-\frac{1}{2})\Gamma(N+\frac{1}{2})}{\Gamma(\frac{1}{2})}{}_2F_2\left(N+\frac{1}{2}, \frac{1}{2}; N-L+\frac{1}{2}, \frac{3}{2}; \frac{P_s}{P}\right)$$
$$\left. + \frac{\Gamma(L+1-N)\Gamma(\frac{1}{2})\Gamma(N)}{\Gamma(1)}\right], \tag{B.5}$$

where we have used the fact that ${}_2F_2\left(N, 0; N-L, \frac{1}{2}; \frac{P_s}{P}\right) = 1$.

APPENDIX C

BER CALCULATIONS FOR SPACE-TIME RECEIVERS

In this section, we derive eqs. (5.36), (5.37) and (5.38).

C.1 Derivation of the BER of the Spatial Combiner

Rewriting the expression for the BER, we have

$$\begin{aligned} P_e &= \int_0^\infty \frac{1}{2}\mathrm{erfc}(\sqrt{\mu}) f_\mu(\mu) d\mu \\ &= \frac{1}{2} - \frac{1}{2}\int_0^\infty \mathrm{erf}(\sqrt{\mu}) f_\mu(\mu) d\mu. \end{aligned} \tag{C.1}$$

Using the identity [42]

$$\mathrm{erf}(\sqrt{\mu}) = \frac{2}{\sqrt{\pi}}\sqrt{\mu}\, e^{-\mu}{}_1F_1\left(1; \frac{3}{2}; \mu\right) \tag{C.2}$$

and the PDF given in eq. (5.15) in eq. (C.1), we get

$$\begin{aligned} P_e = \frac{1}{2} - \frac{(JN+\sigma^2}{\sqrt{\pi}\sigma^2\Gamma(N)h^N}\int_0^\infty \mu^{N-\frac{1}{2}} e^{-\left(\frac{JN+\sigma^2}{P_s}+1\right)\mu} \\ {}_1F_1\left(1; \frac{3}{2}; \mu\right){}_1F_1\left(N-1; N; \frac{JN\mu}{P_s}\right) d\mu. \end{aligned} \tag{C.3}$$

Using the identity [43]

$$\int_0^\infty e^{-st} t^{a-1}{}_1F_1\left(c; d; xt\right){}_1F_1\left(f; g; yt\right) dt = \frac{\Gamma(a)}{s^a} F_2\left(a, c, f; d, g; \frac{x}{s}, \frac{y}{s}\right) \tag{C.4}$$

in eq. (C.3), we get

$$P_e = \frac{1}{2} - \frac{(JN+\sigma^2)\Gamma(N+\frac{1}{2})P_s^{N+\frac{1}{2}} F_2\left(N+\frac{1}{2}, 1, N-1; \frac{3}{2}, N; \frac{P_s}{JN+\sigma^2+P_s}, \frac{JN}{JN+\sigma^2+P_s}\right)}{\sqrt{\pi}\sigma^2\Gamma(N)h^N(JN+\sigma^2+P_s)^{N+\frac{1}{2}}}. \tag{C.5}$$

C.1.1 Derivation of the BER of COSST

Using eqs. (5.22), (5.35) and the procedure shown above, the BER of COSST can be easily derived and is

$$P_e = \frac{1}{2} - \frac{(JN+\sigma^2)^M \Gamma(NM+\frac{1}{2})}{\sqrt{\pi}(\sigma^2)^M \Gamma(NM) h^{NM} (\frac{JN+\sigma^2+P_s}{P_s})^{NM+\frac{1}{2}}} F_2\left(NM+\frac{1}{2}, 1, (N-1)M; \frac{3}{2}, NM; \frac{P_s}{JN+\sigma^2+P_s}, \frac{JN}{JN+\sigma^2+P_s}\right). \quad \text{(C.6)}$$

C.1.2 Derivation of the BER of Joint Space-Time Combiner

Using eqs. (5.33), (5.35) and the procedure shown above, the BER of joint ST processor can be shown to be given by

$$P_e = \frac{1}{2} - \sum_{l=1}^{r} \frac{\Gamma(NM-r+\frac{3}{2})\pi_l}{\sqrt{\pi}\Gamma(NM-r+1)\gamma_o{}^{(NM-r)}\gamma_l(1+\frac{1}{\gamma_l})^{NM-r+\frac{3}{2}}} F_2\left(NM-r+\frac{3}{2}, 1, NM-r; \frac{3}{2}, NM-r+1; \frac{\gamma_l}{\gamma_l+1}, \frac{1-\frac{\gamma_l}{\gamma_o}}{\gamma_l+1}\right) \quad \text{(C.7)}$$

APPENDIX D

DISTRIBUTION OF A RECEIVED BPSK SIGNAL THROUGH A RAYLEIGH FADING CHANNEL

In this section we show that the distribution of a received Rayleigh fading signal at each antenna element, i.e., $\sqrt{P}s(t)c$, is complex Gaussian with mean zero and variance $P\sigma^2$. $s(t) \in \{-1, 1\}$ and c is complex Gaussian with zero mean and variance σ^2. Also, $s(t)$ and c are independent.

Let $y = ax$, where $a \in \{-1, 1\}$ and x is complex Gaussian with zero mean and variance σ^2. We will show that y is also complex Gaussian with zero mean and variance σ^2.

The PDF of the discrete random variable a is

$$f_a(a) = \frac{1}{2}\delta(a+1) + \frac{1}{2}\delta(a-1), \tag{D.1}$$

where $\delta(\cdot)$ is the Dirac impulse function. The PDF of x is given by

$$f_x(x) = \frac{1}{\pi\sigma^2} e^{-\frac{|x|^2}{\sigma^2}}, \tag{D.2}$$

where $\mid x \mid$ denotes the magnitude of x.

Therefore, the PDF of y conditioned on a is given by

$$\begin{aligned} f_{y/a}(y/a) &= \frac{f_x(x)\,|_{x=\frac{y}{a}}}{\left|\frac{dy}{dx}\right|} \\ &= \frac{1}{\pi\sigma^2 \mid a \mid} e^{-\frac{|y|^2}{a^2\sigma^2}}. \end{aligned} \tag{D.3}$$

The PDF of y is given by

$$\begin{aligned} f_y(y) &= \sum_a f_{y,a}(y,a) \\ &= \sum_a f_{y/a}(y/a) f_a(a) \\ &= \sum_a \frac{1}{\pi\sigma^2 \mid a \mid} e^{-\frac{|y|^2}{a^2\sigma^2}} \left[\frac{1}{2}\delta(a+1) + \frac{1}{2}\delta(a-1)\right], \\ &= \frac{1}{2}\frac{1}{\pi\sigma^2} e^{-\frac{|y|^2}{\sigma^2}} + \frac{1}{2}\frac{1}{\pi\sigma^2} e^{-\frac{|y|^2}{\sigma^2}} \\ &= \frac{1}{\pi\sigma^2} e^{-\frac{|y|^2}{\sigma^2}}. \end{aligned} \tag{D.4}$$

Thus, y is a complex Gaussian random variable with mean zero and variance σ^2.

Therefore the received Rayleigh fading signal has a complex Gaussian distribution, i.e., its in-phase and quadrature components have Gaussian distributions.

APPENDIX E

DISTRIBUTION OF SIR AT THE OUTPUT OF THE MAXIMAL RATIO COMBINER UNDER NONFADING/RAYLEIGH MODEL

In this section, we derive the PDF shown in eq. (4.10). The desired signal is assumed nonfading and cochannel interferers are assumed Rayleigh fading. Under this model, the received signal vector is given by

$$\mathbf{r}(t) = \sqrt{P_s}\mathbf{v}s(t) + \sqrt{P}\sum_{k=1}^{L}\mathbf{c}_k s_k(t), \tag{E.1}$$

where $\mathbf{v}^T = [\beta e^{-j\delta_1}, \ldots, \beta e^{-j\delta_N}]$ is the desired signal's antenna array propagation vector. The SIR ρ at the output of the maximal ratio combiner is

$$\begin{aligned} \rho &= \frac{P_S}{P}\frac{\mathbf{v}^H\mathbf{v}\mathbf{v}^H\mathbf{v}}{\mathbf{v}^H\mathbf{R}_1\mathbf{v}} \\ &= \frac{P_S}{P}\frac{N^2\beta^4}{\mathbf{v}^H\mathbf{R}_1\mathbf{v}}. \end{aligned} \tag{E.2}$$

Let $\zeta = \mathbf{v}^H\mathbf{R}_1\mathbf{v}$. Since, $\mathbf{R}_1$ has the complex Wishart distribution $CW_N(\mathbf{\Sigma}, L)$, the distribution of ζ is also complex Wishart $CW_1(\mathbf{v}^H\mathbf{\Sigma}\mathbf{v}, L)$ [57]. The distribution of ζ is given by

$$f_\zeta(\zeta) = \frac{\kappa^{-L}}{\Gamma(L)}\zeta^{L-1}e^{-\frac{\zeta}{\kappa}}, \tag{E.3}$$

where $\kappa = \mathbf{v}^H\mathbf{\Sigma}\mathbf{v}$. Using the transformation $\rho = \frac{P_S}{P}\frac{N^2\beta^4}{\zeta}$, the PDF of ρ can easily be obtained and is

$$f_\rho(\rho) = \frac{1}{\Gamma(L)}\left(\frac{N^2P_s\beta^4}{\kappa P}\right)^L \rho^{-L-1}e^{-\frac{N^2P_s\beta^4}{\kappa\rho P}}. \tag{E.4}$$

APPENDIX F

DISTRIBUTION OF THE MAXIMUM SIR AT THE OUTPUT OF THE OPTIMUM COMBINER UNDER NONFADING/RAYLEIGH MODEL

In this section, we derive the PDF shown in eq. (4.20). The desired signal is assumed nonfading and cochannel interferers are assumed Rayleigh fading. Under this model, the received signal vector is given by

$$\mathbf{r}(t) = \sqrt{P_s}\mathbf{v}s(t) + \sqrt{P}\sum_{k=1}^{L}\mathbf{c}_k s_k(t), \tag{F.1}$$

where $\mathbf{v}^T = [\beta e^{-j\delta_1}, \ldots, \beta e^{-j\delta_N}]$ is the desired signal's antenna array propagation vector. The maximum SIR μ at the output of the optimum combiner is

$$\begin{aligned} \mu &= \frac{P_S}{P}\mathbf{v}^H\mathbf{R}_1^{-1}\mathbf{v} \\ &= \frac{P_S}{P}\nu, \end{aligned} \tag{F.2}$$

where $\nu = \mathbf{v}^H\mathbf{R}_1^{-1}\mathbf{v}$. Since, $\mathbf{R}_1$ has the complex Wishart distribution $CW_N(\mathbf{\Sigma}, L)$, the distribution of $\frac{1}{\nu}$ is complex Wishart $CW_1((\mathbf{v}^H\mathbf{\Sigma}^{-1}\mathbf{v})^{-1}, L+1-N)$ [57]. The distribution of ν can now be obtained and is given by

$$f_\nu(\nu) = \frac{\eta^{N-L-1}}{\Gamma(L+1-N)}e^{-(\frac{1}{\eta\nu})}\nu^{N-L-2} \qquad \nu > 0,\ 1 \le N \le L, \tag{F.3}$$

where $\eta = \left(\mathbf{v}^H\mathbf{\Sigma}^{-1}\mathbf{v}\right)^{-1}$.

Using the transformation $\mu = \frac{P_s}{P}\nu$, the PDF of μ can easily be obtained and is

$$f_\mu(\mu) = \frac{1}{\Gamma(L+1-N)}\left(\frac{P_s}{\eta P}\right)^{L+1-N} e^{-(\frac{P_s}{P}\frac{1}{\eta\mu})}\mu^{N-L-2} \qquad \mu > 0,\ 1 \le N \le L. \tag{F.4}$$

APPENDIX G

DERIVATION OF THE BER FOR MAXIMAL RATIO COMBINER UNDER THE NONFADING/RAYLEIGH MODEL

In this section we derive eq. (4.15). The BER is given by

$$P_e = \frac{1}{2\Gamma(L)}\left(\frac{N^2P_s\beta^4}{\kappa P}\right)^L \int_0^\infty \text{erfc}(\sqrt{\rho})e^{-(\frac{N^2P_s\beta^4}{P}\frac{1}{\rho\kappa})}\rho^{-L-1}d\rho. \tag{G.1}$$

Using the identity [42]

$$\text{erfc}(\sqrt{\rho}) = \frac{1}{\sqrt{\pi}}e^{-\rho}\text{U}\left(\frac{1}{2};\frac{1}{2};\rho\right) \tag{G.2}$$

in eq. (G.1), we get

$$P_e = \frac{1}{2\sqrt{\pi}\Gamma(L)}\left(\frac{N^2P_s\beta^4}{\kappa P}\right)^L \int_0^\infty e^{-(\frac{N^2P_s\beta^4}{P}\frac{1}{\rho\kappa})}\rho^{-L-1}e^{-\rho}\text{U}\left(\frac{1}{2};\frac{1}{2};\rho\right)d\rho, \tag{G.3}$$

where $\text{U}(\cdot)$ is the confluent hypergeometric function of the second kind. Using transformation of variable and rewriting eq. (G.3) we have

$$P_e = \frac{1}{2\sqrt{\pi}\Gamma(L)}\left(\frac{N^2P_s\beta^4}{\kappa P}\right)^L \int_0^\infty e^{-(\frac{N^2P_s\beta^4}{P}\frac{z}{\kappa})}z^{L-1}e^{-z^{-1}}\text{U}\left(\frac{1}{2};\frac{1}{2};z^{-1}\right)dz. \tag{G.4}$$

Equation (G.4) can be evaluated in a closed form [67] and is

$$\begin{aligned}
P_e &= \frac{1}{2\sqrt{\pi}\Gamma(L)}\left[\frac{\Gamma(L)\Gamma(\frac{1}{2})}{\Gamma(1)}{}_1F_2\left(0;\frac{1}{2},1-L;\frac{N^2P_s\beta^4}{\kappa P}\right)+\left(\frac{N^2P_s\beta^4}{\kappa P}\right)^L\right. \\
&\quad \frac{\Gamma(\frac{1}{2}-L)\Gamma(-L)}{\Gamma(1-L)}{}_1F_2\left(L;L+1,L+\frac{1}{2};\frac{N^2P_s\beta^4}{\kappa P}\right) \\
&\quad \left.+\left(\frac{N^2P_s\beta^4}{\kappa P}\right)^{\frac{1}{2}}\frac{\Gamma(-\frac{1}{2})\Gamma(L-\frac{1}{2})}{\Gamma(\frac{1}{2})}{}_1F_2\left(\frac{1}{2};\frac{3}{2},\frac{3}{2}-L;\frac{N^2P_s\beta^4}{\kappa P}\right)\right] \\
&= \frac{1}{2\sqrt{\pi}\Gamma(L)}\left[\Gamma(L)\Gamma(\frac{1}{2})+\left(\frac{N^2P_s\beta^4}{\kappa P}\right)^L\frac{\Gamma(\frac{1}{2}-L)}{(-L)}\right. \\
&\quad {}_1F_2\left(L;L+1,L+\frac{1}{2};\frac{N^2P_s\beta^4}{\kappa P}\right)+\left(\frac{N^2P_s\beta^4}{\kappa P}\right)^{\frac{1}{2}}\frac{\Gamma(-\frac{1}{2})\Gamma(L-\frac{1}{2})}{\Gamma(\frac{1}{2})} \\
&\quad \left.{}_1F_2\left(\frac{1}{2};\frac{3}{2},\frac{3}{2}-L;\frac{N^2P_s\beta^4}{\kappa P}\right)\right],
\end{aligned} \tag{G.5}$$

where we have used the fact that ${}_1F_2\left(0;\frac{1}{2},1-L;\frac{N^2P_s\beta^4}{\kappa P}\right)=1$.

APPENDIX H

DERIVATION OF THE BER FOR OPTIMUM COMBINER UNDER THE NONFADING/RAYLEIGH MODEL

In this section we derive eq. (4.24). The BER is given by

$$P_e = \frac{1}{2\Gamma(L+1-N)}\left(\frac{P_s}{P\eta}\right)^{L+1-N}\int_0^\infty \operatorname{erfc}(\sqrt{\mu})e^{-(\frac{P_s}{P}\frac{1}{\eta\mu})}\mu^{N-L-2}d\mu. \tag{H.1}$$

Using the identity [42]

$$\operatorname{erfc}(\sqrt{\mu}) = \frac{1}{\sqrt{\pi}}e^{-\mu}\mathrm{U}\left(\frac{1}{2};\frac{1}{2};\mu\right) \tag{H.2}$$

in eq. (H.1), we get

$$P_e = \frac{1}{2\sqrt{\pi}\Gamma(L+1-N)}\left(\frac{P_s}{P\eta}\right)^{L+1-N}\int_0^\infty e^{-(\frac{P_s}{P}\frac{1}{\eta\mu})}\mu^{N-L-2}e^{-\mu}\mathrm{U}\left(\frac{1}{2};\frac{1}{2};\mu\right)d\mu, \tag{H.3}$$

where $\mathrm{U}(\cdot)$ is the confluent hypergeometric function of the second kind. Using transformation of variable and rewriting eq. (H.3) we have

$$P_e = \frac{1}{2\sqrt{\pi}\Gamma(L+1-N)}\left(\frac{P_s}{P\eta}\right)^{L+1-N}\int_0^\infty e^{-(\frac{P_s}{P}\frac{z}{\eta})}z^{L-N}e^{-z^{-1}}\mathrm{U}\left(\frac{1}{2};\frac{1}{2};z^{-1}\right)dz. \tag{H.4}$$

Equation (H.4) can be evaluated in a closed form [67] and is

$$\begin{aligned}
P_e &= \frac{1}{2\sqrt{\pi}\Gamma(L+1-N)}\left[\frac{\Gamma(L+1-N)\Gamma(\frac{1}{2})}{\Gamma(1)}{}_1F_2\left(0;\frac{1}{2},N-L;\frac{P_s}{P\eta}\right)+\left(\frac{P_s}{P\eta}\right)^{L+1-N}\right.\\
&\quad \frac{\Gamma(N-L-\frac{1}{2})\Gamma(N-L-1)}{\Gamma(N-L)}{}_1F_2\left(L+1-N;L-N+2,L-N+\frac{3}{2};\frac{P_s}{P\eta}\right)\\
&\quad \left.+\left(\frac{P_s}{P\eta}\right)^{\frac{1}{2}}\frac{\Gamma(-\frac{1}{2})\Gamma(L-N+\frac{1}{2})}{\Gamma(\frac{1}{2})}{}_1F_2\left(\frac{1}{2};\frac{3}{2},N-L+\frac{1}{2};\frac{P_s}{P\eta}\right)\right]\\
&= \frac{1}{2\sqrt{\pi}\Gamma(L+1-N)}\left[\Gamma(L-N+1)\Gamma(\frac{1}{2})+\left(\frac{P_s}{P\eta}\right)^{L+1-N}\frac{\Gamma(N-L-\frac{1}{2})}{(N-L-1)}\right.\\
&\quad {}_1F_2\left(L+1-N;L-N+2,L-N+\frac{3}{2};\frac{P_s}{P\eta}\right)+\left(\frac{P_s}{P\eta}\right)^{\frac{1}{2}}\frac{\Gamma(-\frac{1}{2})\Gamma(L-N+\frac{1}{2})}{\Gamma(\frac{1}{2})}\\
&\quad \left.{}_1F_2\left(\frac{1}{2};\frac{3}{2},N-L+\frac{1}{2};\frac{P_s}{P\eta}\right)\right],
\end{aligned} \tag{H.5}$$

where we have used the fact that ${}_1F_2\left(0;\frac{1}{2},N-L;\frac{P_s}{P\eta}\right)=1$.

APPENDIX I

CORRELATION OF DS-CDMA SIGNALS

Here we evaluate the terms of eq. (6.4). This relation represents the correlation of the received signal at the n-th antenna element at the m-th tap for the l-th symbol with the signature waveform $u_1(t)$ of the desired user. Let the four terms on the right-hand side of eq. (6.4) be denoted X_1, X_2, X_3, and X_4 respectively. X_1 represents the aggregate contributions of the desired user at the m-th tap correlator. It can be further analyzed as follows:

$$X_1 = \sqrt{P} d_1(l) B^{(1)}_{nm(0)} + \sqrt{P} d_1(l+1) B^{(1)}_{nm(1)} + \sqrt{P} d_1(l-1) B^{(1)}_{nm(-1)}, \qquad \text{(I.1)}$$

where the factor $B^{(1)}_{nm(0)}$ represents contributions of $d_1(l)$ to the output of the matched filter at the n-th antenna element and m-th tap. This factor consists of the correlation of the desired signal in the m-th path with the signature waveform $u_1(t)$, as well as inter-path contributions, and it can be written

$$B^{(1)}_{nm(0)} = c^{(1)}_{nm}\ \rho_{11}(0,0,T_b)\ + b^{(1)}_{nm}, \qquad \text{(I.2)}$$

where $\rho_{jk}(\tau, t_1, t_2)$ is the partial correlation between signature sequences of users j and k, with time lag τ between the sequences, and time limits t_1 and t_2. It can be expressed as

$$\rho_{jk}(\tau, t_1, t_2) = \int_{t_1}^{t_2} u_j(\alpha+\tau)\ u_k(\alpha)\ d\alpha, \qquad \text{(I.3)}$$

where $\{*\}$ denotes a complex conjugate. Note that $\rho_{11}(0,0,T_b) = D$, the processing gain.

The complex normal variable $b_{nm}^{(1)}$ (constant during the processing interval) represents contributions of $d_1(l)$'s paths other than the m-th. It consists of paths $i < m$ that arrive prior to path m (which is aligned with the signature $u_1(t)$) and paths $i > m$ that arrive following m. It is given by

$$\begin{aligned} b_{nm}^{(1)} &= \sum_{i=0}^{m-1} c_{ni}^{(1)}\, \rho_{11}((m-i)T_c, 0, T_b - (m-i)T_c) \\ &+ \sum_{i=m+1}^{M-1} c_{ni}^{(1)}\, \rho_{11}((m-i)T_c, (i-m)T_c, T_b). \end{aligned} \tag{I.4}$$

Factors of the form $B_{nm(\alpha)}^{(1)}$ with $\alpha = -1, 1$ represent contributions associated with the $(l+\alpha)$ -th symbol of the desired user. Note that the m-th path waveform of $d_1(l)$ may overlap with the $i < m$-th path waveform of the next symbol $d_1(l+1)$ or with the $i > m$-th path waveform of the previous symbol $d_1(l-1)$. These factors can be written explicitly as

$$\begin{aligned} B_{nm(0)}^{(1)} &= c_{nm}^{(1)}\, \rho_{11}(0, 0, T_b) + b_{nm}^{(1)} \\ B_{nm(1)}^{(1)} &= \sum_{i=0}^{m-1} c_{ni}^{(1)}\, \rho_{11}((m-i)T_c, (i-m)T_c, 0) \\ B_{nm(-1)}^{(1)} &= \sum_{i=m+1}^{M-1} c_{ni}^{(1)}\, \rho_{11}((m-i)T_c, 0, (i-m)T_c). \end{aligned} \tag{I.5}$$

The term X_2 consists of the cochannel interferences' contributions. It is given by

$$X_2 = \sum_{k=2}^{K} \left\{ \sqrt{P} d_k(l) B_{nm(0)}^{(k)} + \sqrt{P} d_k(l+1) B_{nm(1)}^{(k)} + \sqrt{P} d_k(l-1) B_{nm(-1)}^{(k)} \right\}. \tag{I.6}$$

With considerable algebraic manipulations, but in a manner similar to the derivation of eq. (I.5), it can be shown that the terms $B_{nm(\alpha)}^{(k)}$, $\alpha = -1, 0, 1$, $k = 2, \ldots, K$, are given by

$$
\begin{aligned}
B^{(k)}_{nm(0)} &= c^{(k)}_{n\left(m-\left\lfloor\frac{\tau_k}{T_c}\right\rfloor\right)}\rho_{k1}(0,0,T_b)+b^{(k)}_{nm} \\
B^{(k)}_{nm(1)} &= \sum_{i=0}^{m-\left\lfloor\frac{\tau_k}{T_c}\right\rfloor-1} c^{(k)}_{ni}\rho_{k1}((m-i)T_c-\tau_k,(i-m)T_c+\tau_k,0) \\
B^{(k)}_{nm(-1)} &= \sum_{i=m-\left\lfloor\frac{\tau_k}{T_c}\right\rfloor+1}^{M-1} c^{(k)}_{ni}\rho_{k1}((m-i)T_c-\tau_k,0,(i-m)T_c+\tau_k), \qquad \text{(I.7)}
\end{aligned}
$$

where

$$
\begin{aligned}
b^{(k)}_{nm} &= \sum_{i=0}^{m-\left\lfloor\frac{\tau_k}{T_c}\right\rfloor-1} c^{(k)}_{ni}\rho_{k1}((m-i)T_c-\tau_k,(i-m)T_c+\tau_k,0) \\
&\quad + \sum_{i=m-\left\lfloor\frac{\tau_k}{T_c}\right\rfloor+1}^{M-1} c^{(k)}_{ni}\rho_{k1}((m-i)T_c-\tau_k,0,(i-m)T_c+\tau_k). \qquad \text{(I.8)}
\end{aligned}
$$

The notation $\lfloor\cdot\rfloor$ denotes the integer part.

The term X_3 is the narrowband interference after matched filtering and is given by

$$
\begin{aligned}
X_3 &= \int_{lT_b}^{(l+1)T_b} \xi_n(t+mT_c)u_1(t)dt \\
&= \xi_{nm}(l). \qquad \text{(I.9)}
\end{aligned}
$$

Finally, X_4 is the noise after matched filtering and is given by

$$
\begin{aligned}
X_4 &= \int_{lT_b}^{(l+1)T_b} v_n(t+mT_c)u_1(t)dt \\
&= \eta_{nm}(l). \qquad \text{(I.10)}
\end{aligned}
$$

REFERENCES

1. J. E. Padgett, C. G. Gunther, and T. Hattori, "Overview of wireless personal communications," *IEEE Communications Magazine*, vol. 33, pp. 28–41, January 1995.

2. D. J. Goodman, "Trends in cellular and cordless communications," *IEEE Communications Magazine*, vol. 29, pp. 31–40, June 1991.

3. W. C. Y. Lee, *Mobile Communications Design Fundamentals*, John Wiley & Sons, Inc., New York, USA, 2nd ed., 1993.

4. T. S. Rappaport, *Wireless Communications*, Prentice-Hall, Inc., Englewood Cliffs, New Jersey, USA, 1996.

5. A. M. Haimovich, "Designing the Infrastructure of the Next Generation Wireless Communication," *New Jersey Institute of Technology Research*, vol. 4, pp. 8–14, Spring 1996.

6. X. Wu and A. Haimovich, "Space-Time Optimum Combining for CDMA Communications," *Wireless Personal Communications*, no. 3, pp. 73–89, 1996.

7. J. H. Winters, "Optimum Combining in Digital Mobile Radio with Cochannel Interference," *IEEE Transactions on Vehicular Technology*, vol. 33, pp. 144–155, August 1984.

8. J. H. Winters, "Optimum Combining for Indoor Radio Systems with Multiple Users," *IEEE Transactions on Communications*, vol. COM-35, no. 11, pp. 1222–1230, November 1987.

9. J. H. Winters, "Signal Acquisition and Tracking with Adaptive Arrays in the Digital Mobile Radio System IS-54 with Flat Fading," *IEEE Transactions on Vehicular Technology*, vol. 42, pp. 377–384, November 1993.

10. J. H. Winters, J. Salz, and R. D. Gitlin, "The Impact of Antenna Diversity on the Capacity of Wireless Communication Systems," *IEEE Transactions on Communications*, vol. 42, pp. 1740–1751, February/March/April 1994.

11. J. H. Winters, J. Salz, and R. D. Gitlin, "Adaptive Antennas for Digital Mobile Radio," *Adaptive Array Symposium, Bethpage, NY*, pp. 81–85, November 1992.

12. J. H. Winters, "On the Capacity of Radio Communication Systems with Diversity in a Rayleigh Fading Environment," *IEEE Journal on Selected Areas in Communications*, vol. 5, pp. 871–878, June 1987.

13. X. C. Bernstein, *Dissertation: Adaptive Space-Time Processing for Wireless Communications*, Department of Electrical and Computer Engineering, New Jersey Institute of Technology, Newark, New Jersey, USA, 1996.

14. R. A. Monzingo and T. W. Miller, *Introduction to Adaptive Arrays*, John Wiley & Sons, Inc., New York, USA, 1980.

15. D. D. Klovskiy, "Noise Immunity of Binary Systems with Fluctuation Noise and Concentrated Interference," *Telecommunications and Radio Engineering*, vol. 19, no. 2, pp. 7–11, February 1965.

16. I. S. Andronov, "Optimum Noise Immunity of Diversity Reception," *Telecommunications and Radio Engineering*, vol. 19, no. 9, pp. 8–12, September 1965.

17. V. A. Dubrovskiy and V. A. Gordeyev, "Noise Immunity in the Reception of Radio Telegraphy Signals in the Presence of Interference from Adjacent Channel Radio Stations," *Telecommunications and Radio Engineering*, vol. 24, no. 8, pp. 80–84, February 1969.

18. I. A. Kychkin, "Noise Immunity of Fading PT and RPT Signals in the Presence of Fading Concentrated Interference and Noise," *Telecommunications and Radio Engineering*, vol. 20, no. 9, pp. 59–62, September 1966.

19. I. A. Tsikin, "Noise Immunity in the Reception of Signals via A Channel with Unknown Parameters," *Telecommunications and Radio Engineering*, vol. 20, no. 6, pp. 96–102, June 1966.

20. J. H. Winters and J. Salz, "Upper bounds on the Bit Error Rate of Optimum Combining in Wireless Systems," *IEEE Vehicular Technology Conference, Stockholm, Sweden*, vol. 2, pp. 942–946, June 1994.

21. M. V. S. Anderson, M. Millnert and B. Wahlberg, "An Adaptive Array for Mobile Communication Systems," *IEEE Vehicular Technology Conference, Stockholm, Sweden*, vol. VT-40, pp. 230–236, February 1991.

22. S. C. Swales, M. A. Beach and D. J. Edwards, "Multi-beam Adaptive Base Station Antennas for Cellular Land Mobile Radio Systems," *Mobile Radio and Personal Communication Conference, UK*, pp. 341–348, December 1989.

23. Federal Communications Commission, "In the matter of amendment of the commission's Rules to establish new personal communications services," *Second Report and Order, GEN Docket 90-314,FCC 93-451*, October 1993.

24. R. L. Peterson, R. E. Ziemer, and D. E. Borth, *Introduction to spread spectrum communications*, Prentice-Hall, Inc., Englewood Cliffs, New Jersey, USA, 1995.

25. J. E. Padgett, C. G. Gunther, and T. Hattori, "Overview of wireless personal communications," *IEEE Communications Magazine*, vol. 33, pp. 28–41, January 1995.

26. L. B. Milstein et al., "On the feasibility of a CDMA overlay for personal communications networks," *IEEE Journal on Selected Areas in Communications*, vol. 10, no. 4, pp. 655–668, May 1992.

27. D. L. Schilling and E. Kanterakis, "Broadband-CDMA overlay of FM on TDMA in the cellular system," *IEEE Global Telecommunications Conference*, vol. Mini-Conference Volume, pp. 61–65, 1992.

28. R. L. Pickholtz, L. B. Milstein and D. L. Schilling, "Spread spectrum for mobile communications," *IEEE Transactions on Vehicular Technology*, vol. 40, no. 2, pp. 313–322, May 1991.

29. L. B. Milstein, "Interference rejection techniques in spread spectrum communications," *Proceedings of the IEEE*, vol. 76, no. 6, pp. 657–671, June 1988.

30. J. Wang and L. B. Milstein, "CDMA overlay situations for microcellular mobile communications," *IEEE Transactions on Communications*, vol. 43, no. 2,3,4, pp. 603–614, February/March/April 1995.

31. P. Wei et al., "Adaptive interference suppression for CDMA based PCN Systems," *IEEE International Conference on Communications, Geneva, Switzerland*, pp. 1890–1894, May 1993.

32. K. G. Filis and S. C. Gupta, "Coexistence of cellular CDMA and FSM: Interference suppression using filtered PN sequences," *IEEE Global Telecommunications Conference*, pp. 898–901, 1993.

33. M. B. K. Widjaja, H. S. Misser and R. Prasad, "Performance Analysis of an Overlay CDMA System with Multiple BPSK Interferers," *IEEE Global Telecommunications Conference*, pp. 510–514, 1994.

34. L. Li and L. B. Milstein, "Rejection of narrow-band interference in PN spread-spectrum systems using transversal filters," *IEEE Transactions on Communications*, vol. COM-30, no. 5, pp. 925–928, May 1982.

35. J. W. Ketchum and J. G. Proakis, "Adaptive algorithms for estimating and suppressing narrow-band interference in PN spread-spectrum systems," *IEEE Transactions on Communications*, vol. COM-30, no. 5, pp. 913–924, May 1982.

36. R. A. Iltis and L. B. Milstein, "Performance analysis of narrow-band interference rejection techniques in DS spread-spectrum systems," *IEEE Transactions on Communications*, vol. COM-32, no. 11, pp. 1169–1177, November 1984.

37. J. Salz and J. H. Winters, "Effect of Fading Correlation on Adaptive Arrays in Digital Wireless Communications," *IEEE ICC*, pp. 1768–1774, May 23-26 1993.

38. S. Unnikrishna Pillai, *Array Signal Processing*, Springer-Verlag, Inc., New York, USA, 1989.

39. C. A. Baird, Jr. and C. L. Zahm, "Performance for Narrowband Array Processing," *Conference on Decision Control, Miami Beach, Florida*, pp. 564–565, 1971.

40. J. G. Proakis, *Digital Communications*, McGraw-Hill, Inc., New York, USA, 3rd ed., 1995.

41. J.V. DiFranco and W.L. Rubin, *Radar Detection*, Prentice-Hall, Inc., Englewood Cliffs, New Jersey, USA, 1968.

42. L. C. Andrews, *Special Functions for Engineers and Applied Mathematicians*, Macmillan Publishing Company, New York, USA, 1985.

43. H. Exton, *Handbook of Hypergeometric Integrals: Theory, Applications, Tables, Computer Programs*, John Wiley & Sons, Inc., New York, USA, 1978.

44. W. N. Bailey, *Generalized Hypergeometric Series*, Stechert-Hafner Service Agency, Inc., New York, USA, 1964.

45. A. Erdelyi et al., *Tables of Integral Transforms: Volume II*, McGraw-Hill, Inc., New York, USA, 1954.

46. S. Haykin, *Communication Systems*, John Wiley & Sons, Inc., New York, USA, 3rd ed., 1994.

47. V. Bogachev and I. Kiselev, "Optimum Combining of Signals in Space-Diversity Reception," *Telecommunications Radio Engineering*, vol. 34/35, pp. 83–85, October 1980.

48. W. C. Jakes, Jr., *Microwave Mobile Communication*, John Wiley & Sons, Inc., New York, USA, 1974.

49. A. T. James, "Distributions of Matrix Variates and Latent Roots Derived from Normal Samples," *Annals of Mathematical Statistics*, vol. 35, pp. 475–501, 1964.

50. Q. T. Zhang, "Outage Probability in Cellular Mobile Radio Due to Nakagami Signal and Interferers with Arbitrary Parameters," *IEEE Transactions on Vehicular Technology*, vol. 45, pp. 364–372, May 1996.

51. K. W. Sowerby and A. G. Williamson, "Outage Probability Calculations for a Mobile Radio Systems having Multiple Rayleigh Interferers," *Electronic Letters*, vol. 23, pp. 600–601, 1987.

52. A. A. Abu-Dayya and N. C. Beaulieu, "Outage Probabilities of Cellular Mobile Radio Systems with Multiple Nakagami Interferers," *IEEE Transactions on Vehicular Technology*, vol. 40, no. 4, pp. 757–768, November 1991.

53. I. S. Gradshteyn and I. M. Ryzhik, *Table of Integrals, Series and Products*, Academic Press, Inc., New York, USA, 1980.

54. N. C. Giri, *Multivariate Statistical Inference*, Academic Press, Inc., New York, USA, 1977.

55. N. R. Goodman, "Statistical Analysis Based on a Certain Multivariate Complex Gaussian Distribution (An Introduction)," *Annals of Mathematical Statistics*, vol. 34, pp. 152–177, 1963.

56. M. S. Srivastava and C. G. Khatri, *An Introduction to Multivariate Statistics*, Elsevier North Holland, Inc., New York, USA, 1979.

57. Robb J. Muirhead, *Aspects of Multivariate Statistical Theory*, John Wiley & Sons, Inc., New York, USA, 1982.

58. C. G. Khatri, "On Certain Distribution Problems Based on Positive Definite Quadratic Functions in Normal Vectors," *Annals of Mathematical Statistics*, vol. 37, pp. 468–479, 1968.

59. K. C. S. Pillai and G. M. Jouris, "Some Distribution Problems in the Multivariate Complex Gaussian Case," *Annals of Mathematical Statistics*, vol. 42, pp. 517–525, 1971.

60. A. M. Kshirsagar, *Multivariate Analysis*, Marcel Dekker, Inc., New York, USA, 1972.

61. J. N. Pierce and S. Stein, "Multiple Diversity with Nonindependent Fading," *Proceedings of the IRE*, vol. 48, pp. 196–211, January 1960.

62. W. C. Y. Lee, "Elements of Cellular Mobile Radio Systems," *IEEE Transactions on Vehicular Technology*, vol. 35, no. 2, pp. 48–56, May 1986.

63. Y. Yao and A. U. H. Sheikh, "Investigations into Cochannel Interference in Microcellular Mobile Radio Systems," *IEEE Transactions on Vehicular Technology*, vol. 41, pp. 114–123, May 1992.

64. R. Prasad, A. Kegel and J. Olsthoorn, "Spectrum Efficiency Analysis for Microcellular Mobile Radio Systems," *Electronic Letters*, vol. 27, pp. 423–425, February 1991.

65. I. S. Reed et al, "Rapid convergence rates in adaptive arrays," *IEEE Transactions on Aerospace and Electronic Systems*, vol. 10, pp. 853–863, November 1974.

66. A. M. Mathai and R. K. Saxena, *Generalized Hypergeometric Functions with Applications in Statistics and Physical Sciences*, Springer-Verlag, Inc., New York, USA, 1973.

67. A. P. Prudnikov, Y. A. Brychkov and O. I. Marichev, *Integrals and Series*, vol. 4, Gordon and Breach Science Publishers, Philadelphia, USA, 1992.